Dynamic Cyclic Bending, Kinetic to Strain Energy, Deceleration Systems.

By : Antony Johannes Joost Steynberg.

Submitted in partial fulfilment of the requirements for the degree of Master of Mechanical Engineering, in the faculty of Engineering, Built Environment and Information Technology, University of Pretoria, Pretoria.

Submitted in July 2004.

Table of Contents

Abstract

During the period of 2001 to 2003 an investigation has been completed at the University of Pretoria, which explored the application of a cyclic plastic bending deceleration system in a dynamic environment. The system consisted of a user-defined number of inline guide rollers, with a metal element threaded in an over and under arrangement. This metal element, when drawn through the rollers, was subjected to bending and reverse bending as the material moved from roller to roller. This action allowed for kinetic energy to be absorbed by means of the kinetic to strain energy transformation mechanism. In the past, this concept and the performance prediction thereof had been proved reliable under quasi-static conditions however, the performance prediction under dynamic conditions remained uncharted.

The study performed at the University of Pretoria produced a dynamic performance prediction model. The various predictions were compared to scale experimental simulations, as well as dynamic finite element analyses. The comparison between the predictions, (mathematical prediction, experimental model results and the finite element analyses) proved to be extremely accurate and consistent. A full-scale evaluation would be the next remaining step to evaluate the system's suitability for future application in industry.

Opsomming

Gedurende die periode van 2001 tot 2003 was 'n studie afgehandel by die Universiteit van Pretoria, ten einde die toepassing van sikliese plastiese buigings vertraging sisteme, onder dinamiese toestande. Die sisteme behels n gebruiker-gespesifiseerde hoeveelheid staal rollers wat inlyn langs mekaar gerangskik is. 'n Staal strook word tussen die rollers deur gevleg. Wanneer die strook aan die een punt tussen die rollers deur gesleep word, buig die strook herhaaldelik om die spoor tussen die rollers deur te volg. Hierdie buigings proses absorbeer energie deur middle van omskakeling van kinetiese na vervormings energie. In die verlede is n model ontwikkel om briekkrag lewering onder kwasi-satiese toestande betroubaar te voorspel. 'n Dinamiese lewerings model is nog nie ontwikkel nie.

Tydens die Universiteit van Pretoria se ondersoek is n dinamiese model ontwikkel en wiskundig geprogrammeer, wat dan die briekkrag lewering van die sisteem onder dinamiese toestande voorspel. Hierdie wiskundige voorspellings is dan vergelyk meet 'n afgeskaalde eksperimentele model wat gebou is by die Universiteit van Pretoria, asook 'n dinamiese eindige element analise van die model. Die vergelyking van al drie resultate, (wiskundige model, eksperimentele opstelling en die eindige element analise) was baie goed en herhaalbaar. Die volgende logiese ontwikkelings stadium in voorbereiding vir industriële teopassing van hierdie sisteme, sal dus volskalse toetse wees.

Acknowledgements

I wish to thank SIMRAC who financially supported this study.

I would like to thank all the persons involved in this project. I would especially like to thank my promoter from the University of Pretoria, Mr N.D.L. Burger, for his guidance and advice; Mr R. Ottermann for managing the finances of the project; Mr T. Blom for his assistance and advice in the data capturing section of the project and also his general insight; Mr P.R. de Wet from the University of Pretoria, and Mr C. Stone from MSC Africa, for their expertise and help with the FEM analysis, and Mr A. von Wieliegh who helped with the model building and modifications.

In addition my thanks goes out to all the technical personnel of the University of Pretoria who contributed to the model building and solving of problems, which were encountered. Lastly, I would like to thank all the people who put up with the endless conversation concerning the topic, and patiently offered their valued insights and opinions.

List of symbols

a	Acceleration. (m/s^2)
D	Coefficient in stress strain relation. (Mild steel characteristic)
F	Force applied by deceleration system (N)
FEM	Finite Element Method
FEML	Finite Element Model
FEA	Finite Element Analysis
Gs	Gravitational acceleration. ($9.8m/s^2$)
M	Mass of cage. (kg)
Msec	Millisecond. (0.001sec)
n	Number of rollers in roller assembly.
p	Exponent in stress strain relation.
R	Roller radius (m)
t	Strip thickness (m)
w	Roller width (m)
σ_{yd}	Dynamic yield stress approximation. (Mpa)
σ_{yo}	Static yield stress of material. (Mpa)
ε'	Strain rate at the point of plastic deformation. (/s)
ε_x	Strain at distance y from neutral plane.
y	Distance from neutral plane. (m)
ρ	Curvature radius of neutral plane. (m)

List of Figures

List of Equations

List of Tables

1. Introduction

1.1 Introduction to problem

In the modern technological environment, large masses moving at great velocities are a common occurrence. The potential hazard of not being able to control these masses, leaves a gap in industry that needs to be filled in terms of an effective, reliable kinetic energy absorbing system capable of harnessing and dissipating such large forces.

A possible beneficiary of such a device would be the mining industry, which extensively involves the transport of vast amounts of personnel, equipment and minerals. Accompanying these activities are the unavoidable risks of accidental over or under-wind situations, involving the cages and their contents. Mining personnel are exposed to these dangerous situations daily, and numerous fatalities and injuries have been sustained as a result. With this in mind, transport safety in underground mining is of utmost importance.

Against this background, a SIMRAC (Safety In Mines Research Advisory Committee) project GAP638 [1], was undertaken by a design team from the University of Pretoria and a deceleration device was identified as a possible solution. In this project, past accidents involving conveyances were investigated and the shortfalls in the systems were addressed. A literature study was conducted to identify the existing safety devices used to safeguard cages. These devices were evaluated and efforts were made to constructively utilise their strong points and develop their weaknesses to increase their effectiveness [1].

This dissertation deals with the development of the deceleration device identified as a viable option in the SIMRAC project GAP638 [1]. The device can also be used universally in industry to produce specific deceleration forces to any moving mass. With GAP638 as a preceding project base history, a mining specific event known as an under-wind condition is used as a point of reference, as a possible area of application for the device, which is under development. An under-wind condition occurs when a cage, during its downward journey, overshoots the landing platform and strikes the bottom of the shaft. The proposed device to be used as an under-wind protection system makes use of a steel strip threaded between inline rollers which, when pulled through the roller set, repeatedly deforms from one roller to the next. The repeated bending action disperses energy in the form of plastic deformation, which generates heat, and thereby decelerates the mass system.

A prominent problem with this highly effective system used for mass retardation, is its sensitivity to deformation rate, and therefore the velocity of the decelerated mass at impact [1,2]. This factor drastically varies the performance of a specific configuration, under a quasi-static condition, and that of a dynamic, real-life situation [3].

The first complication regarding the application of the system is the need to accurately and consistently predict the performance for any configuration and thus, for any conceivable situation. This is important due to the stringent deceleration specifications which humans can be subjected to for limited periods of time [4]. The challenge is to incorporate the parameters of a dynamic deceleration system into a calculation which, when fed the operating conditions, would deliver an accurate performance prediction.

calculation which, when fed the operating conditions, would deliver an accurate performance prediction.

The next complication is the devices inability to both detect and accommodate for a varying mass to be decelerated. The deceleration force potential of the device would always be constant, and thus for a certain mass to be decelerated, a specifically sized deceleration system would deliver a corresponding deceleration rate (i.e. F = Ma). If, for example, the same system was to be used to decelerate half the mass, (i.e. half full cage) to satisfy the physical description of force, (F) the acceleration (a) would have to be twice as much. To design for conditions allowing for maximum mass deceleration, a worst case scenario, provision has to be made for a means of staying within the specified limit set for the deceleration of a half mass condition, as well as still having the capacity to decelerate a full load condition within the travel distance available. A possible solution to this problem will be discussed in chapter 9.

1.2 Proposed solution

A method selected to fulfil the operational requirements, is an existing system. It is based on the Strain Energy Linear Ductile Arrestor system, (SELDA). [5] The method of energy absorption by means of kinetic to strain conversion was pioneered by Jackson in 1965 [19].

This method of operation involves the absorption of energy through the plastic bending and unbending of material. This system encompasses a metal strip, which is pulled through a set of sequential rollers, between which the strip is threaded (refer: Figure 1, Figure 2).

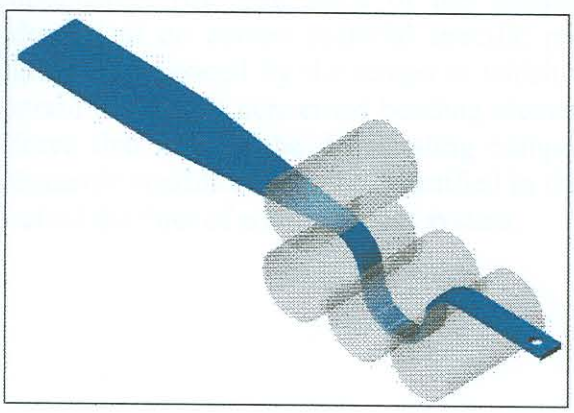

Figure 1 Schematic representation of taper strip energy absorber.

Figure 2 Practical application of wall-mounted, tapered energy absorber.

When the strip is bent and unbent around the rollers, the kinetic energy is absorbed and transformed into low-level heat. The maximum amount of energy that can possibly be absorbed by these means would be a constant force at the maximum specified level for the duration of the deceleration stroke. This, in concept, can be achieved by making use of a strip of constant width, threaded through the rollers, delivering maximum permissible deceleration force.

deceleration profile resulting from the plastic deformation of the strip moving between the rollers, has to be accounted for. This thesis concerns itself with that very investigation.

To alleviate the initial impact effect, the strip or deceleration element, is cut in the profile of a taper, which facilitates a smooth decelerating action, by means of gradual application of the decelerating force (refer: Figure 2). The tapered profile masks the prominent influence of the inertial effect on the deceleration levels experienced by the decelerated body. By these means, the requirement for the primary designed, inline damper system is also eliminated, further simplifying the deceleration system (refer: Appendix C). The narrowest section of the strip, the neck, is designed to have a safety factor of six for static yielding while under application of the maximum expected dynamic load. A design factor of six is acceptable practice according to the Occupational Health and Safety Act and Regulations specifications for all driven machinery [21]. The section of the act is applicable to cables and ropes, and since this application could be classified as a structural member, good engineering principles are required and should be applied. A safety factor of six is more than adequate.

The tapered metal element can only contribute to the decelerating force, once the tapered section enters the roller system. The absorption of kinetic energy takes place during the deformation action of forcing the element to conform to the roller radius. This event occurs once the section of the element leaves the roller radius it had travelled over, and moves to the next radius, bending from one arc to conform to the next. This event is repeated, as many times as there are rollers in the series. The bending and straightening of the element under tension causes slight elongation. This effect has been identified and quantified in past research. It is magnified by specific geometrical and system properties but the effect is still negligible in the current application [6]. The force of the element resisting travel through the rollers is dependant on certain material specific properties. The performance properties are greatly influenced by the tempo at which the process takes place, and therefore the strain rate of the concerned bending element [7]. The element's resisting force is the force that acts as the decelerating component. The performance characteristic for dynamic conditions is to be quantified in this dissertation, which could then be used to retard the "out of control" mass system.

In the proposed application of the deceleration system [1], sets of rollers loaded with deformable strips can be anchored either side of the shaft to the walls, connected by means of pulleys and cables strung across the width of the shaft. When the cage travels past the shaft bottom limit, contact with the cable strung across the path of travel of the cage is made. The cable, which is attached on either of its ends to a deformable strip, would then pull the deformable element through the roller sets, resulting in a decelerating force (refer: Figure 3, Figure 4).

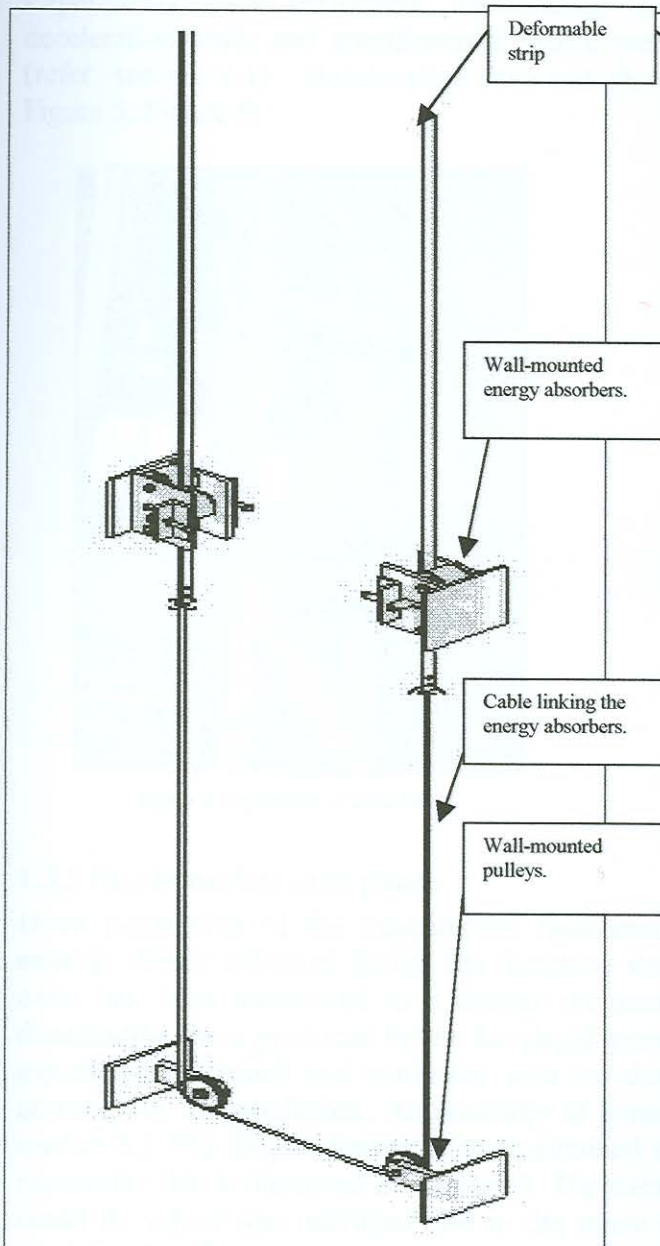

Figure 3 Schematic of retardation system.

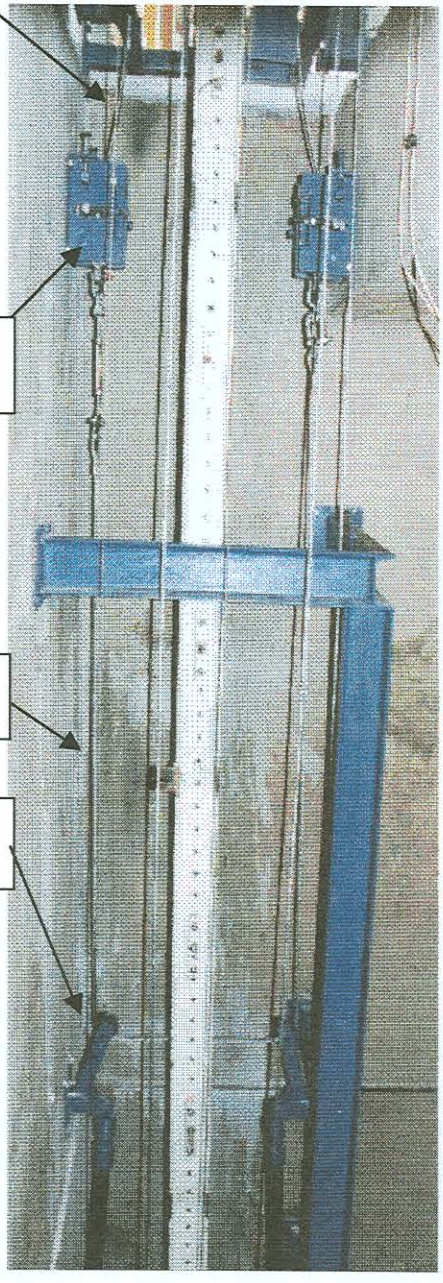

Figure 4 Image showing model retardation system.

1.3 Problem solution approach

1.3.1 Scale model phase

A tenth scale model of a mineshaft, constructed at the University of Pretoria, has been used to implement and evaluate the proposed under-wind protection system. This model was also used for the test work for the SIMRAC project GAP638 [1]. Experiments were performed, decelerating the model cage within the desired deceleration limits and specifications, which were established in the literature study (refer: section 2.1). Deceleration data was recorded during the experiments (refer: Figure 5, Figure 6).

Figure 5 Top section of model shaft.

Figure 6 Lower section of model shaft.

1.3.2 Mathematical code phase

Upon completion of the experiments, mathematical code was developed based on existing theory collected during the literature study (refer: section 4.) [3], [7]. This code has been automated in a design program to predict the magnitude of the deceleration force produced by the simulated geometry. Various geometries were then experimentally tested and compared with the design program's output to verify the accuracy of the prediction. An accuracy of between 75%-99% was obtained (refer: section 8.). The largest deviations were obtained with the small force simulations. The reason for this is discussed in chapter 9. The extent of which the experimental set-up could be varied was restricted due to the space constraints in the scale shaft (refer: section 6.2). These restricting factors, i.e. roller radius and drop height, which would vary in industrial applications, required to be investigated by other means of testing to verify that the prediction program delivers accurate information, and to further ascertain its accuracy domain. During the course of the study it has been noted that the developed design program's output only significantly deviates from the true situations once the inertia factors reach a significant size. This is when the combined mass of the strips used to perform the retardation, are within 10% of the mass being decelerated. This is in an extreme situation that will be discussed at a later stage (refer: section 8.).

1.3.3 Dynamic finite element analysis phase

Further testing has been achieved by means of a dynamic Finite Element Analysis (FEA) simulation, making use of MSC Patran and MSC Dytran. Firstly a model was created similar to the scale experiments already performed, and the results were compared to the captured experimental data. This is considered to be the benchmarking phase. The predictions of the design program also compared well with the experimental data captured (refer: section 8.). Having gone through this process of calibrating the FEA, it could be accepted that the Finite Element Model (FEM), was delivering sound information. The correlation between the FEM and the experimentally recorded data was between 75%-99% (refer: section 8.). This is an acceptable degree of accuracy considering the finite element program only delivers a velocity output, which had to be filtered and differentiated to obtain an acceleration figure. Some degree of inaccuracy would this be expected.

The restrictions of the experimental model mentioned in the above paragraph, could thus be changed and tested in the FEM, where space and velocity have no limits. The simulation can be performed, and the output can be used as a reference or yardstick, since the quality of the FEM predication has been established as being of an acceptable standard, allowing for the design program to be further explored and quantified.

Various possible real life conditions have been simulated by means of the FEM. The outputs of the simulated conditions were compared to the output of the design program to determine the deviation of the prediction from the true conditions obtained from the FEM (refer: section 8).

1.4 Conclusion

This dissertation describes the development and testing of a reliable design tool, in the form of mathematical code, which predicts the performance of the dynamic strain energy converting deceleration system under various dynamic conditions, and in various forms. This project is thus an extension of the preceding SIMRAC project, GAP638 [1], which investigated the possibility of utilising the proposed deceleration system for application in the mining industry.

2. Literature Survey

2.1 Human deceleration specification literature survey

2.1.1 Introduction

Man, as a mechanical system, is extremely complex and his mechanical properties readily undergo changes under dynamic conditions. Information quantifying the magnitude of forces which produce physical and psychological damage to the human body, is scarce [9]. The study of positive longitudinal short duration acceleration is closely linked to the development of upward ejection seats used for escape from aircraft.

The term impact describes the force applied to a body coming into sudden contact with a second body where momentum transfer then takes place. Impact forces by nature are of considerable magnitude, with no exception during the scenario where a human body decelerates independently from a rapidly decelerating cage.

In the literature survey conducted, it has been noted that the duration of the impact, combined with its magnitude, form the crux in defining the degree to which human injury would occur. The magnitude of the acceleration alone without the time duration of the force exposure is not enough information to draw any conclusion [9], [10]. Another defining characteristic is the level to which the human body is supported while being subjected to the deceleration. A person who is seated and strapped down can withstand greater vertical accelerations than a person who is free-standing, such as someone standing in an elevator or a mine cage [9], [10]. A wide range of literature concerning automobile as well as aircraft crashes, has also been perused. Experiments with dummies or manikins, and live subjects reveal that complete body support and restraint of the induced motion extremities, provides maximum protection against acceleration induced, impact forces and offers the subject the greatest chance of survival [11].

In summary, specifically concerning freestanding vertically ascending acceleration, the human body can survive large decelerations for short durations (roughly 200Gs for 2Msec). Based upon the minimal research undertaken for longer duration exposure, the survivable limit is estimated to be in the region of 20Gs for 200Msec [10]. The G-loading decreases as the time exposure increases further from the estimated values above (refer: Table 1). Control or prevention of injury is critically dependant on body positioning and restraint to minimise unwanted, forceful flexion of the spinal column. The fracture tolerance limit is influenced by age, physical condition, clothing, bodyweight and many other factors. All can greatly alter the stress that the subject can or cannot survive. When limits are exceeded, fractures of the lumbar and thoracic vertebrae occur first (injuries of the lower back and back). While in itself this injury is not classified as severe, small changes in orientation are enough to involve the spinal cord, which is extremely sensitive and susceptible to problems with forced posture disturbance. Neck injuries occur at considerably higher levels of vertical accelerations than back injuries [10].

2.1.2 Human deceleration specifications

Deceleration specifications are scarce and usually incomplete, with certain degrees of uncertainty involved with the application thereof. This study highlights four applicable criteria found in literature, which serve as comparisons for the two mining specifications, to validate and compare their order of magnitude.

2.1.2.1 Deceleration criteria 1 [10]

The envelopes of deceleration listed in Table 1 below have been set up from extensive experiments conducted in the field under operational conditions. The limits which indicate possible death, have been based on the post crash analysis of experts estimating the conditions of exposure experienced by the occupants, or victims.

Type of operation.	Acceleration, G's	Duration, sec
Man:		
Parachute opening, 40 000ft (vertical)	33	0.2 to 0.5
6 000ft (vertical)	8.5	0.5
Parachute landing (vertical)	3 to 4	
Fall onto firemans net (vertical)	20	0.1
Approx limit of survival with well distributed forces (fall into deep snow bank)	200	0.015 to 0.03
Aircraft: (Horizontal)		
Ordinary take-off	0.5	>10
Catapult take-off	2.5 to 6	1.5
Crash landing (survivable)	20 to 100	<0.1
Seat ejection (vertical)	10 to 15	0.25
Automobiles: (Horizontal)		
Comfortable stop	0.25	5 to 8
Very undesirable	0.45	3 to 5
Maximum obtainable	0.7	3
Crash (survivable)	20 to 100	<0.1
Public transport: (Horizontal)		
Normal acceleration and deceleration	0.1 to 0.2	5
Emergency stop from 70 mph	0.4	2.5
Elevators: (vertical)		
Average (fast service)	0.1 to 0.2	1 to 5
Comfort limit	0.3	
Emergency deceleration	2.5	

Table 1 Approximate Duration and Magnitude of Some Short-Interval Acceleration Loads [10].

2.1.2.2 Deceleration criteria 2 [9]

Arthur E. Hirsch considered all the available data published by a variety of experts in the field and combined it into a single figure with three defining axes (refer: Figure 7). The three defining axes are firstly, the exposed Gs rating, secondly the time of exposure and lastly the condition or injury that is likely to be encountered at that stage (refer: Figure 7). This information is currently extensively used in industry as a guideline for acceptable human deceleration limits.

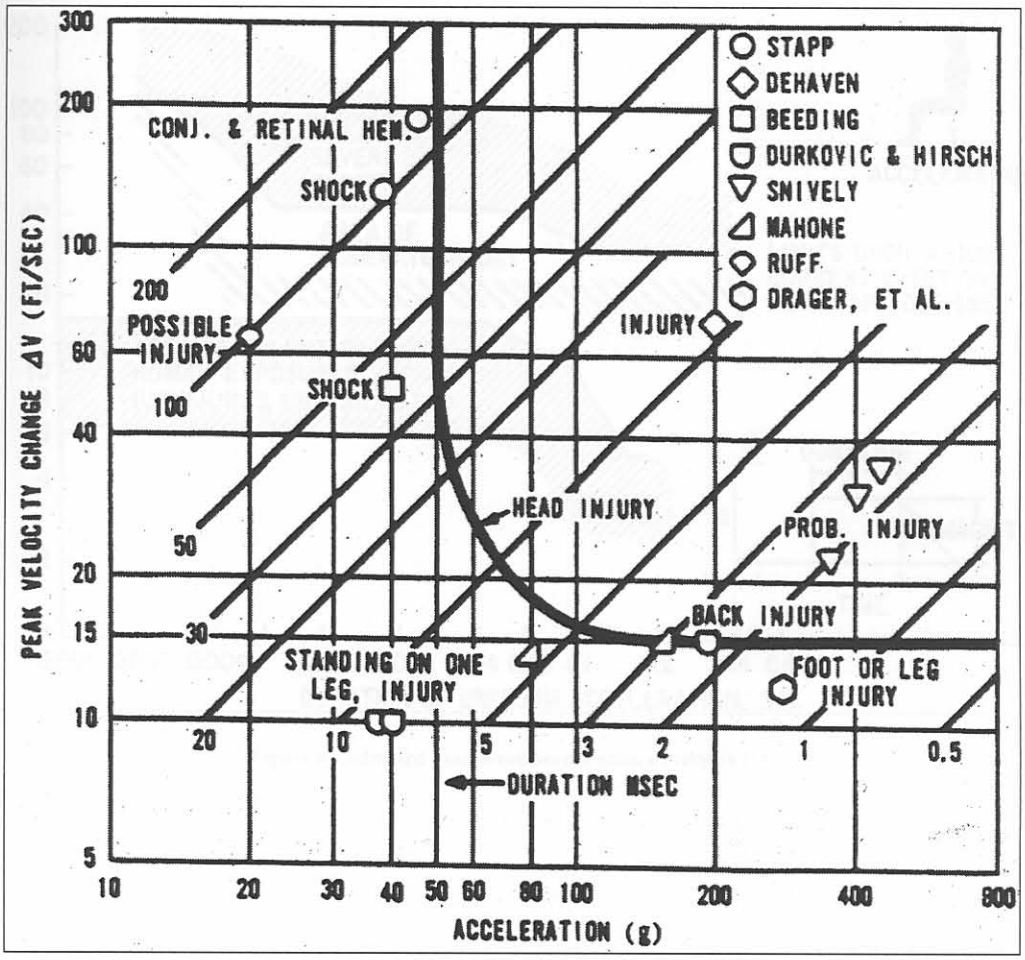

Figure 7 Acceleration tolerance limits [9].

2.1.2.3 Deceleration criteria 3 [11]

The human tolerance for vertically seated ascending acceleration for various exposure intervals was investigated by Arthur Eiband. The research was performed for the National Aeronautics and Space Administration (NASA). His findings are summarised in a figure depicting various limits of comfort (refer: Figure 8).

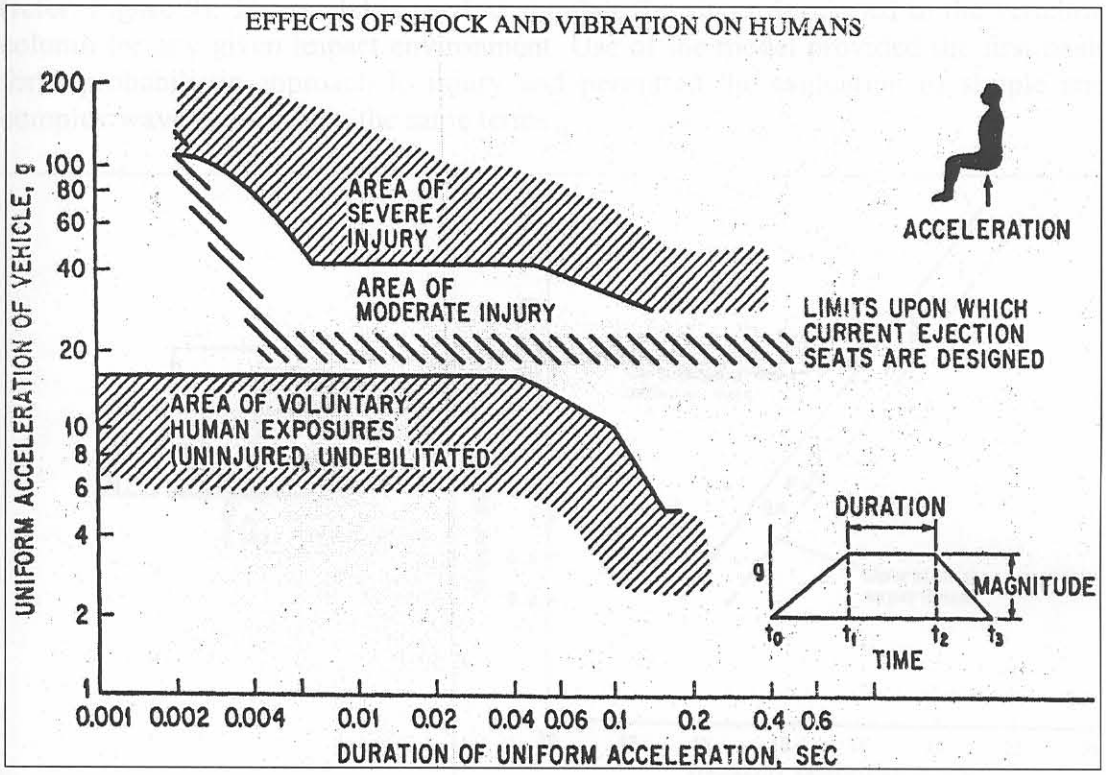

Figure 8 Estimated head ward acceleration envelopes [11].

2.1.2.4 Deceleration criteria 4 [13]

Investigations indicate that the human body's ballistic response can be predicted by means of analogue computations by making use of the frequency response characteristic of the body. The simplest analogue model used for the study of positive vertical accelerations, is the single degree of freedom mechanical resonator composed of the lumped parameter with elements comprising of a mass, spring and damper (refer: Figure 9). The model is used to simulate the stress developed in the vertebral column for any given impact environment. Use of the model provided the first basis for a probabilistic approach to injury and permitted the evaluation of simple and complex waveforms within the same terms.

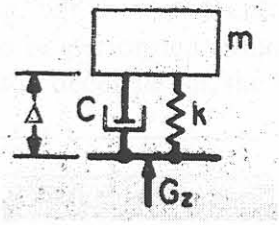

Figure 9 Ballistic model of human body.

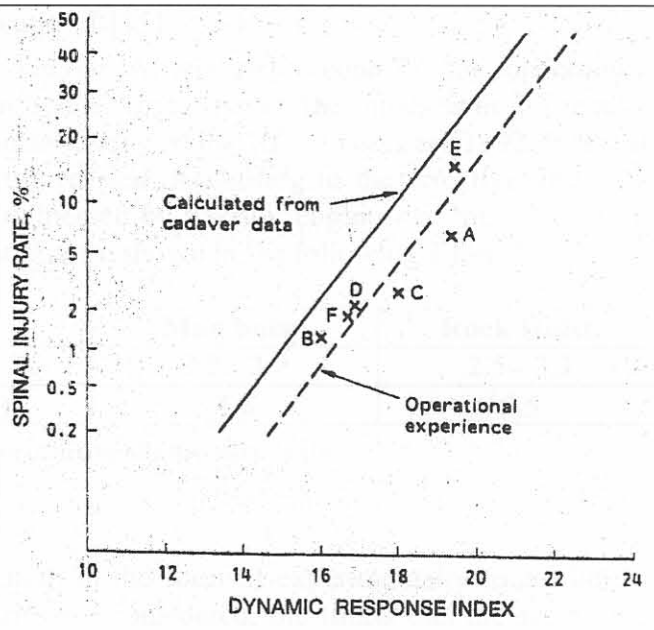

Figure 10 Spine injury probability % vs. DRI.

The maximum dynamic deflection of the spring, Δ_{max}, may be calculated for a given input acceleration-time history to the model. The potential for spinal injury was then estimated by forming the *dynamic response index* (DRI),

which is defined as $DRI = \frac{\omega^2{}_n \Delta_{max}}{g}$,

where the natural frequency of the model is $\omega_n = \sqrt{\frac{k}{m}}$,

and the damping ratio $\frac{c}{2}\sqrt{km} = 0.224$.

Experience with 361 non-fatal ejections from military aircraft, shown by the crosses and dashed line in Figure 10, suggests a 5% probability of spinal injury from exposure to a dynamic response index of 18. An estimate of the rate of spinal injury from cadavers is shown in the same figure as the solid line. The success of the model has led to its adoption for the specification of ejection seat performance, as well as the measure of ride comfort for exposure to repeated impact in some land and water vehicles [10].

2.1.2.5 Mining Deceleration Specification 1 [14]

The Ministry of Mines for British Columbia set up specifications that cannot be exceeded while bringing mine man conveyances to an emergency halt. These limits are described as follows.

- While the conveyance is travelling upward the deceleration should be no more than $9.8 m/s^2$ (1Gs).
- While travelling downward the maximum deceleration limit is $24.5 m/s^2$ (2.5Gs).

These retarding limits are specified to be applied by means of; "a safety device in any shape or form".

2.1.2.6 Mining Deceleration Specification 2 [15]

The Department of Mineral and Energy Affairs, who controls the operational regulations for all licensed mines in South Africa, issued the mines with a directive for the dynamic testing of winding installations on the 10th of February 1992. It is still binding, but the act is currently being revised. According to the directive, the tests have to be performed annually and witnessed by a senior engineer of the mine. With respect to deceleration, the specifications are shown in the following Table 2.

	Man hoist.	**Rock Hoist.**
Average brake deceleration. (m/s^2)	2.2 - 2.7	2.5 - 3.3
Maximum brake deceleration. (m/s^2)	4.8	5.5

Table 2 South African Deceleration Specifications [14].

2.1.2.7 Summary

When the above sources of information in the form of experimentally found limits, prediction models and data summaries are considered, the limits that are set by the mines are based on a sound safety foundation. They also have a sufficient buffer zone to allow for human survival under slightly larger retardation rates if and when the moment called upon it. Further confirmation of these limits can also be seen with reference to Macaulay [17].

2.2 Shaft protection requirements

2.2.1 Functional analysis of under wind system

The investigation undertaken for SIMRAC, project GAP638 [1], focussed on the safe control of mine cages. From this investigation the following functional requirements were developed.

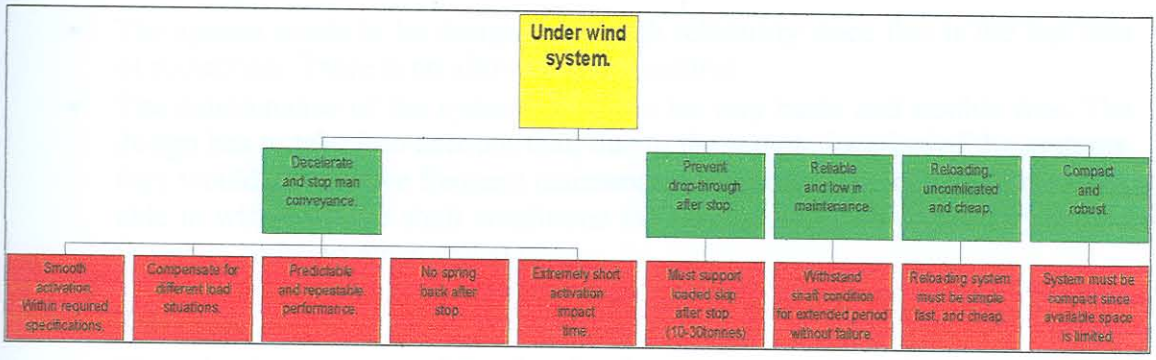

Figure 11 System functional requirement.

2.2.1.1 Decelerating conveyance

- A smooth activation of the decelerating force would be required. This is the primary function of the taper section, introduced to the front of the parallel strip (refer: Figure 2). The retardation force has to be within the specified 2.5Gs average limit, even under dynamic circumstances.
- Compensation has to be made for both a fully and partially loaded. The deceleration force needs to be varied for the change in mass to accommodate the specification of the maximum deceleration limit as explained in chapter 3.
- The performance of the chosen deceleration system needs to be predicted accurately for any given probable situation. The dynamic aspect needs to be accounted for, given the application of the systems. This is discussed in great detail in chapter 4 of this study.
- The ability of the system to absorb the kinetic energy of the moving conveyance without spring back once the cage was brought to rest, is important. A bungee effect would need to be avoided in the shaft as this could then cause secondary rebound damage, which would be unnecessary.
- In the event of two mass systems colliding, as is the case of the conveyance connecting with the deceleration system, forces are introduced upon each other to satisfy the law of conservation of energy. The system has to be developed to maintain this impulse force introduced into the conveyance by the decelerating systems to an acceptable minimum time, to ensure the safety of the occupants (refer: Figure 7).

2.2.1.2 Prevent drop through

- When an emergency deceleration has taken place, the design of the systems has to be of such a nature as to ensure that the conveyance would not fall through the braking zone under static conditions. Thus the system has to be able to support the full static mass of the conveyance.

2.2.1.3 Reliability and Maintenance

- The system needs to be designed for high reliability since this is the last area of protection. There is no allowance for misfires.
- The maintenance of the systems needs to be very basic and trouble free. The design has to take into account that, due to the remote location of the systems, they would not receive frequent maintenance attention. The systems have to be able to withstand the shaft conditions for extended periods of time whilst not failing to function when called upon.

2.2.1.4 Reloading

- The reloading process of the deceleration system needs to be uncomplicated and easy. Intricate settings and adjustments needed to allow the system to operate, as well as extremely expensive disposable sections, are out of the question. In an industry where standing time causes great financial losses economic time consumption is of the essence.

2.2.1.5 Compact System

- The absence of space in the shaft for the building of elaborate deceleration systems is also a considerable problem. The system needs to be compact enough to be retrofitted in confined spaces, yet still have the ability to fulfil all the other requirements.

2.3 Existing and probable solutions

2.3.1 Introduction

The technique of absorbing and converting a large quantity of kinetic energy to another form of energy is subject to many conditions. The amount of energy to be absorbed by the device is equal to the integral of the force over the stroke length. The required performance of the device is defined by the maximum deceleration that can be applied to the moving mass and the space available to arrest it.

When the mass under deceleration contains human beings, which are susceptible to injury or death in the event of rapid deceleration, the rate of energy dissipation is of great importance. There are thus some limits, which regardless of what means are used to decelerate a human cargo, would remain unchanged for all cases. These conditions are nonnegotiable if the survival of the occupants are of importance.

- The first condition is the deceleration rate, which cannot be exceeded (refer: Table 2). The state of the bodily restraint of the person under deceleration plays a major role in the survival limit [11].
- The second fixed condition is the distance that would be required to decelerate the mass, given a velocity at which it would be moving when striking the emergency decelerating system. Certain environments have limitations and cannot accommodate this.
- The third important requirement of all possible deceleration systems is the minimal size of the initial contact force to be transferred, thus the inertial effects of the system.

All three factors require careful consideration before a deceleration system can be successfully implemented.

2.3.2 Existing protection

The existing protection against the under wind accidents is limited to the control of the cable drum, which comprises of a trigger which activates the emergency brakes to retard the conveyance. As a result there are thus no specific protection devices in the shaft itself, at the point of impact, in the current systems.

The statement in the Mining Act, under which the mines in South Africa fall in terms of shaft operational law, states the following:

"Chapter 16, Winding:

Retarding device: 16.59 For a winding system in a vertical shaft or winze where the winding rope is not fastened to the drum or sheave of the winding engine –

16.59.2 the over-run space at the bottom of the shaft below the lowest established stopping place shall be provided with rigid guides or *other appliances* arranged so that an under wind conveyance is retarded and arrested before it can come into contact with any fixed obstacle.

16.61 The shaft or winze shall be carried sufficiently deep to allow an overrun space of *at least 7.5m* in which the conveyance can travel below or beyond the lowest landing place for persons before it comes into contact with any fixed obstacle *excluding any retarding appliance provided in terms of regulation 16.59"* [16].

2.3 Possible solutions

For information purposes, some possible concepts that would enable the safe deceleration of the mine cages in the event of an under wind, are discussed. There are, however some operating conditions that make the systems non-viable. A deceleration system developed to comply with all the requirements does not have to be restricted to the mining industry. Various industrial applications would benefit from a system capable of performing a large mass deceleration function.

Under mining conditions, an application problem is the shaft bottom, usually being the deepest part of the mine and thus attracting all free water, flooding the bottom of the shaft. Another important problem to be considered is the dropping of debris down the shaft, especially in the form of conveyed rock spillage. In a report from Vaal Reef, it was stated that 180 metric tonnes of rock was removed from the shaft bottom [1]. The time period over which spillage accumulated is not known.

The following concepts are some of the mechanisms, which were considered as candidates to solve the problem at hand [1].

2.3.1 Concept 1

A concept under evaluation, which has recently made great progress, is the use of aluminium honeycombs as energy absorbing structures [18]. These systems are used as bases to alleviate the impact during landing of air dropped cargo. During trial experiments, crushing of the honeycomb platforms were done up to velocities of 300m/s. The dynamic versus the quasi-static performance of the honeycomb deceleration force significantly increased by 74% under dynamic conditions. This is due to the strain rate influence as well as the inertia of the structure itself. This is an effective method of energy absorption with a low probability of misfire. Problems would however arise with the specific application, when these platforms are stacked in layers at the bottom of the shaft. In the case of the flooding, the system's performance would be greatly affected, due to the incompressibility of water. The energy absorption should occur with the crushing of hollow compartments in the honeycomb. If the bottom of the structure were submerged, the cavities would be filled and be rendered solid, with no energy absorbing capabilities. This would have severe implications upon the energy absorbing capacity of the structure. With respect to the rock spillage, the platforms would be covered and crushed, and again be rendered useless.

2.3.2 Concept 2

Tube inversion is also a very effective energy absorbing method. The dynamic properties are good and the reliability is impeccable due to the simplistic method of execution [18]. This method of energy absorption is used in submarines to isolate the nuclear reactors from the ships hull in the event of a shock wave during depth charge demolition detonations. For the application of under wind protection, the length of stroke required, would place the tube length in an Euler buckling situation. This type of retardation method would be used for considerably higher acceleration applications with shorter travel distances. Pipes or shells can be used in various other configurations as well. Tube flattening or lateral compression, is a good absorber but has a low stroke length. Local or transverse collapse, for instance the bumper of a car, also has good energy absorbing characteristics. Useable stroke length remains an application problem. Axial or concertina buckling in a bellows fashion has proved a

popular energy absorber and also delivers a constant retarding force profile. The load however, must be applied exactly axially to these devices, to prevent Euler collapse. The length of the pipes must also be restricted to eliminate Euler buckling [20].

2.3.3 Concept 3

Bellamble Mining proposed the use of visco-elastic shock absorbers in the event of an accidental under wind [5]. The energy of the moving cage would be absorbed by the visco-elastic properties of the fluid in the device. The viscosity (10-20m^2/s) and the compressibility (15% at 400 MPa) of the fluid would allow the single device to function as both a shock absorber and a spring to retard the moving mass. The problem with this application would again be the flooding of the shaft, as well as the spilling of conveyed rock. These viscous devices are cumbersome and heavy, do not provide very long stroke lengths and are expensive. They also have an inherent sealing problem when exposed to high velocity rates.

2.3.4 Concept 4

Coulomb damping was also considered as an for the energy dissipation application. Coulomb friction force is generally accepted to adhere the following characteristics.

- It is dependant on the materials in contact and their surface preparation.
- The magnitude of the force is also proportional to the normal force across the interface.
- It is also independent of the sliding speed and apparent area of contact.
- Static friction force is larger than that of kinetic friction force.

The magnitude of the force resisting relative motion between the surfaces in contact is greatly dependant on the coefficient of friction of the surfaces. This, in turn, is dependant on the condition and temperature of the surfaces. Devices of this nature also tend to have low specific energy absorbing capacity per unit mass, and are thus typically applied in rotational applications [20], as is the case with the winder drums.

2.3.5 Concept 5

The concept of energy dissipation by means of converting kinetic energy to strain energy when repeatedly deforming a steel element by dragging it through a set of inline rollers is not new technology [refer: section 1.2]. The principle was introduced and developed by Seltrust Engineering, as the Strain Energy Linear Ductile Arrestor or the so-called SEDA system. This principle was applied in the SIMRAC project GAP638 investigating arrestors for cage under-wind conditions [1].

This concept holds great promise since it is mechanical and, therefore, perfectly reliable. The system is mounted against the walls of the shaft, keeping it from shaft bottom and therefore has no problem with water, until the shaft fills to within the intended path of travel of the conveyance. It also makes use of cables strung across the shaft opening and not platforms, thus the spilled rocks would not impede its function as long as a full distance of travel is allowed for (refer: Figure 3). The problem is the various conditions in terms of speed and mass to be retarded, and the determination of exactly what configuration would be ample to fulfil the deceleration requirements.

The task of defining the specifications and performance of such as system for operational conditions is the focus of this dissertation.

2.4 Conclusion

The deceleration of the cage is possible by means of concept 5, applying the kinetic to strain energy conversion technique. The hindrance involving shaft flooding and rock spillage would still have to be monitored, but would be less prominent than with the other systems. The specification of the required geometry of the system to perform the deceleration within the prescribed limits would be described by means of a design prediction program, as discussed in chapter 5, thus making it the most attractive option. For these reasons concept 5 has been chosen for further development (refer: section 1.2).

3. Cyclic Bending Theoretical and Experimental History

3.1 Introduction

The mechanism for energy dissipation by means of plastically deforming metals is commonly used as a means of irreversibly absorbing kinetic energy, in one or another form of motion, and converting it to heat. Many of these devices designed to absorb impact energy are common structural elements such as bars, tubes, wires and frames. The performance prediction of these devices as deforming structures involves taking into account large geometrical changes, strain hardening, strain rate sensitivity and modes of deformation. Oversimplifying these assumptions can lead to inaccurate predictions of performance. In this chapter past research conducted in this field is investigated.

Devices making use of plastic bending and unbending of metal elements to provide a resistive force are of great interest to industry. Many areas can benefit from the accurate magnitude prediction of the resulting resistive force produced when a metal element is plastically deformed.

3.1.1 Cyclically Loaded Devices

The SELDA system has already been implemented and used in industry by Seltrust Engineering [5]. To the authors knowledge no clear performance prediction is available, and the application specification as stated by the manufacturer, is a force range or envelope, which will be delivered by the systems. There are three different sizes of deceleration systems; small, medium and large, which are available to cover a small range of forces. The assumption is that the specified performance envelope covers the variations in performance of the deceleration systems, under quasi-static and dynamic conditions.

Rosslee developed two analytical equations predicting the performance of cyclic bending energy absorbers, in his master's thesis [3]. These models were meant for quasi-static application. Rosslee experimentally verified them for a variety of geometries. The predictions and the experiments showed a very good correlation (refer: 4). In Rosslee's paper the dynamic application of this system as an energy absorber was suggested, provided testing was done to verify a prediction model.

Sheet metal bending as a function of thickness has been studied in the light of air bending by De Vin [22]. The bending performance is important when predicting forces required to press out certain patterns, accounting also for spring back and bend radii. A plane strain bending model was developed on the basis of a moment curvature model. The model was used to simulate the bending process for materials with different work hardening behaviour.

A metal strip being pulled over a roller was considered by Alexander [23], and a theoretical analytical model was developed to predict the difference in magnitude of tip forces required to pull the strip over the roller while conforming to the arc. According to Alexander the device delivered nearly constant resistive force and this was increased with each unit of width and thickness (refer: section 4.). These findings were under quasi-static conditions.

Johnson and Mamalis [4] developed an approximate theory for the force required to bend a metallic strip over a roller while forcing it to conform to the roller radius. It was suggested that this method of energy dissipation should be used to absorb the kinetic energy of a moving conveyance in order to protect the occupants. The magnitude of the force was also a function of width and thickness of the strip that was bent and unbent over the radius (refer: section 4.3). This mechanism was applied to a moving mass of 23 tonnes, but the equation does not make use of strain rate sensitivity.

During sheet metal forming on a double action press, drawbeads on the blank holder supply the restraining force, which controls the flow of metal into the die. As the metal is drawn through the drawbead, the restraining force has two components, bending deformation and friction. In an investigation performed by H.D. Nine, these two components were separated by means of a simulated drawbead and the use of rollers to eliminate friction, isolating the bending component [24]. It was found that the strain rate hardening should be modelled for steel and not for aluminium. Strain as a function of position was measured on the strip by means of grids accurately drawn on the undeformed strip prior to bending. The changes in spacing of the gridlines were closely monitored during the process. The distance needed for the strip to conform to the following arc radius when leaving the roller it had just passed over, was repeatedly recorded as being between 2-3 times that of the strip thickness (refer: section 4.). The experiments were done and verified against a statically calculated value, which compared well, within 5%. The effect of cyclic strain softening was neglected, which was compensated for by the lack of the strain rate hardening component.

3.2 Conclusion

The preceding theory has been scrutinised and summarised, and combined into a theoretically functional form to estimate the performance of the cyclic bending retardation systems. Four analytical equations have been collected and modified to accomplish the task. These have been automated into MATLAB code and allowed to deliver predictions of resistive performance. The results were gathered and compared (refer: section 7.).

4. Relevant Applied Theory

4.1 Introduction

The theoretical approach used to solve the presented problem did not encompass the development of new models. It was based on the manipulation of existing models and verifying whether the dynamic aspect applied to them delivered a prediction that coincided with the experimental readings gathered, as well as the FEA results. When a model was found to deliver comparable answers, the range of accuracy had to be evaluated.

In this dissertation, four analytical equations have been gathered, based on work from various authors (refer: section 3). The quasi-static prediction models have been automated into mathematical code (MATLAB), supplemented with the dynamic strain rate effect equations applicable to high strain rate situations, and allowed to predict the response of specific roller strip systems (refer: section 5).

In this chapter, the theory gathered and the application thereof is discussed.

4.2 Important Physical Considerations

4.2.1 Baushinger Effect

When a material is loaded into the plastic regime, unloaded and reloaded in the opposite direction, it is generally observed that the yielding during reloading occurs at a stress level lower than the initial load. This direction dependant yield behaviour is known as Baushinger effect, as discovered by J. Baushinger, a civil engineer in 1881 (refer: Figure 12). There is a dynamic aspect, which affects the degree to which the Baushinger behaviour influences the material characteristics [25]. The materials that were tested by Thakur [25] in the dynamic Baushinger effect experiments were exposed to significantly higher strain rates than the application considered in this study, but the same tendencies were expected. It was assumed that the Baushinger effect is a significantly smaller contributing factor to the dynamic effects of the systems performance.

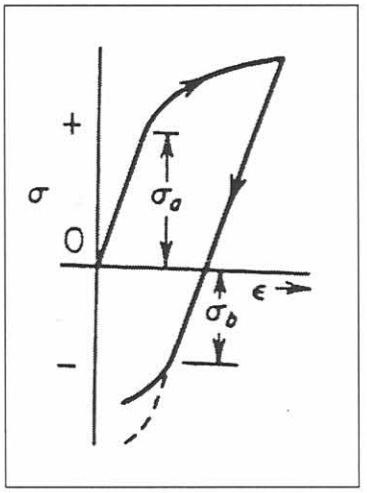

Figure 12 Baushinger effect.

The Baushinger effect is commonly ignored in plastic theory [26]. This was the case in the development of the analytical equations considered in this study, which have been sourced and used as performance predictors [3]. The yield stress was assumed to be the same in both directions of bending.

The roller radius and the thickness of the strip, as well as the velocity of the mass that is retarded, defines the strain rate of the current application. There are checks stipulated in the design protocol, specified by the author for the prevention of situations where the ratio of the thickness of the strip relative to the size of the roller radius are too large. This would prevent situations where the bending angle is too sharp, i.e. when a thick strip bends around a small roller, creating high surface strains.

4.2.2 Material Elasticity or Plasticity Component

During his experiments, H.D. Nine found that the total energy absorbed by a strip which was pulled through a series of rollers, was far greater than the amount of energy that the strip could store elastically [24]. This would then support the assumption that elasticity effects could be neglected in the cyclic plastic bending energy absorber, given that the ratio of roller radius to strip thickness is such that a large percentage of the strip cross section is plastically deformed [3].

4.2.3 Material Strain Hardening

There are two reasons why the material strain hardening effect has a small influence on the performance of the system considered in this study. The first reason is that strain hardening decreases with the increase of strain rate [27]. The second reason is that mild steel, as used in the cyclic plastic bending energy absorber, has moderate strain hardening characteristics, and the influence of this on the results would be negligible [28].

For these reasons, the four authors who developed the theory which was used as the prediction models in this study, ignored the material strain hardening effects.

4.2.4 Material Strain Rate Sensitivity

It has been identified that materials which have a tendency to be strain rate sensitive under high deformation rate conditions, should be modelled accordingly. The dynamic yield stress of a material has been known to increase by 300% from the static yield stress, at high rates of deformation (refer: Figure 13). In an investigation conducted by Perrone, reference was made to the well-known Cowper Symonds model for strain rate sensitive materials [29], [8]. This model was developed for the situation involving the impact loading of cantilever beams, which exhibit strain hardening or strain rate sensitivity.

The investigations performed by Perrone and Cowper Symonds was adopted as the basis for applying the strain rate sensitivity effects to the cyclic plastic bending retardation system, considered in this dissertation.

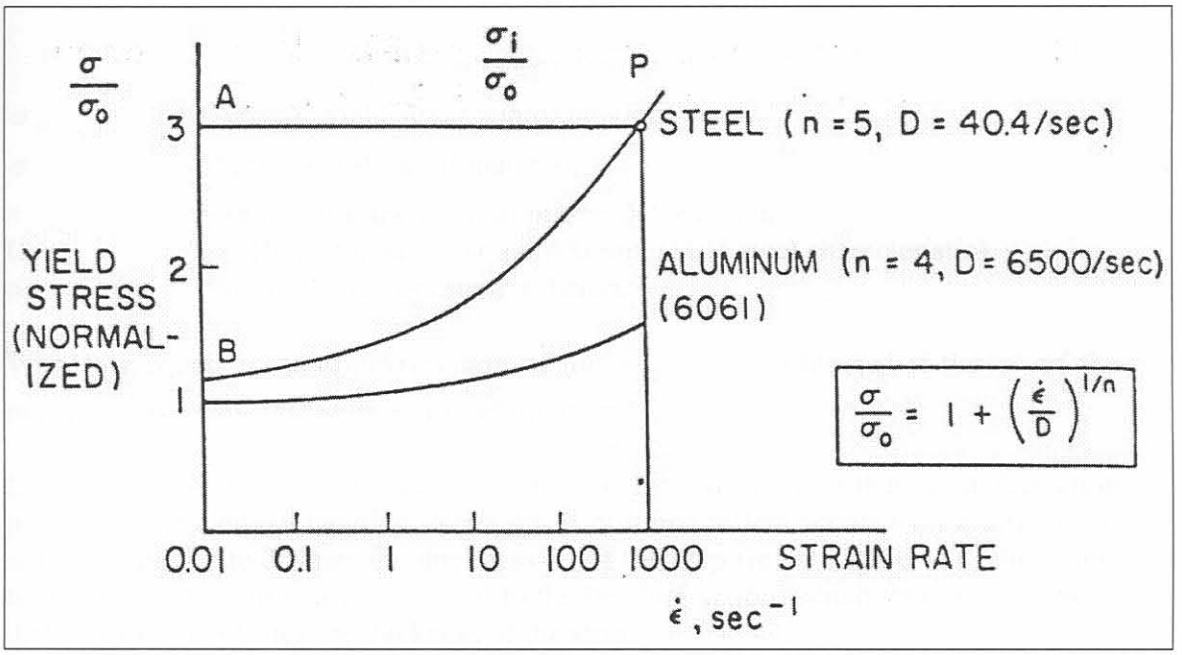

Figure 13 Dynamic yield effect, Perrone.

4.3 Applied Equations

4.3.1 Strain Rate Sensitivity Compensation

The strain rate sensitivity is appended to the prediction equations in the form of the Cowper Symonds formulation [8]. This is combined with a deduction made from the research of H.D. Nine [24] concerning the period in which the straining of the material takes place. When the distance is known, for the strip deformation process at each point of bending to take place, the velocity of the moving material is also known, thus the strain rate at that point can be calculated and the dynamic yield stress at the point of strain deformation can be determined.

The Cowper Symonds formulation is the following:

$$\frac{\sigma_{yd}}{\sigma_{yo}} = 1 + \left(\frac{\varepsilon'}{D}\right)^{\frac{1}{p}}$$

Equation 1 Cowper Symonds. [8]

σ_{yd}	=	Dynamic yield stress approximation.
σ_{yo}	=	Static yield stress of material.
ε'	=	Strain rate at the point of plastic deformation.
D	=	Coefficient in stress strain relation. (Mild steel characteristic)
p	=	Exponent in stress strain relation.

With this equation, an approximation of the σ_{yd} can be obtained if the ε' of the material was known at the point of deformation.

During the investigation of drawbead forces, H.D. Nine showed that the deformation process of the element bending over a series of inline rollers occurs over a distance of approximately 2 to 3 times the thickness (t) of the strip (refer: Figure 14). This refers to the length of strip that is subjected to the bending action, which then occurs over a distance of 2 to 3 times the thickness of the strip.

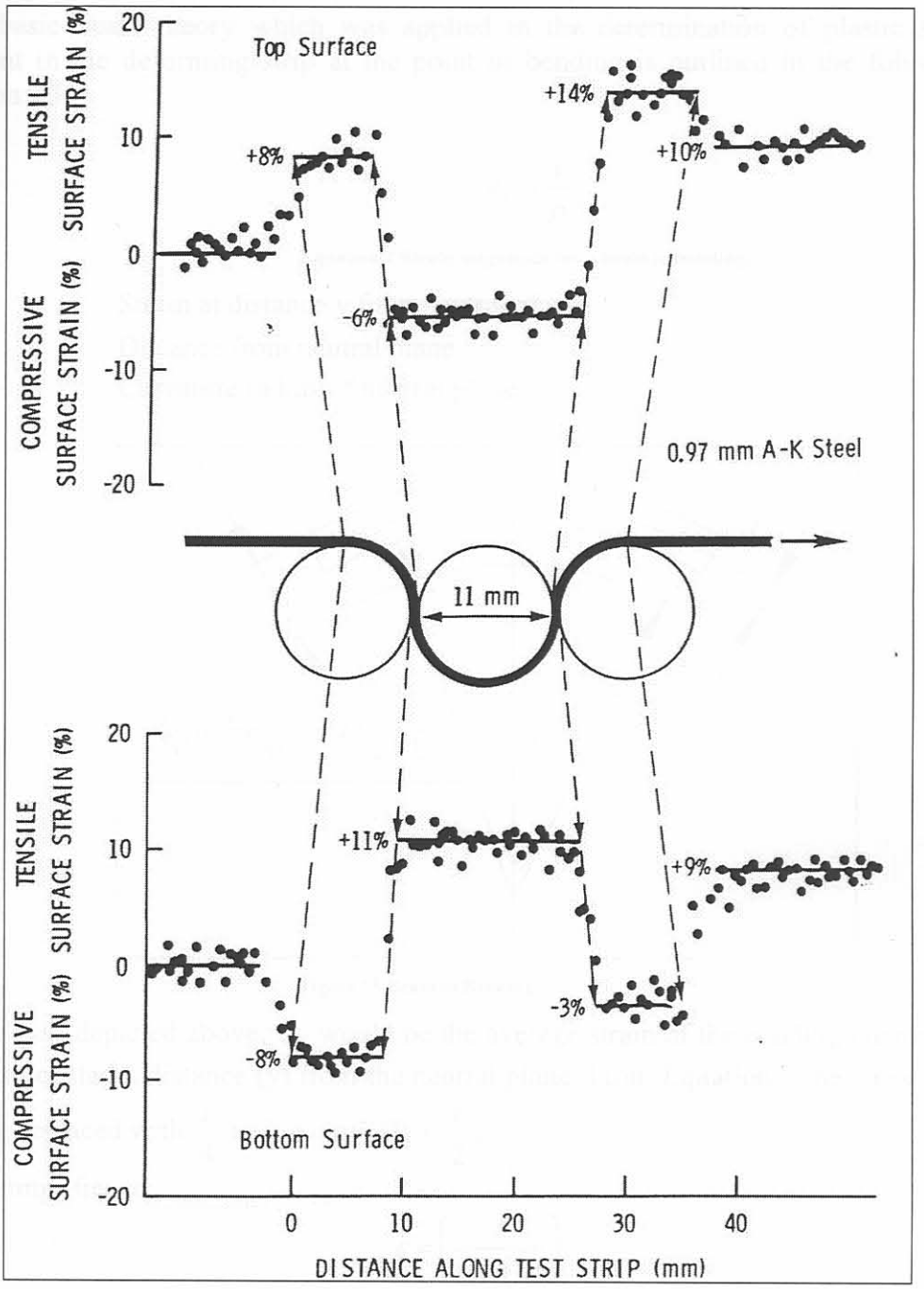

Figure 14 Surface strain relative to position, H.D. Nine.

A further explanation of Nine's research would be as follows [24]. The bending element, upon leaving the roller it had just passed over to conform to the next roller in line, would undergo strain deformation for a distance of approximately three times its thickness. With this fact in mind, knowing the velocity at which the strip is moving, and the magnitude of the average strain the strip is experiencing during bending based on beam theory for bending over a roller of specified radius, the strain rate at the point of plastic strain can be calculated. In turn, the dynamic yield stress can be determined.

The basic beam theory which was applied in the determination of plastic strain present in the deforming strip at the point of bending is outlined in the following section: [30]

$$\varepsilon_x = \frac{y}{\rho}$$

Equation 2 Strain magnitude for a beam in bending,

ε_x = Strain at distance y from neutral plane.

y = Distance from neutral plane.

ρ = Curvature radius of neutral plane.

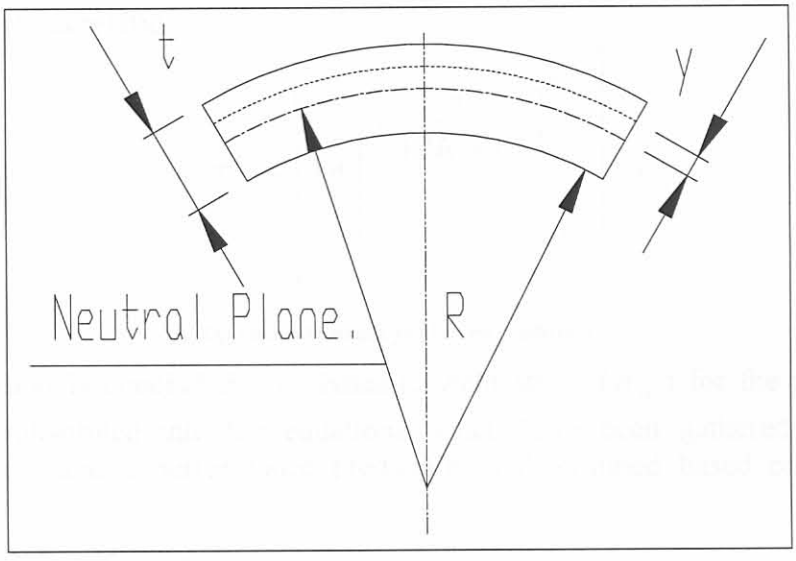

Figure 15 Beam in Bending.

In the case depicted above, ε_x would be the average strain of the bending element, at a point located a distance (y) from the neutral plane. From Equation 2 the value for y can be replaced with $\frac{t}{4}$ and ρ with $(R + \frac{t}{2})$.

This simplifies to

$$\varepsilon = \left(\frac{t}{4R + 2t} \right)$$

Equation 3 Strain as a function of radius and thickness.

Considering Figure 14 of H.D. Nine, the assumption that the plastic strain takes place within 3 times the thickness (t) of the strip, moving at a velocity (v), leads to the following:

$$\text{Duration of strain} = \frac{3 \times t}{v} \qquad \text{(in seconds)}$$

Equation 4 Time duration of strain.

This is true for infinitesimally small time segments, which would reveal constant velocity during the considered interval.

A combination of equations 3 and 4, results in the following:
If

$$\varepsilon' = \left(\frac{t}{4R+2t}\right) \div \frac{3\times t}{v}$$

then becomes,

$$\varepsilon' = \left(\frac{v}{12R+6t}\right)$$

Equation 5 Bending Strain Rate equation.

Since the strain rate (ε') is now quantified for any bending radius magnitude and velocity, Equation 5 can now be combined with Equation 1. This would deliver the dynamic yield stress relation.

$$\sigma_{yd} = \left[1+\left(\frac{\left(\frac{v}{12R+6t}\right)}{D}\right)^{\frac{1}{p}}\right]\times\sigma_{yo}$$

Equation 6 Dynamic yield stress prediction.

Once this relation is concluded, the dynamic yield stress (σ_{yd}) for the prescribed condition, is substituted into the equations which have been gathered from the literature survey, and a performance prediction is determined based on the new material property.

4.3.2 Force Prediction Model 1 [3]

The analytical model presented in this section, has been developed by Rosslee [3]. The model is based on bending moment theory. Consider a metal strip being bent over a roller radius (R) under a pure bending moment (M). The strip has thickness (t) and width (w) and plane strain deformation conditions prevail. If the roller radius is very large, only elastic deformation occurs. As the radius decreases the deformation becomes elastic-plastic and finally almost purely plastic. When nearly the whole section is plastically deformed, the effects of elasticity can be neglected and rigid-perfect-plasticity can be assumed. When the radius becomes too small, tensile and compressive failure of the material at the surfaces of the strip will start to occur.

When a strip is being pulled over a single roller, the strip would be subjected to a bending and tensile force simultaneously. In this formulation it was assumed that:

- The strip shows rigid perfectly plastic behaviour.
- The transverse planes would remain plane during and after deformation, distributing axial strain linearly through the strip cross-section.
- The yield stress is equal in both directions of deformation, tension and compression.
- Plane strain under frictionless roller conditions exist.

Referring to Figure 16, the strip bends to conform to the first roller radius at point 1, and then straightens to leave the curve again at point 2. These points are assumed to be two plastic hinges. These hinges transform energy and dissipate it through heat created by plastic deformation work.

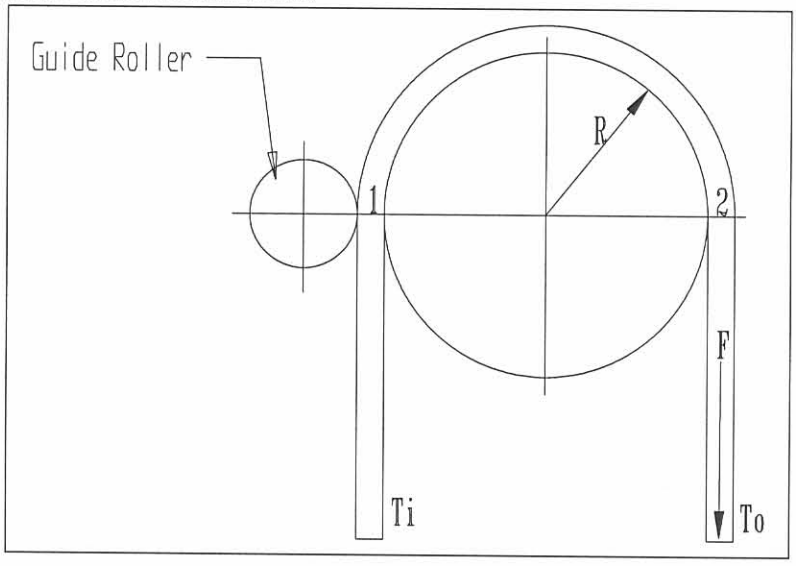

Figure 16 Element conforming to roller radius.

The two hinges are considered similar, only acting in opposite directions. By following basic principles, Rosslee concluded that: [3].

$$F = 2\sigma_y w\left[(2R+t)-\sqrt{(2R+t)^2-t^2}\right]$$

Equation 7 Rosslee bending model.

This expression can now be used as an approximation of the force required to pull a strip of metal over a single roller, given the initial assumptions. From the above formulation notice can be taken that the arc of contact between the roller and the strip

is not represented. The number of times the strip bends and unbends determines the magnitude of the applied force, and not the arc of contact.
Equation 7 can then be expanded with the addition of Equation 6 to produce the first of the dynamic cyclic bending approximation models.

$$F = 2\left(\left[1+\left(\frac{\left(\frac{v}{12R+6t}\right)}{D}\right)^{\frac{1}{p}}\right]\times\sigma_{yo}\right)w\left[(2R+t)-\sqrt{(2R+t)^2-t^2}\right]$$

Equation 8 Force Prediction Model 1.

This is one equation that has been used to deliver predictions of cyclic plastic bending performance when automated into mathematical code, as detailed in section 5.

4.3.3 Force Prediction Model 2 [3]

Rosslee also used deformation energy techniques to model a solution for cyclic plastic bending [3]. Consider a wide strip of metal being pulled over a frictionless roller, as shown in Figure 16. The strip of original width (w) and thickness (t), undergoes plastic bending and elongation as it passes over the roller of radius (R).

It is assumed that the strip bends suddenly as it reaches position 1 in Figure 16, to conform to the roller contour. This curvature is maintained for the duration of contact with no additional deformation occurring, until the strip again straightens suddenly, at position 2. The experiment conducted by H.D. Nine shows this assumption to be fairly accurate (refer: Figure 14) It is further assumed that the ratio of roller radius to strip thickness (R/t) is such that complete plasticity exists at the bending points 1 and 2. Rigid plastic behaviour with infinite plasticity and no strain hardening is assumed. It has also been proven experimentally [24], that if (w) is much greater than (t), then no deformation takes place in the width of the strip. Therefore, plane strain can be assumed. It is further assumed that all the energy absorbed is dissipated in plastic deformation. The energy is absorbed in cyclic plastic straining, as well as elongation and thinning of the strip. The bending positions 1 and 2 are also assumed to be exactly the same thus the combined energy absorbed would merely be twice the amount at point 1.

Keeping all these factors in mind the following has been determined:

Deformation work at a point (W), is calculated by:

$$W = Volume \cdot \int \bar{\sigma} \cdot d\bar{\varepsilon}$$

Equation 9 Strain work integral at one hinge.

then the following equation was deduced from basic principles [3],

$$F = \frac{2 \cdot w \cdot t \cdot \sigma_y \cdot \left[\ln\left(\frac{R+t}{R+\frac{t}{2}} \right) - \ln\left(\frac{R+t}{R+\frac{t}{2}} \right) \right]}{2 \cdot \sqrt{3} - \left[\ln\left(\frac{R+t}{R+\frac{t}{2}} \right) + \ln\left(\frac{R+t}{R+\frac{t}{2}} \right) \right]}$$

Equation 10 Rosslee's deformation energy formulation [3].

The formulation of Equation 10, can be appended to the strain rate dependant dynamic yield stress predictor, Equation 6, which reveals,

$$F = \frac{2 \cdot w \cdot t \cdot \left[\left[1 + \left(\frac{\left(\frac{v}{12R + 6t} \right)}{D} \right)^{\frac{1}{p}} \right] \times \sigma_{yo} \right] \cdot \left[\ln\left(\frac{R+t}{R+\frac{t}{2}} \right) - \ln\left(\frac{R+t}{R+\frac{t}{2}} \right) \right]}{2 \cdot \sqrt{3} - \left[\ln\left(\frac{R+t}{R+\frac{t}{2}} \right) + \ln\left(\frac{R+t}{R+\frac{t}{2}} \right) \right]}$$

Equation 11 Force Prediction Model 2.

This force prediction model has also been automated into mathematical code to deliver an indication of performance (refer: section 5.).

4.3.4 Force Prediction Model 3 [4]

Another analytical model has been developed by W. Johnson and A.G. Mamalis, based upon plastic work principles [4]. The formulation predicts that for a wide rectangular strip of width (w) and thickness (t), being bent across the arc of a roller with radius (R), the difference in tension between the taut and slack sides, applied to the ends of the strip to ensure conformation to the roller curvature (refer: Figure 16) would be equal to :

$$(T_o - T_i) \times (R + \frac{t}{2}) = 2M_p$$

Equation 12 Plastic work equation [4].

Where:

T_0 = Tension on the taut side of the bending element. (N)
T_i = Tension on the slack side of the bending element. (N)
M_p = Plastic bending moment. (N.m)

The reason for the double representation of the plastic moment in Equation 12 is that firstly, the bending element is plastically deformed to conform to the arc of the roller it is being bent over and then secondly, is bent away from the surface to straighten again.

The assumptions made are the following:

- The ratio of t/R is assumed to be much smaller than 1.
- Perfect plasticity exists.
- There is no friction of the rolling roller element.

Ignoring the Baushinger effect as previously discussed in section 4.2.1, the bending moment can be considered of the same magnitude in both directions of application. This bending moment magnitude is represented by:

$$M_p = \frac{w \times t^2 \times \sigma_y}{4}$$

Equation 13 Plastic bending equation.

Where:

σ_y = mean yield stress. (Mpa)

After substituting Equation 13 into Equation 12, the following result is obtained.

$$(T_0 - T_i) = \frac{w \times t^2 \times \sigma_y}{2 \times R + t}$$

Equation 14 Combined plastic bending equation [4].

The static force prediction depicted in Equation 14 was expanded with Equation 6 to deliver the deformation rate dependence element of the formulation.

The above substitution process results in the following:

$$F = \frac{w \times t^2 \times \left[1 + \left(\frac{\left(\frac{v}{12R + 6t}\right)}{D}\right)^{\frac{1}{p}}\right] \times \sigma_{yo}}{2 \times R + t}$$

Equation 15 Force prediction model 3.

The above force prediction model, has also been automated in mathematical code and used to generate force resistance estimations of a steel element or strip being drawn over a roller of given dimensions, as is discussed in greater detail in section 5.

4.3.5 Force Prediction Model 4 [23]

The final model predicting the resistance force generated by a metallic strip being drawn between inline rollers (refer: Figure 16) was developed by J.M. Alexander, and then published by W. Johnson and S.R. Reid [23], [4].

The model assumes a plane strain condition, implying that the width of the strip is much larger than the thickness. Further assumptions are that the roller radius is much larger than the thickness of the strip and lastly, that the elastic effects are neglected. With these conditions established, the observation was made by Alexander that the device being tested, provides a nearly constant resistive force and that this force increases with unit width. The relation of the forces applied to the strips ends, referring to Figure 16, is then:

$$\Delta T = \frac{T_o - T_i}{w}$$

Equation 16 Alexander's basic formulation [23].

where :

$$\Delta T = \frac{4 \times \sigma_y}{\sqrt{3}} \times (t - 2k)$$

Equation 17 Tension difference equivalent.

with :

$$k = R\left[\sqrt{1 + {}^{t}/_{R}} - 1\right]$$

Equation 18 Roller radius and strip thickness ratio.

Combining all the above components delivers the following:

$$T_o - T_i = \frac{4 \times \sigma_y \times w}{\sqrt{3}} \times \left(t - 2 \times R\sqrt{1 + \frac{t}{R}} + 2R \right)$$

Equation 19 Static force prediction equation.

Equation 6 combined with Equation 19, accommodates for the dynamic aspect of the required prediction formula. The units of the value predicted in Equation 20 are, force per unit width.

$$T_o - T_i = \frac{4 \times \left(\left[1 + \left(\frac{\left(\frac{v}{12R + 6t} \right)}{D} \right)^{\frac{1}{p}} \right] \times \sigma_{yo} \right) \times w}{\sqrt{3}} \times \left(t - 2 \times R\sqrt{1 + \frac{t}{R}} + 2R \right)$$

Equation 20 Force prediction model 4.

4.4 Conclusion

In this chapter, the four prediction models used to mathematically predict the dynamic performance of the bending element's resistive force have been developed. The determining factor of the generated force magnitude is the number of bend deformations the strip would encounter during its travel between the rollers. The angle of contact with the roller surface is inconsequential to the resistance force produced since energy is absorbed, and thus resistance is produced, only when bending of the element takes place, upon arrival on the roller surface or departing from it, and not during contact. These models have been based upon previous existing quasi-static models. In the following chapter these models have been automated into mathematical code and allowed to evaluate similar scenarios to those physically tested, in an attempt to produce comparable data.

5. Mathematical Code Evaluation Design Program

5.1 Introduction

A common characteristic, which can be identified in most approximation programs, is the need for a realistically estimated input of the workable solution by the user. The hindrance is usually that the user has no idea of what the expected solution's parameters are going to be, thus has no starting point from which the simulation program can work. For this reason the author decided to use two versions of a prediction program. The first version is spreadsheet based, and has all the permissible ratios of geometry inserted in envelope form ($limit<X<limit$), for the user to simply check whether the chosen values are of correct proportion. This version produces an appropriate force, based on a simplistic calculation, ignoring the change in speed of the mass during the retardation process. The second version of the simulation program, which is MATLAB code based, is then fed the result of the first version, which would be a reasonable estimation of the final outcomes proportion. The second version of the program then delivers an accurate approximation, based on realistic scenario estimations, allowing for the change in speed during the deceleration process.

There are two basic differences between the two versions of the prediction programs. The first difference is the taking into account of the effect which the changing in speed of the mass or conveyance during the retardation process has on the system. In the first spreadsheet version the assumption is made that the deformation rate remains constant throughout the process of deceleration, which is clearly incorrect. This assumption however produces a valuable estimation of the scale of parameters to be expected. The second version of the program, which is automated code executing in MATLAB version 5.3 for students, takes into account the effect of diminishing speed during the retardation process. This diminishing speed greatly affects the performance of the retardation process, causing a transition from dynamic to quasi-static performance. The gradual decrease in arresting force with the decrease in speed is witnessed in the practical experiments, the FEA as well as the analytical program's prediction. This will be mentioned again in chapter 7, where the comparisons between all three methods, namely experiments, FEA and computer generated analytical prediction, are compared.

The second difference is the program's ability to account for the effect of the taper section of the strip, mentioned in section 1.2 (refer: Figure 1). The spreadsheet version of the program cannot account for this and thus assumes a parallel section. The resulting answer, based upon this assumption, is used as the maximum width for the taper in the MATLAB version of the program. The thin section of the strip is determined by calculating the factor of safety upon yielding when subjected to the maximum deceleration force and ensuring that this safety factor is no less than six, which is the acceptable amount based on the Occupational Health and Safety Act and Regulations [21]. The Act is applicable to ropes and cables. In this application the strip could be classified as a structural element, which then requires a design factor of a magnitude consistent with "good engineering practice", which would not need to be as large as the factor required for the ropes and cables. The higher factor specification is still maintained and applied, for total peace of mind.

Through the experimental phase of the project it has been found that the length of this taper section, generally required to fulfil the task of deceleration is between 5 and 10 times the difference in taper width. This implies that a taper of 10mm to 40mm would generally be applied between 150mm and 300mm, as illustrated in Figure 17, depending on the deceleration space available and whether or not the deceleration limit is of application concern. The deceleration magnitude is influenced by the profile of the strip, and can thus be adapted according to specific requirements.

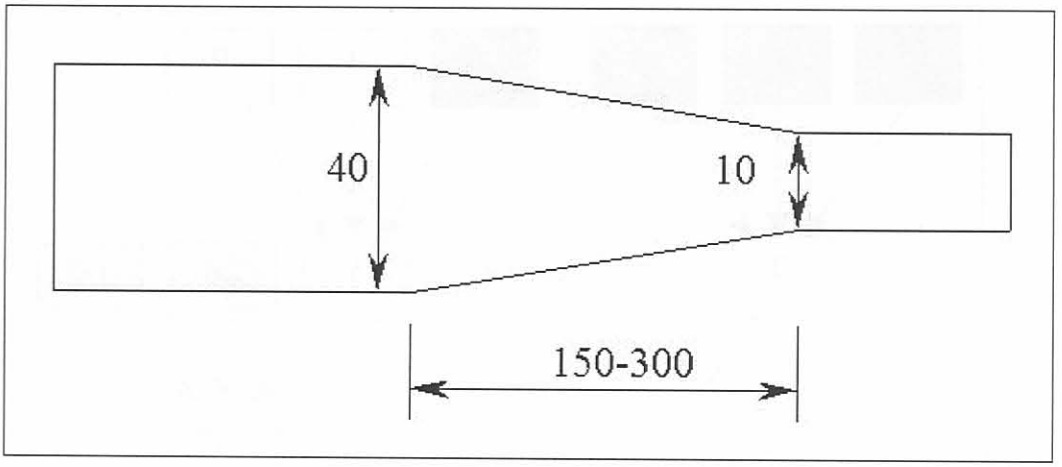

Figure 17 Schematic profile of a typical deceleration strip.

5.1.1 First version of prediction program

The flow diagram Figure 18 illustrates the method of execution of the spreadsheet version prediction program. This illustrated process is converted into the examples shown in Table 3 and Table 4. The selection choices and implications thereof are discussed in the following text, with reference to the shown example.

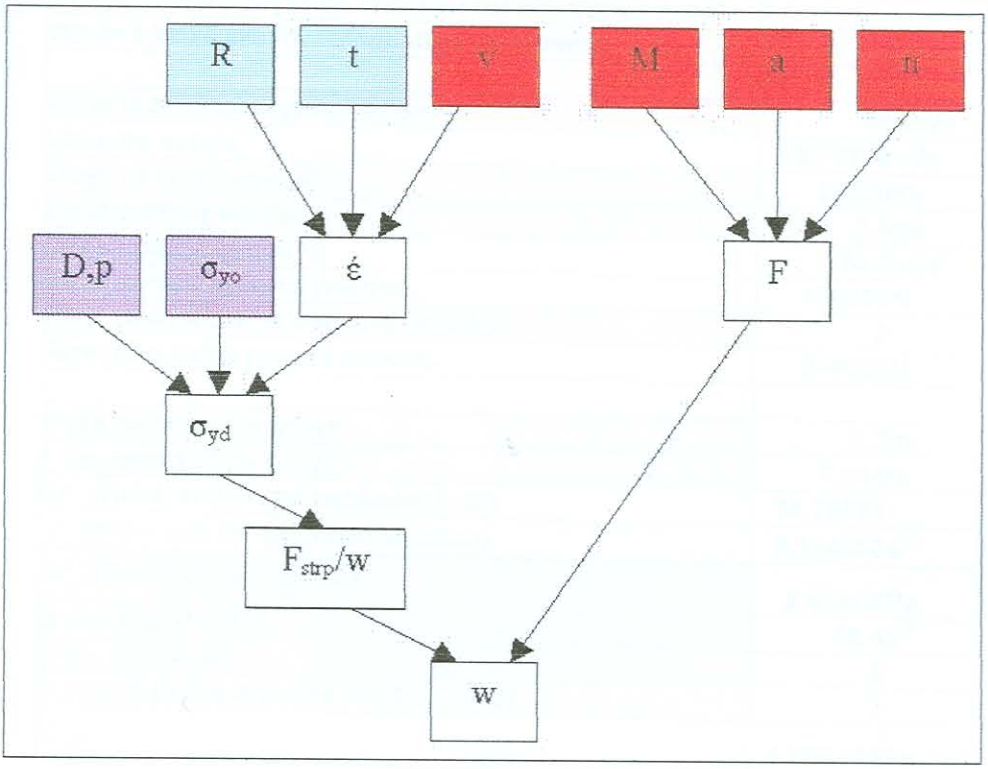

Figure 18 Flow chart of spread sheet program.

Design Process.	
Red blocks are the design variables for the user to specify, based on expected scenario!!	
Blue blocks are the arrester design variables for the user to specify!	
Purple blocks are the material variables!	
Yellow blocks are to be checked for envelopes spec!	
White blocks are for information purposes!	
What is the conveyance speed?	46km/h
Velocity in m/s	12.77778m/s
Mass of conveyance?	20000kg
Deceleration wanted!	2.5gs
Deceleration in m/s^2	24.5m/s^2
Total arresting force needed.	490000N
How many arrester sets are needed?	2
Arresting force per set needed.	245000N
R (as selected by user)	0.2m
t (as selected by user)	0.014m
R/t (Ratio should be between15-25)	14.28571
ε' (strain rate for described situation)	5.144033s^{-1}
σ_{yd} (Dynamic yield stress)	2.8E+08Pa
D (for mild steel)	40.4s^{-1}
p (for mild steel)	5
n rollers in the arrester set (Usually 3)	3
σ_{yd}	4.65E+08Pa

Table 3 User input variables for spread sheet prediction program.

Table 3 illustrates the actual view of the spread sheet, set up to guide the user to a reasonable base decision. The user describing the problem scenario to which the deceleration systems are to be applied, fills in the red blocks. Following that, the two blue blocks referring to the radius of the roller and the thickness of the strip are chosen. This is done in such a way that the R/t ratio is within the ranges specified. This ratio controls the geometric aspect in terms of having a thick strip bending around a small radius and thus creating the opportunity for extremely high strain rates or surface tearing due to excessive surface straining (refer: section 4.2). The information block indicating strain rate (ε') is for the current application at the points of bending, and is the solution of Equation 5. The purple blocks allow for the material characteristics of the material chosen for the strip. The variables (D) and (p) are the specific strain rate sensitive qualities of 300W mild steel. These variables allow for the evaluation of Equation 6, which is the magnitude of the dynamic yield stress (σ_{yd}) of the material.

Fstrpdyn/w (Model 4, Alexander)	763501.7	N/m	
w	0.32089	m	(Arresting force needed/Fstrpdyn/m)
w/t (Should be 15-25)	22.92071		
Fstrpdyn/w (Model 1, Rosslee Bending)	661211.9	N/m	
w	0.370532	m	(Arresting force needed/Fstrpdyn/m)
w/t (Check for ratio 15-25)	26.46655		
Fstrpdyn/w (Model 2, Rosslee Energy)	763322.4	N/m	
w	0.320965	m	(Arresting force needed/Fstrpdyn/m)
w/t (Should be 15-25)	22.92609		
Fstrpdyn/w (Model 3, Mamalis and Johnson)	661022.8	N/m	
w	0.370638	m	(Arresting force needed/Fstrpdyn/m)
w/t (Should be 15-25)	26.47413		

Table 4 Second part of spreadsheet program.

Table 4 summarises the force prediction results produced by the deceleration systems specified by the user in this example. The four models which have been adapted and selected for dynamic prediction, as described in section 4.3.2, have been utilised. The dynamic force per strip width indicator, (Fstrpdyn/w) describes the force per unit width (N/m). This is a convenient result, since when planning to retard a moving mass (M) at a specific rate (g), the magnitude of required force is then F = Mg. This is the combined deceleration force required, and is divided between the number of arrestor sets, of which there are two in this case. If the required deceleration force is divided by the force per unit width capability of the strip, the remaining value is the width of strip required to retard the mass at the desired deceleration rate. This describes the method followed to arrive at the strip width (w). The width over thickness ratio (w/t) is again a geometrical constraint check, prohibiting the development of a situation where the strip is paper thin and many meters wide or vice versa, narrow and extremely thick. The limits set are guide lines to be considered by the user. To change the ratio, the thickness of the strip must be altered, influencing the R/t ratio, which should also be evaluated again for position in the prescribed envelope.

The following figures depict the relationship between three fundamental variables of the deceleration systems, namely the roller radius (R), the strip thickness (t), and the resulting predicted retarding force the system would deliver, relative to the width of the strip (w).

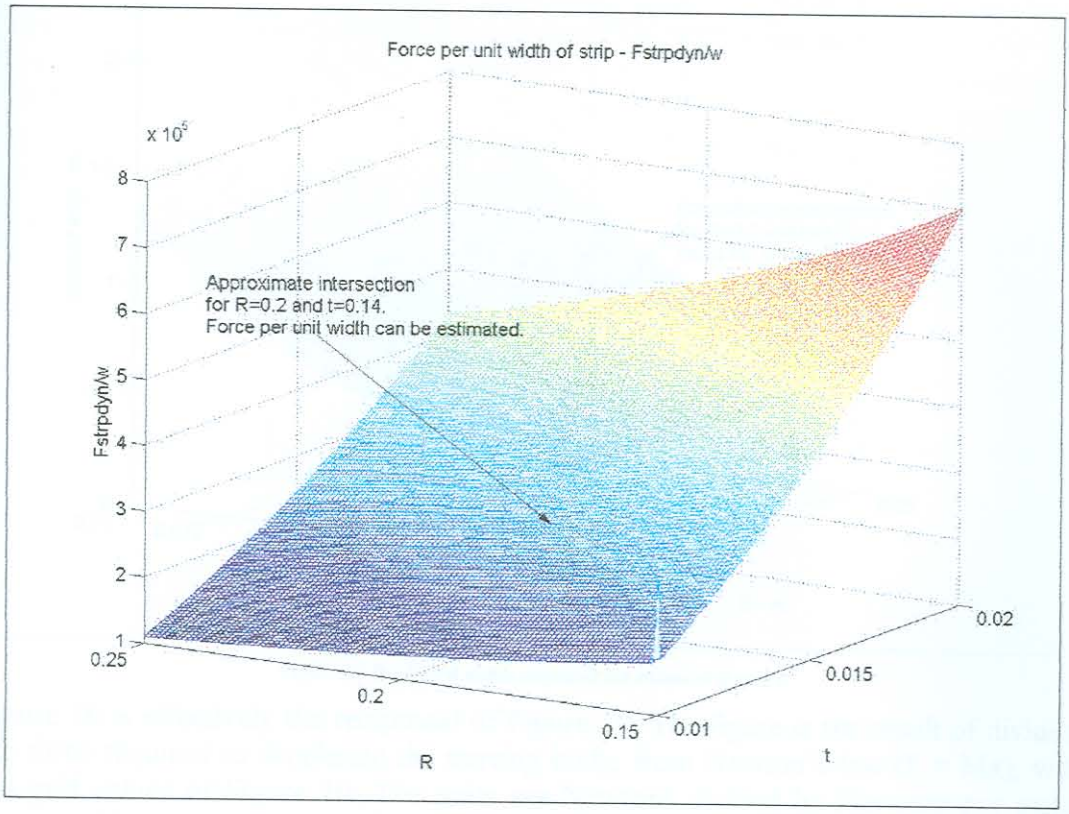

Figure 19 Predicted force per unit width for ratios of R and t.

With reference to Figure 19, the predicted performance of the strip and roller deceleration systems follows a logical trend. The vertical axis recording $F_{strpdyn}/w$, which is the retarding force per unit width of the strip, increases to the corner where the roller radius decreases and the strip thickness increases. This is a logical trend since a sharper angle, or smaller roller radius, will increase the force required to draw the strip over the roller. The effect of a thicker section of material having a larger resistance to bending than a thin section also follows logic. This would lead to the conclusion that the position of the peak for the expected maximum force per unit width is correct.

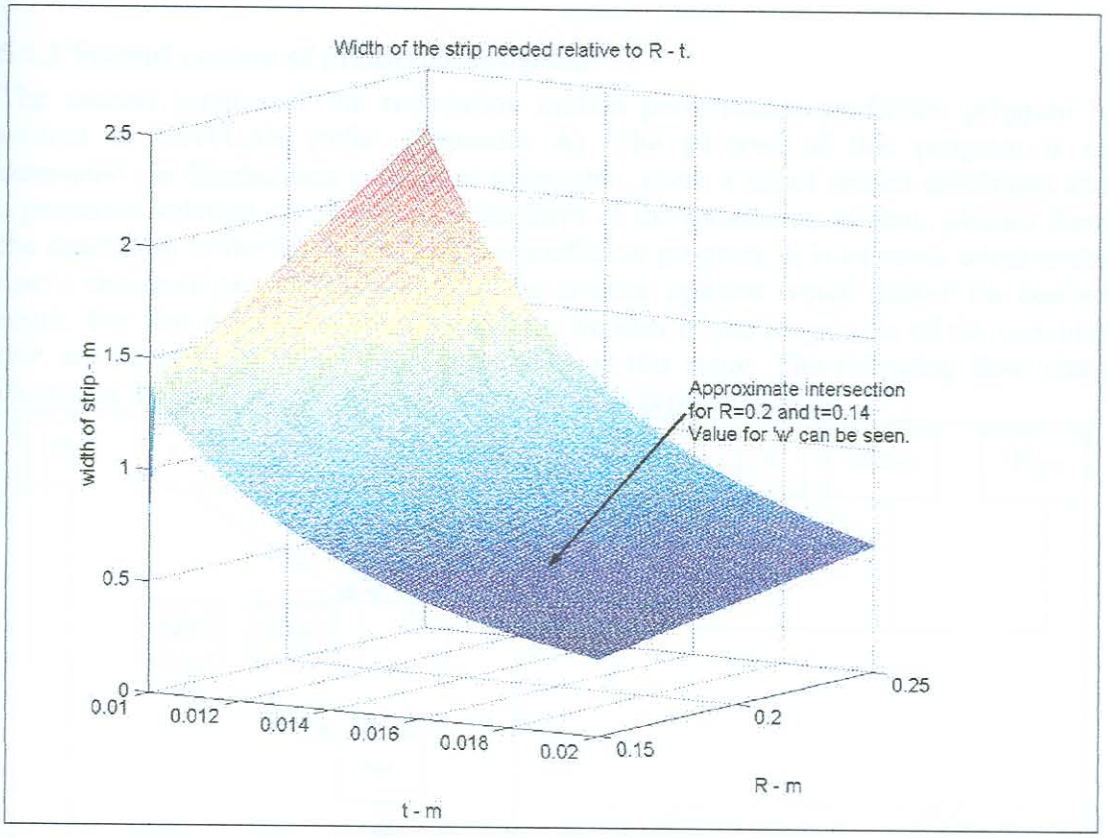

Figure 20 Predicted width required for ratios of R and t.

Figure 20 is effectively the reciprocal of Figure 19. The figure is the result of dividing the force required to decelerate the moving body, from Newton's law (F = Ma), with the grid values of Figure 19. The units are Newtons divided by Newtons per meter thus resulting in meters, which is the width of the strip required to decelerate the moving mass (M) moving at a velocity (v), at a specific deceleration rate (g). The strip width (w) is displayed on the vertical axis, relative to the roller radius (R) and strip thickness (t) on the horizontal axes. Similar to Figure 19, the displayed graphical result of Figure 20 is a logical conclusion. The width of strip needed to decelerate the mass reaches a maximum where the thickness of the strip (t) is the least, and the roller radius (R) is the largest. In this position the thin strip has a large bending radius and would have the minimum resulting resistive force, thus requiring a wide section to accommodate the required deceleration.

5.1.2 Second version of prediction program

The second version of the retardation system performance prediction program is written in MATLAB (refer: Appendix A). The purpose of this program is to determine the deceleration conditions achievable, given a set of system conditions and a proposed solution specification in the form of the retardation system, gleaned from the estimation of the first version of the prediction program. It is to verify whether the user's choice of geometrical values of the arrestor systems would deliver the desired result. For this reason the user should have an idea of the magnitude of the variables that are expected to fulfil the requirements at this stage. The following flow chart illustrates the route of execution of the MATLAB program's code.

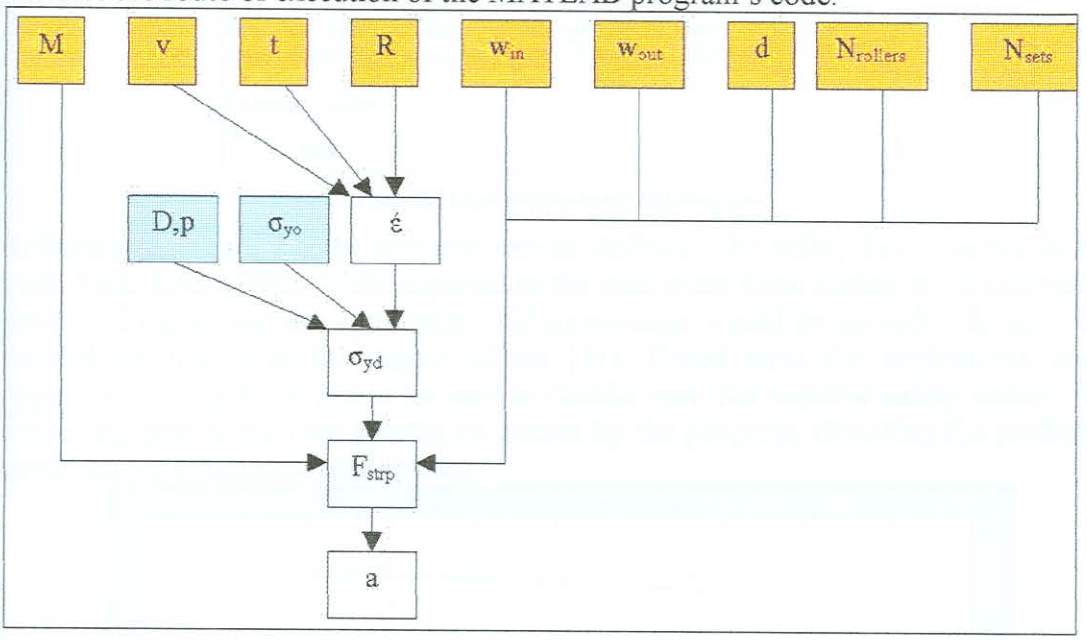

Figure 21 Flow chart of the Matlab program.

When comparing the two flow diagrams Figure 18 and Figure 21, the difference between the first and second versions of the prediction program is evident. Referring to Figure 18, the outcome of the first version can be seen to be a geometrical output, namely the width of the strip and in Figure 21 the result can be seen to be a performance parameter, namely acceleration. In the second version prediction program certain geometrical variables are entered by the user: the strip thickness (t) roller radius (R), the widths of the taper and the distance over which it occurs, as well as the number of rollers in the arrestor set ($N_{rollers}$) and the number of arrestor sets themselves (N_{sets}). The final outcome is then the resulting deceleration of the mass or conveyance, and all the other parameters can also be determined such as distance travelled during the retardation process and the velocity profile. These results can be scrutinised to see whether the chosen set-up conforms to the desired deceleration requirements. The entire process is discussed in the following section.

The effect of guide rail friction in the system is also accommodated in the MATLAB code. During experimentation it has been noted that a maximum of 0.8Gs is reached during free-fall and is thus defined as such in the MATLAB program (refer: section 8.1.1).

5.1.2.1 Second version prediction program output

An example of the MATLAB program is shown in Figure 22. The same values used in the first version of the prediction program will be used here for comparison purposes in order to demonstrate how the two programs are to be used as a combination.

```
» case2
What is the mass of the conveyance? kg - 20000
How many roller sets are needed? - 2
How many rollers in each set ?  - 3
Speed of conveyance, at impact? km/h - 46
Enter the choice of roller radius. m - 0.2
Enter the choice of strip thickness. m - 0.014
What is the thinnest width of the taper? m  - 0.22
What is the thickest width of the taper? m  -  0.37
Over what distance does the taper occur? m  -  1.5

Safety_Factor =

    4.8422
```

Figure 22 Input text for MATLAB program.

Referring to Figure 22, the scenario can be defined. The safety factor output is the yield limit safety factor while exposed to the maximum force during the deceleration process. In this case the application and importance would be considered, since the desired amount is in the region of six [21]. Based upon the application, good engineering judgement would be used to decide upon the required safety factor. The following graphs are then printed on screen by the program, depicting the predicted performance of the proposed system.

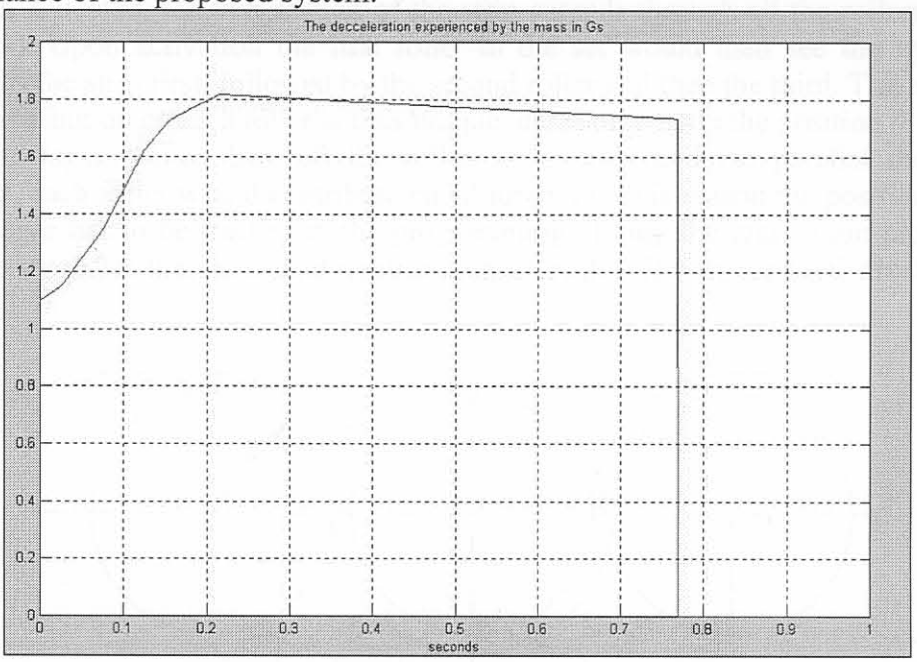

Figure 23 Predicted deceleration of the mass/conveyance.

In Figure 23 the diminishing deceleration effect can clearly be seen. This effect is due to the strain rate decreasing during the slower deformation of the material as the mass is retarded. From this the influence of strain rate on the system's performance can be identified. This phenomenon will be compared again to the experimental results in chapter 8. The predicted deceleration level is less than that predicted by the spread sheet version of the program (refer: Table 3). The discrepancy is due to the slowing of

the mass or conveyance during the transition on the taper section of the strip. By the time the main section is reached, considerable speed has been lost (refer: Figure 27).

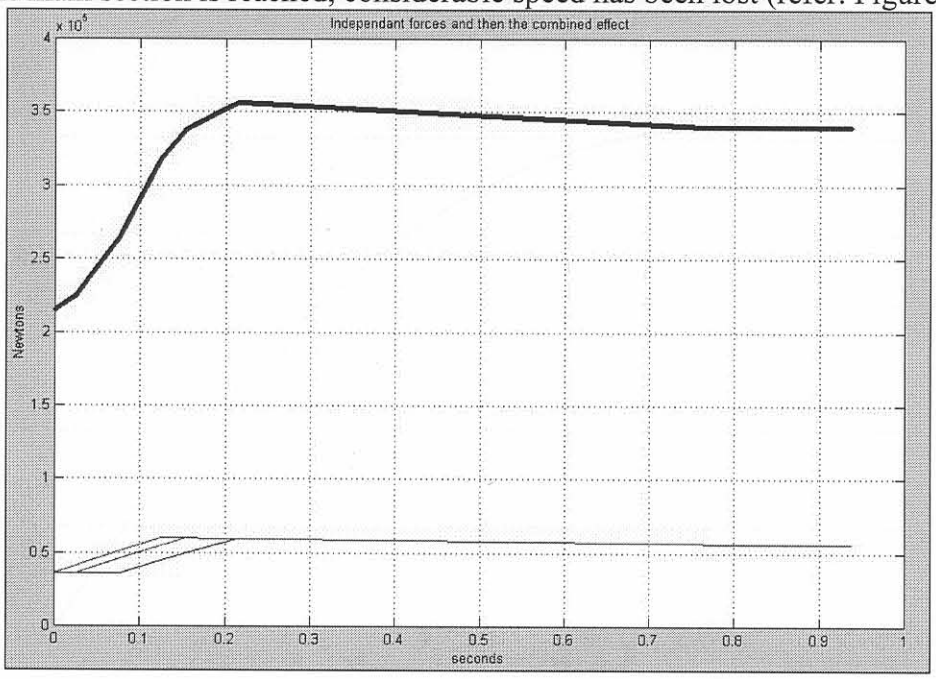

Figure 24 Predicted force delivery from rollers.

Figure 24 shows the force components applied to the mass or conveyance by the individual rollers and then the roller set as a unit. Initially, before the arresting device has been activated, the thin section of the strip extends through all the rollers (refer: Figure 1). Upon activation the first roller in the set would then see the widening section of the strip first, followed by the second roller and then the third. The resistive force contribution of each roller is thus unique, depending upon the position in the set. Once the taper section has left the roller set entirely and the parallel section is threaded, each roller would contribute equal force. For this reason the position of the strip's taper has to be tracked in the programming, during the retardation process to accurately predict the individual contribution of each roller to the total deceleration force.

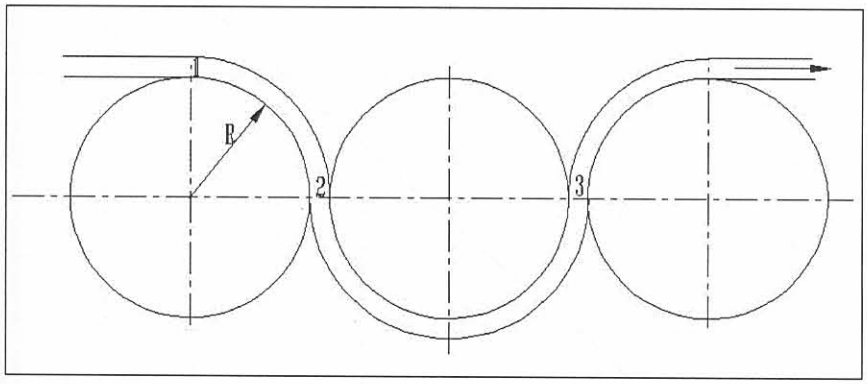

Figure 25 Bending positions of strip element.

In Figure 25 the bending positions of the strip can be seen. Position 1 and 2 can be seen to be only 90° apart, and then position 2 and 3 are separated by 180°. The individual roller force contribution shown in Figure 24 confirm this, since the interval between the increase in force of roller 1 and roller 2, is half the duration of the interval between roller 2 and roller 3. The bold blue line shows the sum total of the

resistive force created by the arrestor set. The initial input can be seen to be gradual which is favourable when decelerating living cargo, for any application.

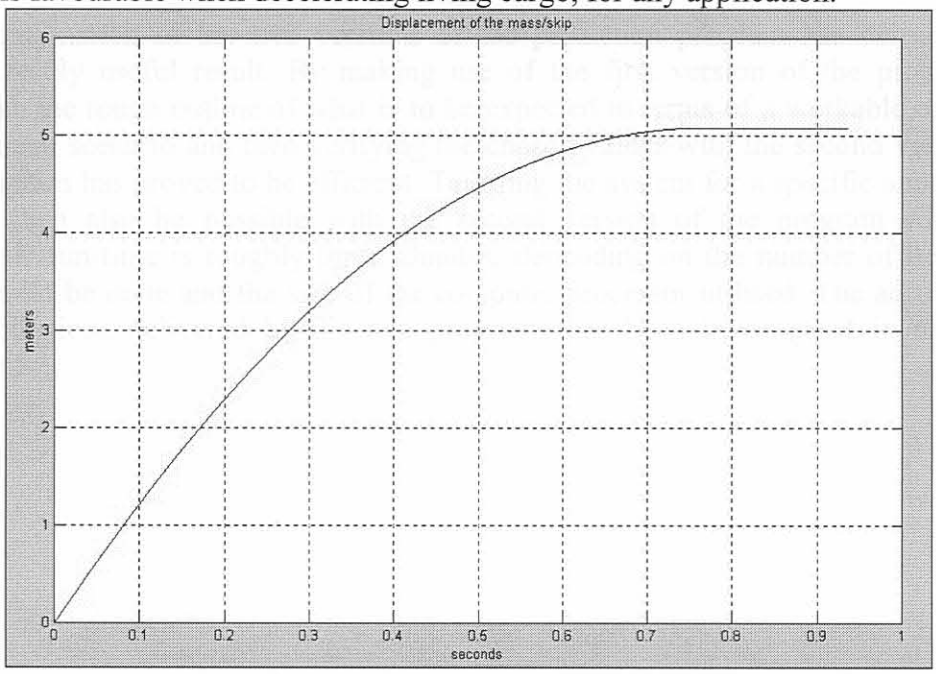

Figure 26 Predicted displacement of mass or conveyance.

In Figure 26 the projected distance travelled by the mass or conveyance during the deceleration can be seen. From Figure 24, the taper takes approximately 0.15 seconds to travel through all three rollers and the corresponding displacement is 1.5 meters which is the specified taper length (refer: Figure 22).

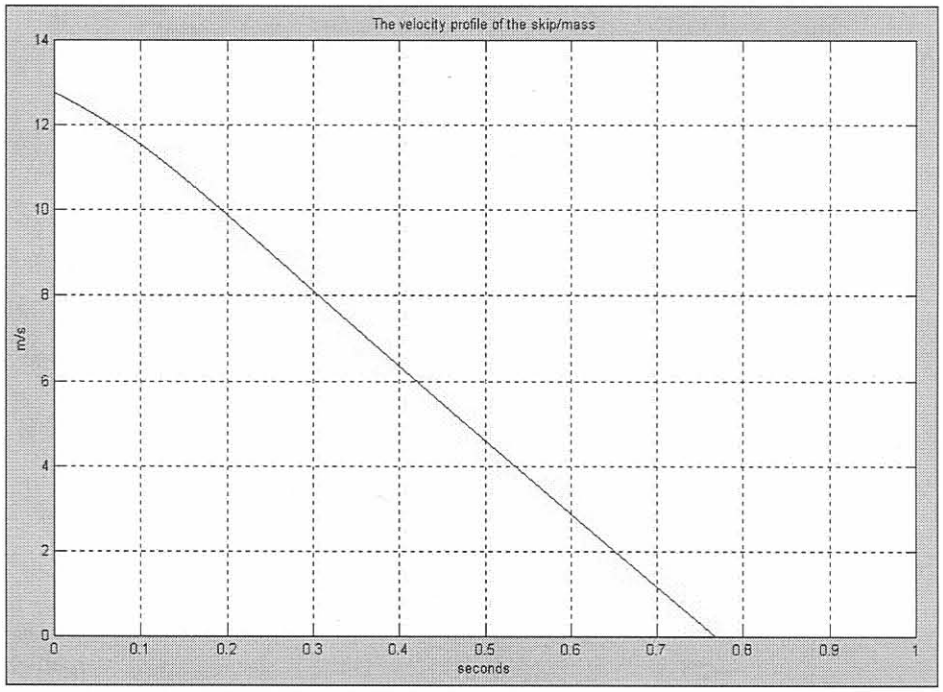

Figure 27 Predicted velocity profile of mass/conveyance.

Figure 27 projects the velocity profile of the mass or conveyance during the retardation process. The taper section takes roughly 0.15 seconds to move past all three rollers, by which time 2m/s or 15% of the initial velocity has already been decelerated.

5.2 Conclusion

The combination of the two versions of the prediction program has delivered an operationally useful result. By making use of the first version of the program to establish the rough outline of what is to be expected in terms of a workable outcome for a given scenario and then verifying the chosen values with the second version of the program has proved to be efficient. Tailoring the system for a specific application would then also be possible with the second version of the program since the computer run-time is roughly three minutes, depending on the number of iterations that would be done and the size of the computer processor utilised. The accuracy of the predictions delivered by the two programs has been investigated in detail in chapter 8.

6. Experimental Procedure

6.1 Introduction

The experimental verification was carried out on a scale model of a mineshaft and conveyance which has been constructed for past research at the University of Pretoria. This tenth scale model had been used to simulate dynamic, scaled down conditions, similar to real-life applications. For the purposes of this study, the existing model was adapted to accommodate the dynamic bending deceleration systems (refer: Figure 5, Figure 30). A piezoelectric accelerometer was attached to the model cage, and acceleration readings were captured during the experiment (refer: Figure 28). The data was recorded by means of a laptop and 'spider' (refer: Figure 29). The 'spider' is a data buffer, implying that it stores data and then transfers it to the laptop. Since the computer is unable to sample at a high enough frequency, the spider takes the initial readings and stores it for later retrieval. The sampling frequency is 3200Hz. The recorded data was then compared to the performance estimation of the design program, as well as the FEA at similar conditions (refer: section 5 and 7).

Figure 28 Accelerometer mounted on model cage.

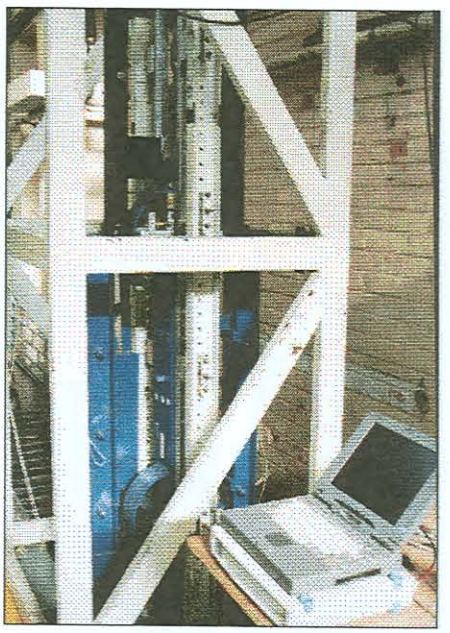

Figure 29 View of model and data capturing equipment.

The experimental procedure used to evaluate the performance of the arresting systems is as follows. The cage was hoisted to a set height above the installed arrestors, determined by the velocity that was to be achieved in the experiment, and released to fall freely. The cage velocity was measured by placing trip switches, a set distance apart, in the cage path. The time taken to trigger the switches was recorded and thus the velocity was calculated.

It was noted that a certain amount of friction occurs in the model's rails, since free-fall on achieved an acceleration of $8m/s^2$. This is understandable and would be encountered in full-scale situations as well. This has been compensated for in the programming of the design program, and can be easily adjusted to suit various conditions, as explained in section 5.1.2.

The model cage was then decelerated by the deformation process of the strips bending and unbending around the rollers, while being dragged through the roller sets. The process was triggered when the cage passed the cable contact point, which connected the two deceleration systems mounted to either side of the shaft walls (refer:Figure 30, Figure 31).

Figure 30 Loaded strips before cage impact.

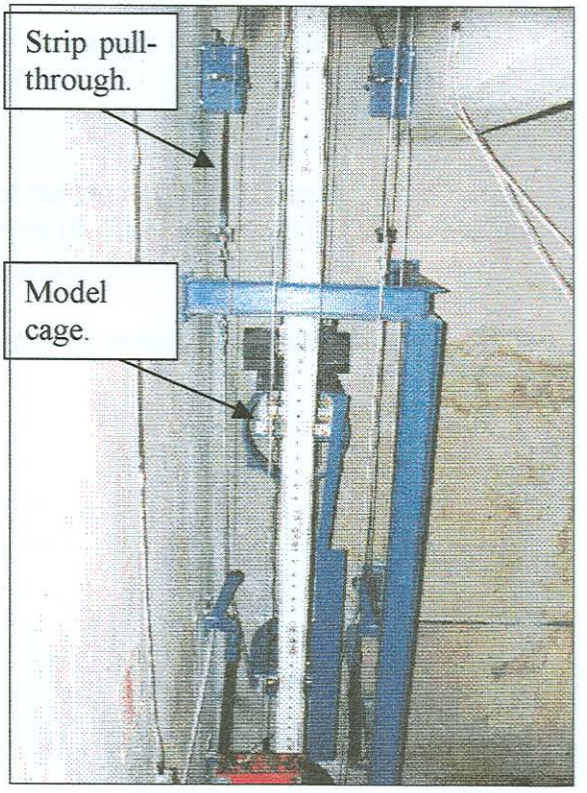

Figure 31 Pulled through strips, after impact.

6.2 Experimental model variables

Geometrical aspects of the model were identified as variables to be changed according to the arresting performance desired. Some of these variables were restricted in the experimental set-up and therefore only a few could be altered. The main reason for these restrictions was due to limited working space. The gap available to vary the roller size was limited, and would require a considerable amount of labour to change this, becoming financially and practically unviable. The space at the bottom of the model shaft, which was available to decelerate the cage, was also cramped in. As a result the achievable velocity for the cage was limited, since the braking distance available before reaching the bump-stops was only 1.5 meters.
The possible variables are the following.

- R = radius of the roller around which the strip bends.
- t = thickness of the strip.
- w = width of the strip. A taper has been introduced so there is a starting taper width and an end width.
- l = length of the taper.
- v = the velocity at which the process takes place was changed, which in turn influenced the strain rate of the material. This was varied by altering the height from which the model cage was dropped.
- M = the mass of the cage.

In the experimental procedure the thickness of the strip (t) was changed, as well as the width of the strip (w) and the length of the taper (l). The velocity (v) of the impacting cage was also varied by changing the drop distance.

The size of the rollers and the mass of the cage were maintained throughout.

6.3 Testing schedule

A testing schedule was set up to evaluate the program over a selection of conditions (refer: Figure 32).

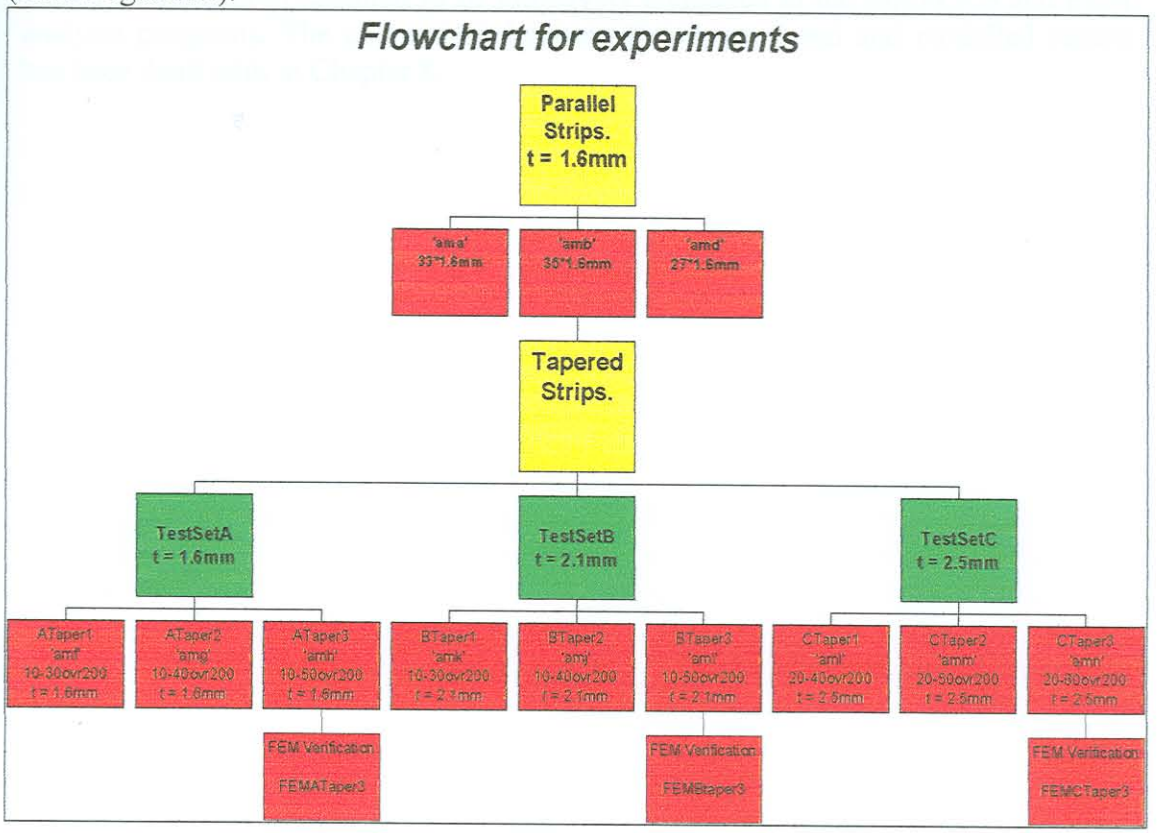

Figure 32 Testing schedule.

6.4 Experimental details

Figure 32 represents the entire history of testing for this project. The results of the parallel strip testing phase were considered as developmental and will not formally be dealt with in this manuscript. The results thereof are appended in Appendix C for interest sake and for the sake of completeness.

During the tapered strip phase of testing, TestSetA experiments were performed with a strip thickness of 1.6 millimetres (mm). The height from which the 130kg model cage was dropped was 1 meter (m). The taper profile increased as described in the flow diagram. 10-30ovr200 implies that the taper profile had a thin section of 10mm wide, increasing to 30mm over a distance of 200mm, and then remaining a uniform width for the remaining length (refer: Figure 17).

TestSetB experiments made use of a strip with thickness of 2.1mm and a drop height of 1.5 m. The taper profile variation for the scope of testing is described in Figure 32 as explained above.

TestSetC which was the final phase of testing, had a strip thickness of 2.5mm and drop height of 2.5 m. The taper profiles varied as described in Figure 32.

6.5 Experimental Conclusion

The experimental phase of the project determined the performance of the decelerating systems under various scaled down conditions. Considering the limitations, enough usable data has been captured to be effectively compared to the MATLAB and FEM analysis programs. The comparison between tested, predicted and modelled results has been dealt with in Chapter 8.

7. Dynamic Finite Element Simulation

7.1 Introduction

The finite element analysis (FEA) is a numerical method for solving problems of engineering and mathematical physics. Typical areas of application are structural analysis, heat transfer, fluid flow, mass transport and electromagnetic potential problems. For situations involving complicated geometry, loading and material properties, analytical equations are difficult to determine and solve. Hence, the numerical method of the FEA application is the only viable solution. The finite element formulation of the problem results in a system of simultaneous algebraic equations for solutions, rather than requiring solution of differential equations. These numerical methods yield approximate values of unknowns at discrete numbers of points in the continuum. The method of modelling a body by dividing it into an equivalent system of smaller bodies or units (finite elements) interconnected at points common to two or more elements (nodal points or nodes) and/or boundary lines and/or surfaces is called discretization. For an FEA the equations for each element are formed and combined to obtain the solution of the entire body, instead of solving the entire body in one step, as for the case with an analytical solution. Typically the solution of structural problems involves the determination of displacements for each node and the stresses within each element within the structure under the applied loads. With non-structural cases, the nodal unknowns would be temperatures or fluid fluxes, depending on the application.

The condition encountered in this FEA case is classified as structural impact. The reason for the FEA was to explore the geometrical limitations of the experimental scale model. The first limitation was the inability to change the roller diameter easily. In the experimental model this was physically difficult since there was limited space available. In the FEA it was a trivial exercise to change roller diameters. The geometrical factors which were readily varied in the experimental model were the strip thickness and the strip profile, the drop height and therefore the velocity. The second limitation was the under wind space available to decelerate the cage being limited, therefore restricting velocity range that could be experimentally simulated. Once again, the velocity of impact can easily be changed to suit the requirements in the FEA model.

During scale model testing, the data of accelerations experienced by the model conveyance was recorded (refer: section 6.). The finite element model (FEM) was then built (on computer) and dynamically excited to emulate the tested situations. For the purpose of this investigation, MSC Dytran was used for the FEA. The pre and post processing of the model was done in MSC Patran. The FEA results were compared to the tested readings and the comparison was of such accuracy that the FEA output was accepted as reliable and accurate. The maximum deviation was 25% and this is considered acceptable since the FEA was consistently non-conservative (refer: section 8.). A 25% error can at worst mean a 0.75g difference in a probable mine conveyance application where the limit is 2.5g. The envelope allowed for human deceleration is wide enough to compensate for the deviation (refer: Table 1). The accuracy of the FEA is considered adequate to form a comparative reference, against which to gauge the range of application of the MATLAB prediction program.

Having established the reliability of the FEM analysis output, the next step was to vary the roller radii, strip thickness and taper profile in the FEM for different situations and compare the data readings to the output predictions of the MATLAB design program. This simulation was used to further verify the accuracy of the design program.

An extreme situation involving a 40 tonne cage moving at 100 km/h was simulated and compared to the output of the MATLAB design program. The only difference between the two sets of results was the initial deceleration profiles (refer: Figure 33). In the figure showing the FEA velocity plot, a sharp decline in velocity at impact could be seen, where the design program output did not have the initial velocity dip. The reason for this is that the FEA takes the strip inertial impact into account and the design program does not. The mass of the strips capable of absorbing 15,5 mega joules of kinetic energy would be 900 kg each. (t = 20mm, R = 200mm, l = 18m, w = 380mm, material = 300W steel) In this case four strips would be required, so the combined mass of the strips, compared to the mass of the total system to be retarded, would be nearly 10%, which would have a significant inertial effect. In concept the following would occur: two masses collide, one of four tonnes (strips) and another of forty tonnes (cage). The initial dip in the velocity predicted by the FEM in Figure 33, was due to the inertial load caused by the forty tonne cage having to accelerate the four tonne mass. The forty tonne mass (cage) would have to accelerate the four tonne mass (strips), which is initially at rest, and since the strips are one tenth the mass of the cage, the deceleration effect on the cage is significant. After the initial deceleration, the combined mass would move on as a lumped mass body of forty-four tonnes. When the design program was fed the total mass, of the conveyance and the strips, (44 tonnes) the resulting velocity gradient of the FEM and the design program were the same. The only difference was the initial profile where the FEM took into account the mass ratio of the colliding masses and the design program did not, as depicted in Figure 33.

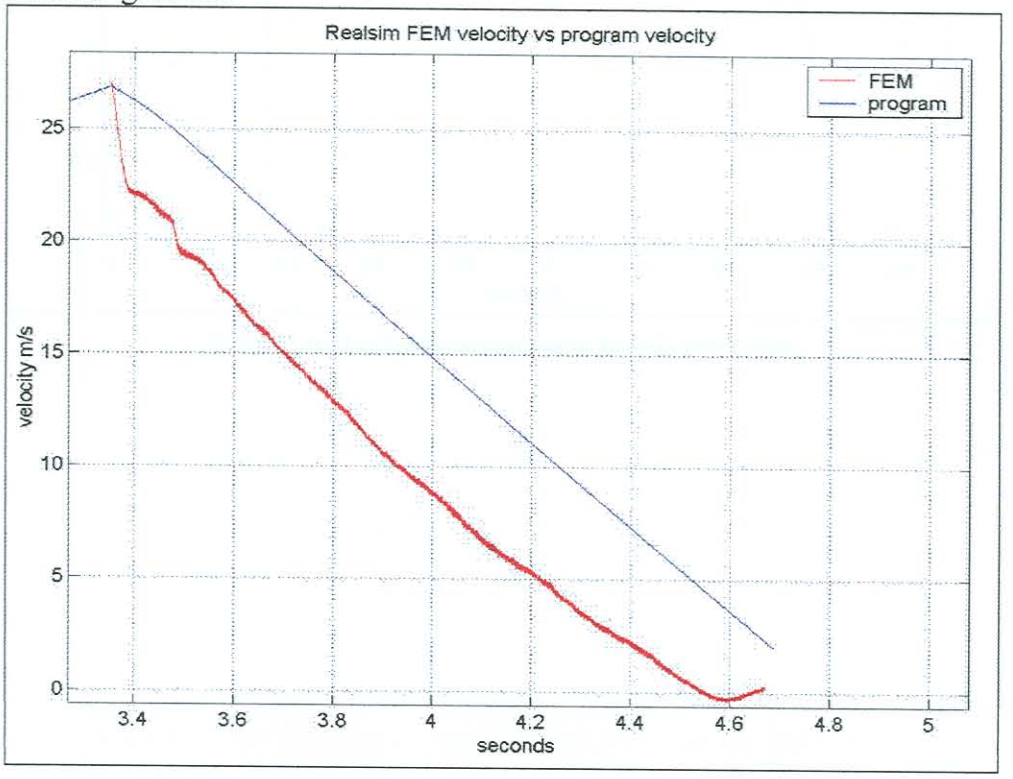

Figure 33 Velocity plot of program vs. its comparative FEM.

The initial velocity gradient drop of the FEM result as depicted in Figure 33, would result in a large impact deceleration effect experienced by the cage. This is confirmed in Figure 34 where the FEM acceleration plot has a high initial deceleration profile and then levels off to the same level as that of the design program, before coming to rest.

These conditions represented an extreme situation and it is unlikely that this would be encountered in a real life situation. This simulation was done purely to explore and identify the limitation of the design program and the possible scope of application.

It is still important to note that the time interval of exposure to the deceleration, had this event occurred, would have been in the order of three tenths of a second (refer: Figure 34). The FEM deceleration level peaked at four Gs for the impact and for that time interval would still have been safely within the survivable limits for head-ward (vertical) decelerations as discussed in section 2.1.2.

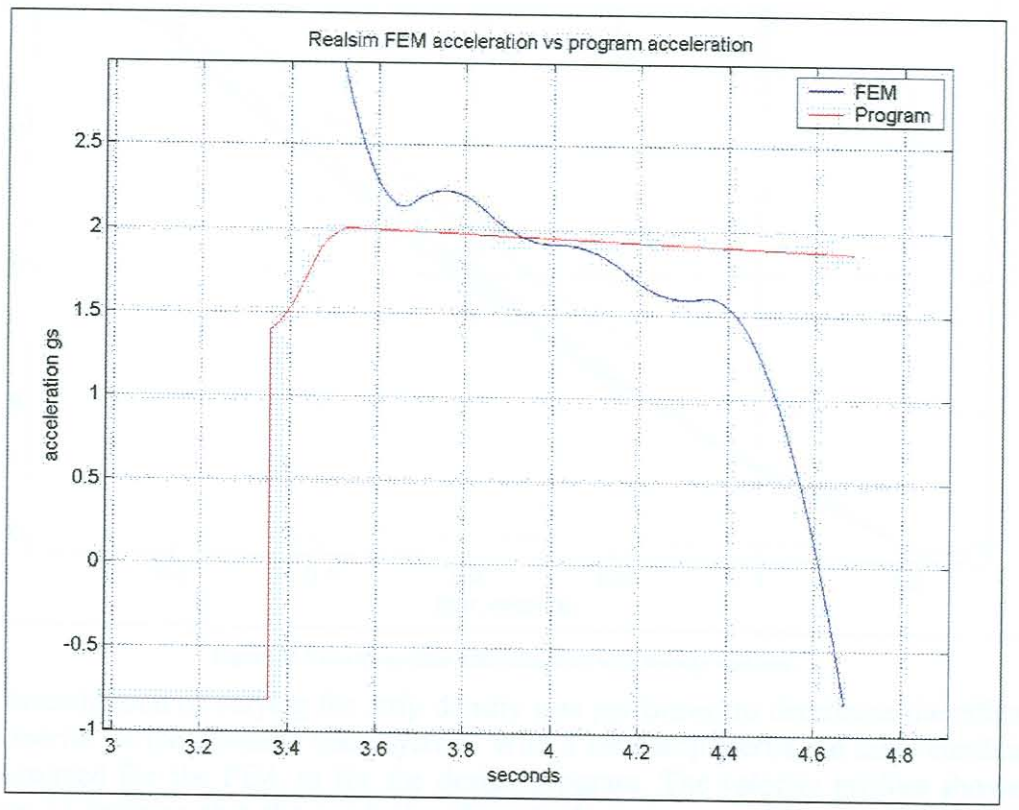

Figure 34 Acceleration plot of program vs. its comparative FEM.

A further investigation has been performed to determine the influence of the inertial effect on the performance of the braking systems. The capability of the FEA made it possible for the density of the strip material to be modified. The full-scale extreme condition, (as previously described) was simulated once more, but this time with strip element densities equal to 0% (1kg/m^3), 25% (1850kg/m^3) and 60% (6000kg/m^3). The resulting velocity and acceleration plots have been superimposed onto the previous 100% strip density condition and the differences were evaluated (refer: Figure 35, Figure 36).

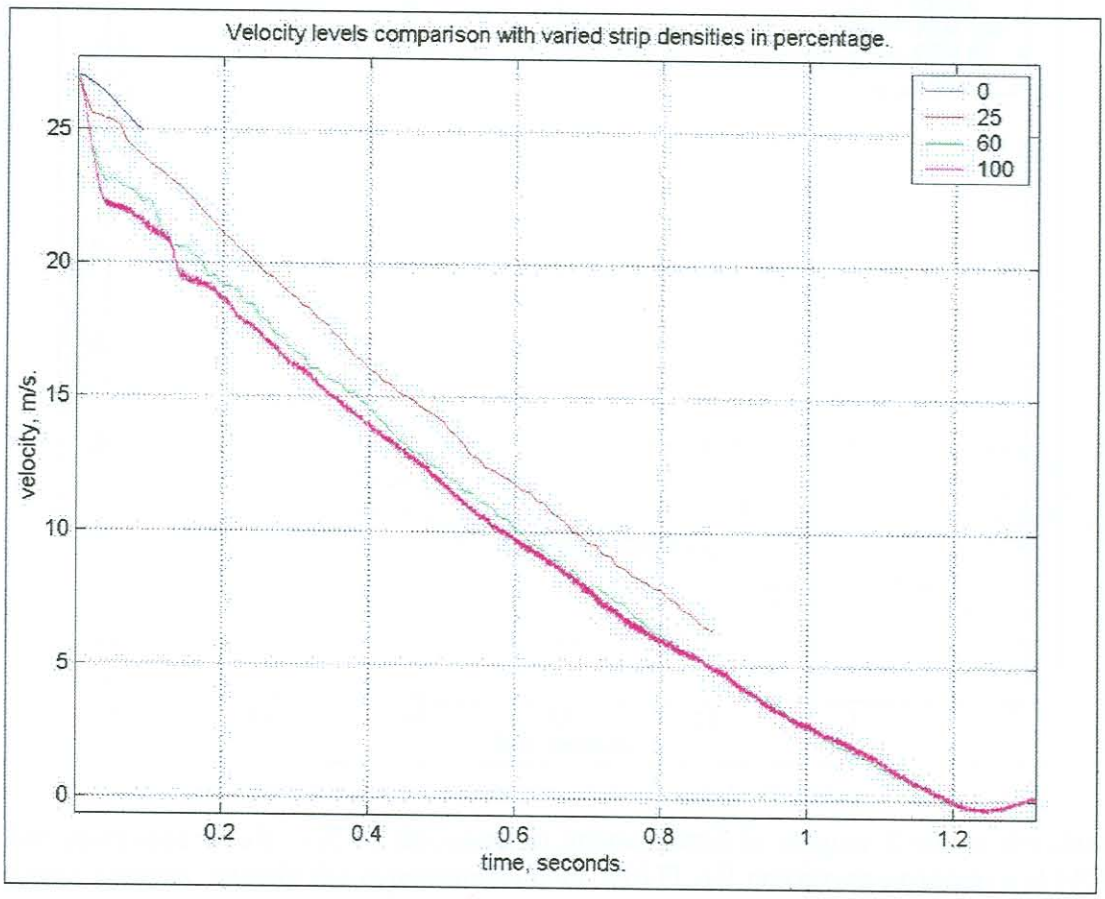

Figure 35 Velocity profiles difference with strip density variance.

The investigation of varying the strip density was performed to determine the effect of strip inertia on the colliding mass system. With a zero strip inertia the same conditions are assumed for the FEA as for the design program. The velocity profiles shown in Figure 33 indicate that the prediction from both sources are the same for the same conditions.

The selection of a low density for the 0% strip material density simulation, caused an extremely long computer running time of 110 hours for the data captured, covering only one tenth of the full event. For this reason the analysis was stopped prematurely revealing the short 0% curve in Figure 35. This still provided an indication of the gradient to be expected during deceleration and the effect of initial impact on the system.

A note can be made of the gradient change between the 0% and 25% curves, relative to the 100% curve. The gradient of the 0% and 25% curves are marginally steeper than the 100% density curve.

The acceleration curves in Figure 36 accentuated some important points. The first of these was the inertial deceleration effect. In Figure 36 curves FEM100 and FEM60 showed virtually the same initial deceleration levels. FEM25 was then substantially lower and finally FEM0 had an obvious trend of not showing inertial effects at all.
The second point highlighted was that the deceleration levels of all the cases, once past the impact zone, were at the same level.

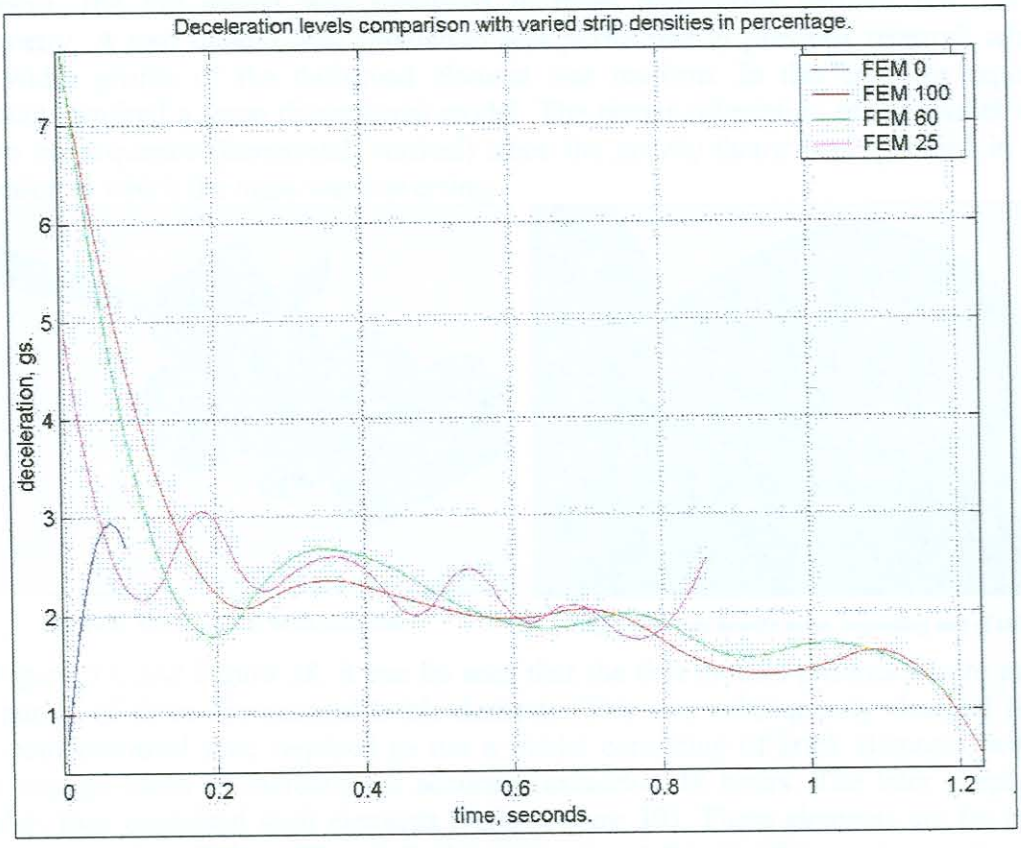

Figure 36 Acceleration profile comparison with strip density variance.

The compared results will be discussed in greater detail in chapter 8 where the three output sources, namely the experimental data, MATLAB prediction program and FEA are compared and evaluated in greater detail.

7.2 Model description

7.2.1 General Aspects

Due to the complex nature of the model, great manipulation and variation was required to produce a functional version. As a result of the dynamic nature of the scenario, the full model was simulated in three dimensions without the use of symmetry. A two dimensional simulation was performed in previous research where the width profile of the deformed element was uniform. In this case the tapered element required a three dimensional model. The planar orientation of the model was of no consequence (horizontal, vertical) since the gravity factor was specified in the direction in which the mass was traversing.

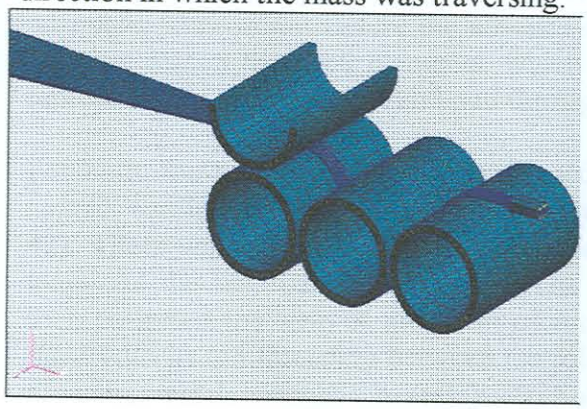

Figure 37 First model in brick elements.

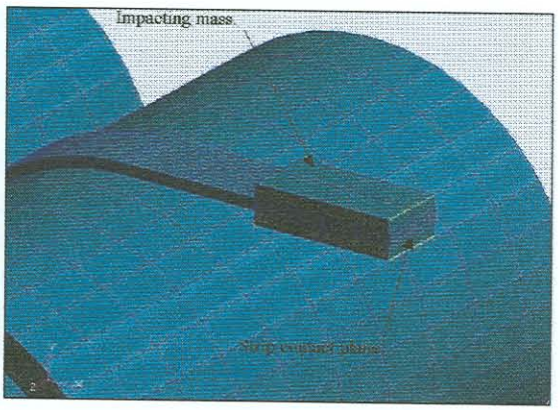

Figure 38 High density mass, impacting end of strip.

In Figure 37, and Figure 38, it can be seen that the first models produced were made up purely of three dimensional brick elements. This was subsequently changed since the computational time required to run a model consisting of brick elements, with a fine enough mesh to increase the accuracy exceeded 48 hours. The later simplified models thus contained shell elements (refer: Figure 39). These elements are far more computationally efficient. The shell elements were defined with a centre surface for every component. The surface was then meshed or divided into elements and given a thickness for each section as required to resemble the model to be simulated. It was possible to use shell elements since the material used was thin sheet metal. In the FEA model, only the relevant sections of the rollers were modelled. The non-participating sections of the rollers were omitted to improve the model's efficiency (refer: Figure 39).

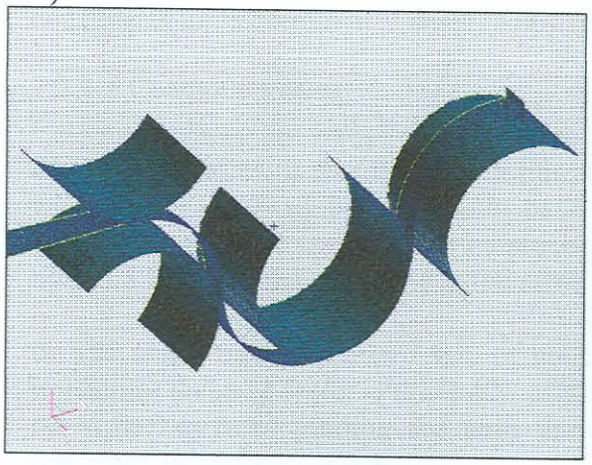

Figure 39 Shell element model.

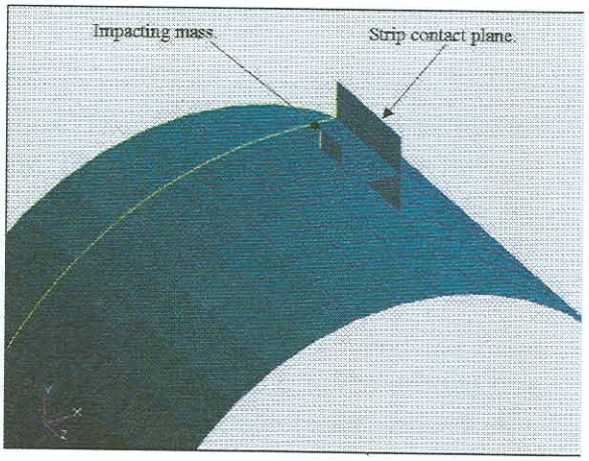

Figure 40 Shell mass surface and strip impact plane.

In this application the material deformation was not expected to be great, in terms of strain, since the bending of the strip took place around large curvatures. Although the component displacements were considerable, the strains are reasonably small. For the purpose of this study the points of interest were the deformation regions of the strip as it threaded between the rollers. The shell elements were capable of adequately predicting these events.

The strip was designed with a static safety factor of six, which is required by the Occupational Health and Safety Act for all lifting equipment with ropes or cables [21]. In this case the element can be regarded as a structural member and would thus only require a safety factor based upon good engineering judgement. A decision was made that for this application a factor of six based upon material yield limit was adequate. This would ensure the absence of necking in the thin section of the strip. For this reason the shell elements, which were selected, would deliver an accurate representation of the impact and pull through event.

For both, the brick and shell element models, the modus operandi was the same: a contact surface was defined between the roller sets and the strip itself (refer: Figure 42). There was also a contact surface created at the front of the strip, between the mass and the strip (refer: Figure 40). The mass was given an initial velocity, which then collected the strip at the point of impact. The strip was dragged along by the mass with its tail threading between the rollers, while applying a deceleration force to the mass, which brought it to rest (refer: Figure 39).

7.2.2 Constraints

In a FEA, many bodies are created, meshed and given material properties. When this process is completed the bodies must be combined into an assembly resembling the true scenario accurately. This is achieved by means of constraints.

Constraints are the definitions that are given to a model in order to closely describe the simulated scenario. These definitions can be applied in many ways, for example restricting motion, rotation or force applications. They represent mountings, initial velocities or contact surfaces. Many more situations could be applied, tailored to represent each unique real situation as accurately as possible.

Knowing how this particular system was to be used in practice enabled the choice of constraints to be confidently made, while not affecting the real life correlation.

7.2.2.1 Contact surfaces

Contact surfaces are inter-body, interface limits. These limits are defined as master and slave partners as was the case in this study. They indicate the boundaries through which other involved bodies cannot pass. This prohibits the interpenetration of the participating bodies and ensures the practical law of space, which cannot be occupied by more than one mass particle at the same instant.

In this study there were two sets of contact surfaces. The one simulated the mass impacting the strip (refer: Figure 40), as discussed in section 7.2.2.3. The second was the roller surfaces guiding the strip through the bending path (refer: Figure 42), described in section 7.2.2.2.

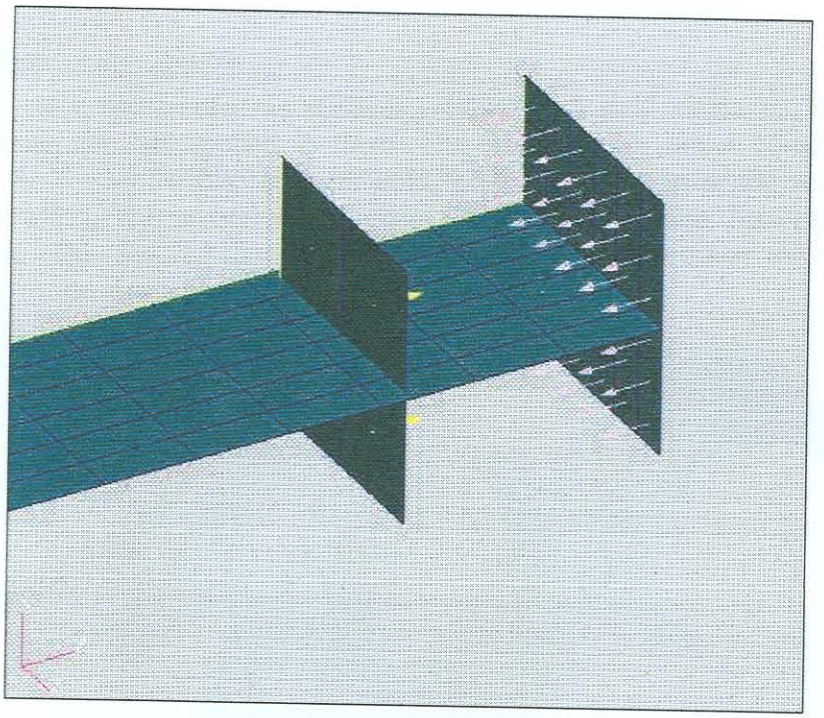

Figure 41 Mass and strip contact pair, master and slave.

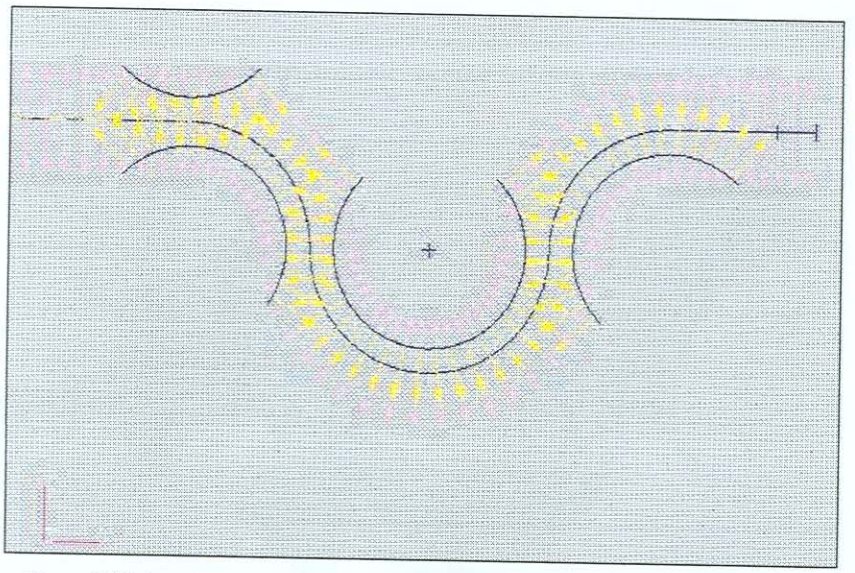

Figure 42 Strip and rollers contact pair, master and slave (Direction of contact support).

Figure 41 represents the contact mode definition of the mass surface. The yellow and purple arrows indicate the direction in which the surface was expecting contact from its master or slave partner.

In Figure 42, the pink arrows point in both directions, thus the strip expected contact from the rollers from both sides. The rollers were only defined in one direction, supporting and guiding the strip. The one direction of contact for the rollers was indicated by means of the yellow arrows. It was defined from the roller towards the strip, for each roller. The correct definition of the expected directions of interaction from neighbouring bodies in the model, drastically decreased the computational time of the analysis.

7.2.2.2 Rollers

The rollers were represented as surfaces meshed with shell elements. These rollers had two constraint sets applied to them. The first was the mount constraint that is applied in the form of a displacement hold, preventing motion of the roller surfaces (refer: Figure 43). The second was the contact surface constraint, between the rollers and the strip. This ensured the strip to travel along the path between the rollers while conforming to the arcs (refer: Figure 44).

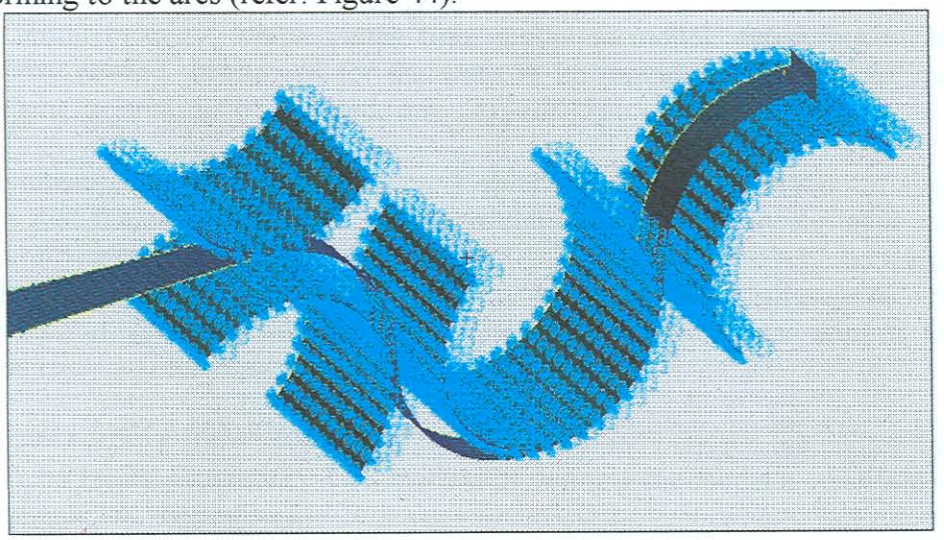

Figure 43 Displacement constraint definition of rollers

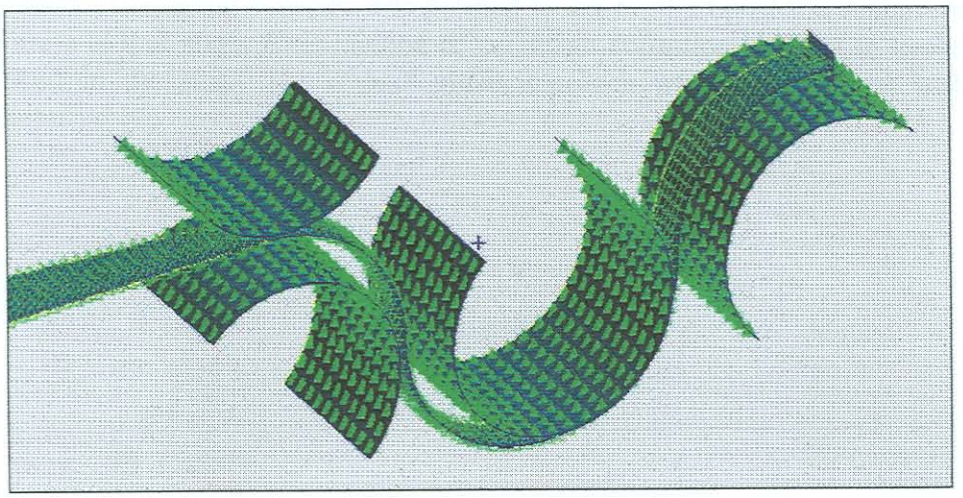

Figure 44 Contact constraint definition of rollers

The light blue points on the rollers in Figure 43 indicate the applied constraint at the nodes. In this analysis they prohibited displacement in the X,Y and Z directions. The rollers were therefore portrayed as stationary surfaces.

The contact between the strip and rollers was also discussed in section 7.2.2.1. In Figure 44 the solid triangles indicate the master surface and the empty triangles show the slave surface. The friction force between surfaces was simulated as zero since the experimental model rollers were mounted on bearings. For this analysis it was assumed that the friction force contribution from the rollers was negligible.

7.2.2.3 The impacting mass

The impacting mass was also represented by a surface and defined as shell elements. Gravitational acceleration was simulated as a constant acceleration in the direction of motion.

It had three constraints applied to it:

An initial velocity, which varies from model to model, depending on the impact severity needed. It allowed for the mass to be moving at the defined speed at the moment the analysis was started (refer: Figure 45).

Movement was restricted to only the X direction, since the situation of application is such that the strip would be drawn through the rollers by means of a cable (refer: Figure 3) towards a fixed point, the pulley. With this in mind, the assumption of planar motion was representative. In Figure 46 the blue dots represent the nodal Y and Z direction, displacement constraint. The same constraint was applied to both the strips ends, and the mass centre.

Contact surfaces (refer: section 7.2.2.1) were defined between the end of the strip and the mass (refer: Figure 47). This method of defining the model's conditions ensured a representative simulation.

An earlier attempt of simulating the scenario was to model the mass and the strip as one body. The initial velocity was defined to act on the tip of the strip, representing the mass at that stage. This method of condition definition resulted in necking being induced in the strip. The impact plane approach was then adopted with greater success.

Referring to Figure 45, the mass plane and the strip seem to be merged. This is only a visual impression since they were modelled as separate entities. In the FEM the mass and the strip only interacted with each other once the impact planes met (refer: Figure 41). Before that occurred they had no effect on each other, even though they seem to be merged. Figure 45 shows the initial velocity definition applied to the mass. Figure 46 shows the definition of X-axis motion of the mass and the end of the strip. In Figure 47 the solid triangles represent the master surface and the empty triangles define the slave surface, between the mass and the end of the strip. Contact surfaces are defined as master and slave pairs, with no preference to which ones remain stationary or move.

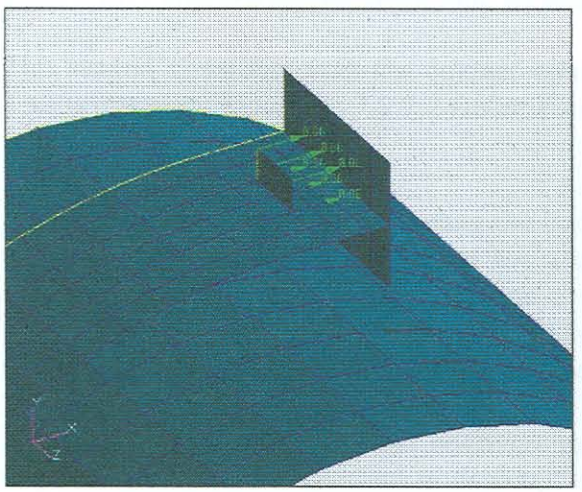

Figure 45 Mass initial velocity definition

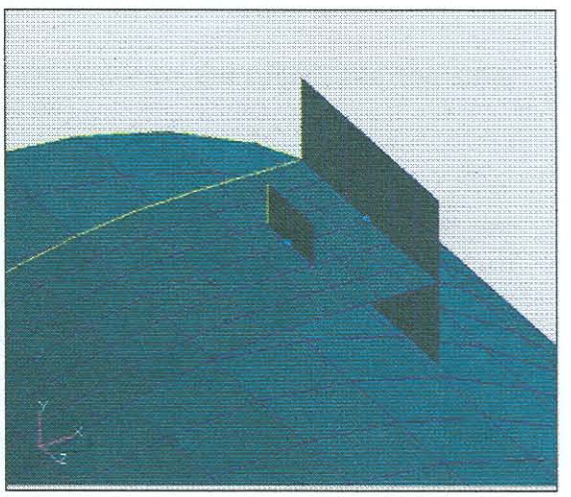

Figure 46 Mass and strip displacement guide

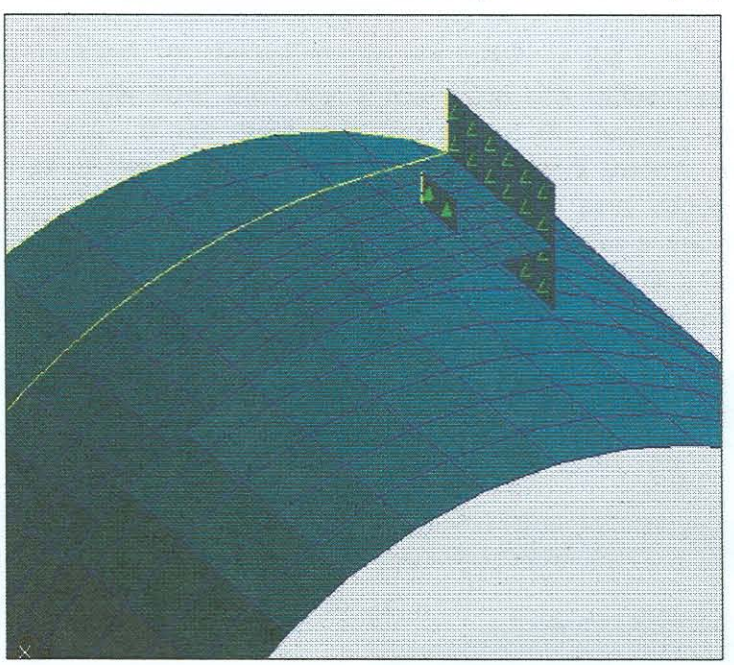

Figure 47 Mass and strip master and slave contact pair

7.2.2.4 The strip

For this analysis the strip was represented as a mid-surface and meshed with shell elements. There were two constraints applied to the strip.

The first constraint was a guide application. The constraint was applied by means of confining only one node on the front of the strip in the Y and Z direction, thus allowing only for travel in the X-axis. This was done to eliminate unnecessary degrees of freedom, which often occur in dynamic simulations. When there are too many degrees of freedom allowed, the models tend to diverge from real motion. (refer: Figure 46) (This is a similar constraint, as was applied on the mass.)

The second constraint was the contact constraint between the rollers and the strip. This is discussed in section 7.2.2.2 (refer: Figure 44).

7.2.3 Meshing

Meshing is the term used for dividing the body into blocks or finite elements. The size of the finite elements, greatly affect the accuracy of the FEA prediction. A rule of thumb is that the user specifies as fine a mesh as practically possible (processing power limitations influence this) in the expected high stress or critical areas in the geometry, to ensure a creditable degree of accuracy.

In this case the geometry was relatively simple and there was only one area that required some mesh refinement as depicted in Figure 48. This area was in the neck of the strip where the taper thins to its minimum width.

It was found that the mesh on the rollers did not influence the results significantly, however the mesh on the strip did play a roll since this influenced the bending performance of the strip. If the mesh was too coarse the bending arc would be simulated as a series of flat, disjointed surfaces and not as a smooth arc. The edge effect can be seen in Figure 49. The rollers (as indicated) have edges and are not smooth curves. The strip, shown between the rollers, clearly has a smoother surface. If the mesh on the strip were coarse, with similar edges as the rollers, a hooking rather than a sliding effect would have occurred. This would have obstructed the smooth pull-through of the strip.

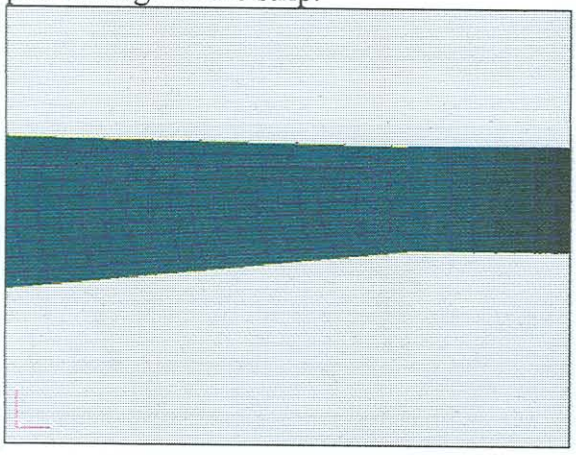

Figure 48 Strip mesh refinement.

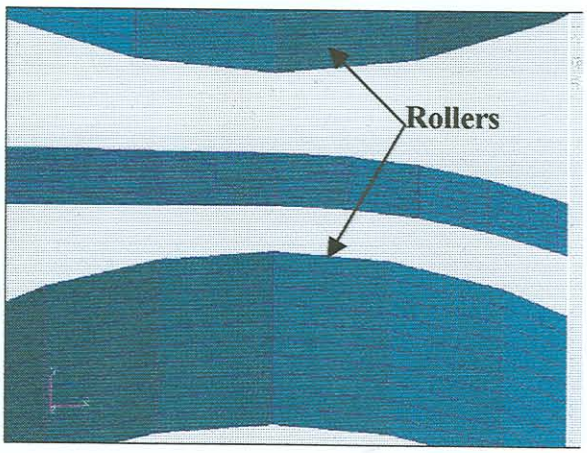

Figure 49 Strip and roller mesh difference.

7.2.4 Material properties

The material properties assigned to the various parts of the model are standard options in the FEM package. An advantage was that the Cowper Symonds (refer: section 4.3.1) material characteristics [8] were available as one of the constitutive models. This model was applied to the strip as discussed in section 7.2.2.4, since this was the component to be influenced by the high strain rate condition. The Cowper Symonds formulation has been used in the past to a great extent to accurately predict the performance of steel members under high strain rate conditions [7].

The rollers were given basic elastic plastic properties, as would be the case in standard steel under quasi-static circumstances. A density of 7800kg/m^3 as is the case for standard 300W mild steel.

For the impacting mass no great deformation was expected. A standard elastic plastic material property was thus assigned, with a variable density. The impact masses for the various simulations were heavy, but the impact areas were kept small, in order not to complicate the geometry. The mass was therefore simulated by means of an artificially high-density material to give the correct mass. Since no major part was played by the mass in terms of deformation, the consequences were considered to be minor.

7.3 The analysis

7.3.1 Analysis objectives

The objective of the finite element analysis phase in this study was to establish the accuracy of the code that was written. First of all a FEA benchmark was to be created, representing the experiments performed. The analysis plan was divided into three segments:

1. Simulation of experiments already done in the laboratory at the University of Pretoria to verify FEA accuracy, since the MATLAB code already showed close correlation to the experiments.
2. Simulate scenarios outside the practical experimental scope, in progressive stages of severity. The results are compared to the output of the MATLAB code for similar conditions.
3. Simulation of the real life scenario. The same scenario was fed into the MATLAB program and the results of both were compared to determine the degree of accuracy of the MATLAB code, when applied to the full-scale industrial conditions.

The stages of progression were followed in the above mentioned order, to establish where the MATLAB code output, and the FEM analysis output, diverge.

Verification of FEA relative to experiments performed.		
ATaper3	Btaper3	CTaper3
Taper = 10-50ovr200 t = 1.6mm R = 30mm Drop height = 1m	Taper = 10-50ovr200 t = 2.1mm R = 30mm Drop height = 1.5m	Taper = 30-50ovr200 t = 2.5mm R = 30mm Drop height = 2.5m

Exploring the experimental restrictions with FEA	
DeltaRoll1	Taper = 30-60over300 t = 6mm R = 80mm Velocity= 8m/s Mass = 500kg
DeltaRoll2	Taper = 40-100over500 t = 10mm R = 150mm Velocity= 12.5m/s Mass = 1000kg
DeltaRoll3	Taper = 100-250over1500 t = 20mm R = 300mm Velocity= 18m/s Mass = 5000kg

Full scale simulation. (4 roller sets, Mass = 40Tonnes, velocity = 100km/h)	
RealSim	Taper = 220-320over3000 t = 20mm R = 300mm Velocity= 27m/s Mass = 10000kg (per roller set)

Figure 50 FEM analysis Verification and Benchmarking Specifications.

7.3.2 FEA output

The output generated by the FEA was displacement of each element in the finite element model. From the displacement relative to time output, velocity was calculated. These results are closely compared to those produced by the MATLAB code and are discussed in detail in chapter 8. The FEA program used to perform the dynamic simulation also has the capability to deliver a visual display of what the model under went during the analysis. This function greatly enhanced the understanding of the process which took place during the deceleration event. A series of frames of one such play-back is shown in the following images, Figure 51 to Figure 54.

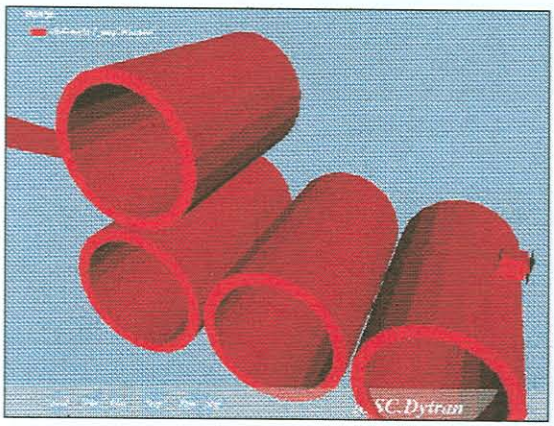

Figure 51 Threaded taper strip before impact.

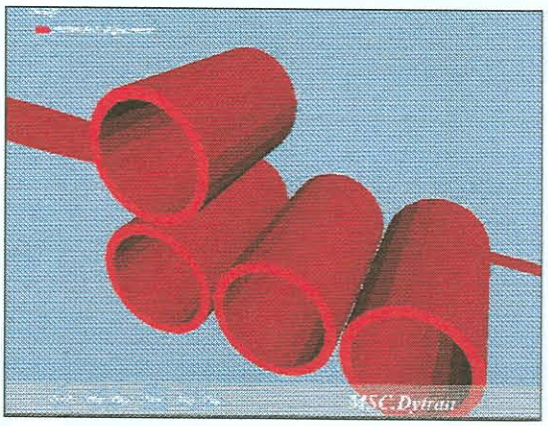

Figure 52 Threaded taper strip after impact.

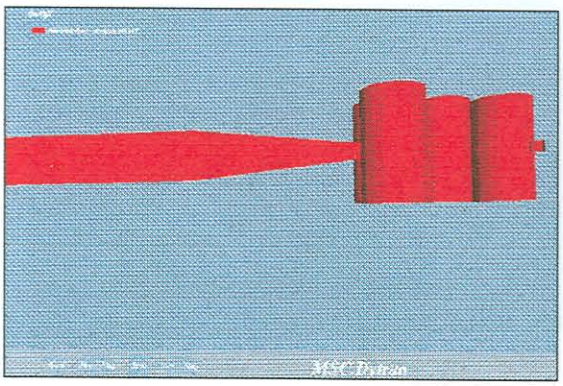

Figure 53 Top view of arrestor set, showing taper strip before impact.

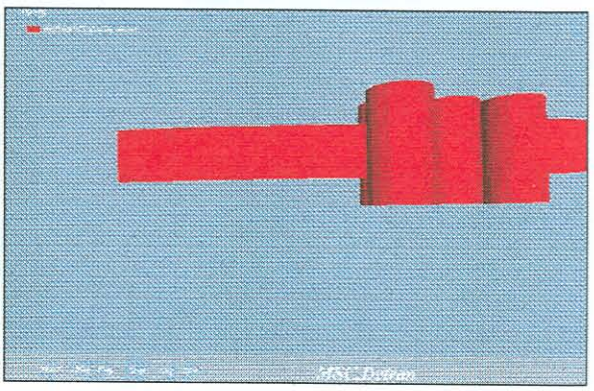

Figure 54 Top view of arrestor set, showing taper strip after impact.

Figure 51 illustrates the visual output prior to impact of the high-density mass, with the surface on the end of the strip. In section 7.2.2.3 the process of the mass colliding with strip and drawing it through the rollers is clearly explained. Figure 52 depicts the strip having progressed through the rollers for a certain distance. Figure 53 and Figure 54 show the top view of the same situations as the aforementioned, displaying the taper section of the strip moving through the roller assembly.

The following images are sequential images of an analysis playback, showing the progression of the strip being drawn between the rollers by the travelling mass, until finally coming to rest. The fact that gravity in the analysis is set to operate in the direction that the mass is moving should be kept in mind with regard to this example. The geometrical scale of the mass in the analysis is also not representative of the true mass used. This aspect is discussed in section 7.2.4.

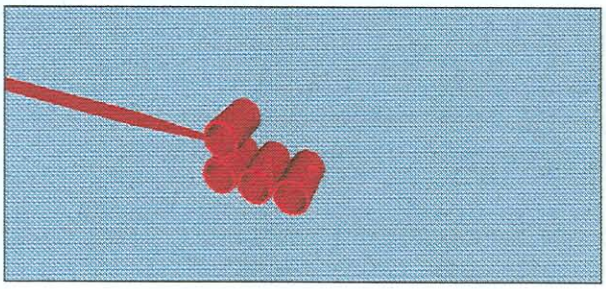

Figure 55 Arrestor set before impact.

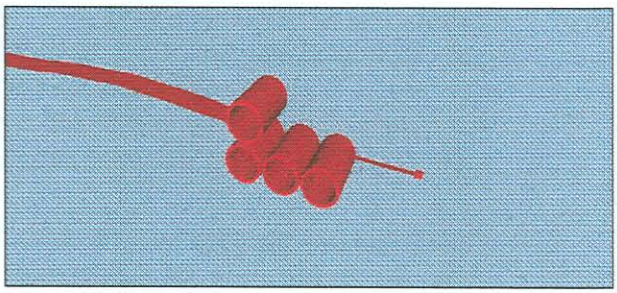

Figure 56 Strip being drawn through after impact

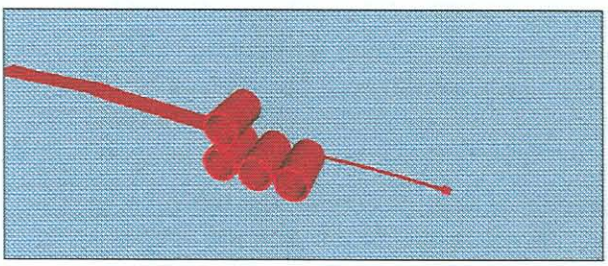

Figure 57 Strip taper section passing through rollers.

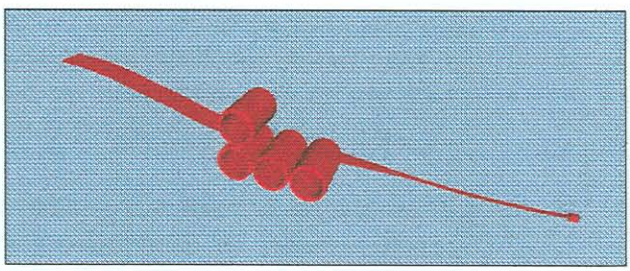

Figure 58 Strip parallel section between rollers.

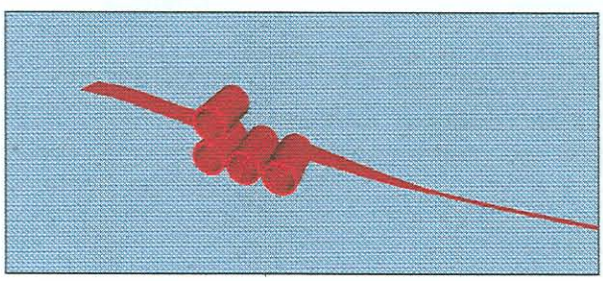

Figure 59 Strip at rest after deceleration complete.

7.4 Conclusion

The finite element analysis program DYTRAN, delivered sound information confirming the generated results delivered by the MATLAB code and the recorded experimental data. The details of these results have been discussed at length in the next chapter.

8. Results comparison

8.1 Introduction

Contained in this chapter are the summarised results of the various outputs encountered during the course of this investigation. They were compared to each other to ascertain their accuracy and shortcomings. The output sources compared are those of the experimental data, the finite element simulation and the results of the composed MATLAB code. The sequence of comparison is as follows:

- The experimental data was captured from the scale model as outlined in section 6. Preliminary comparisons were drawn between these results and the MATLAB code.
- When the range of experiments was completed, a finite element model of the experiments already completed was generated. A simulation of the experiments was executed and the results were compared to the data captured during the experiment itself (refer: section 7.).
- Once the quality of the FEM had been confirmed by accurate comparison to the experimental data, the assumption was made that further exploration of the MATLAB code could be done by means of comparison with the FEM simulated output. This was a sound assumption given the good correlation that was achieved (refer: section 7.1).
- A further investigation was conducted involving the inertial effects of the system on the deceleration levels and the performance of the deceleration systems. The inertia of the system was varied by means of adjusting the density of the strip material in the FEM, and simulating the same full scale scenario.

By making use of this technique, the restrictions encountered with the physical scale model testing were avoided, yet the reliability of the MATLAB code could still be comprehensively evaluated. Further, an understanding of the inertial effects was obtained and quantified.

8.1.1 Experimental data compared to Finite Element Analysis output

The physical component measured in the experimental data capturing process was acceleration (refer: section 6.). The output of the FEM for the simulations was the velocity of the strip and impacting mass. For this investigation to have a common ground on which to compare the systems, the velocity output from the FEM was differentiated to obtain an acceleration profile. Once the acceleration profile was determined, a comparison could be drawn based upon the same reference plane. One experiment from each group was selected for FEM simulation, which was compared to the recorded data (refer: Figure 60). The MATLAB program output was included in the velocity and deceleration comparisons for preliminary evaluation.

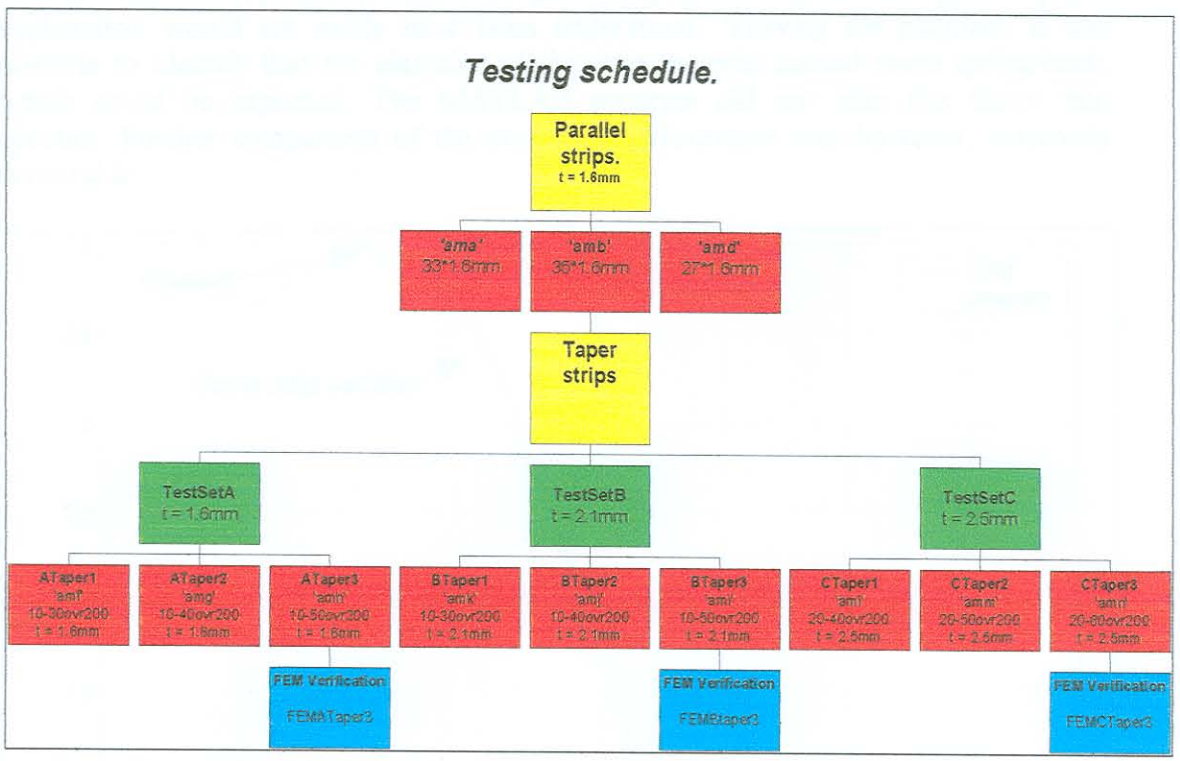

Figure 60 Finite element analysis verification schedule.

8.1.1.1 First comparison set

The schedule seen in Figure 60 shows which of the experiments had been chosen for simulation. Since the output of the FEM was velocity, the velocity output could be directly compared to the velocity output of the MATLAB program (refer: Figure 61). The FEM data was unfiltered. Referring to Figure 61, the FEM velocity profile only started at the indicated contact point. The FEM simulation was initiated at the contact, with the mass having an initial velocity equal to that of the experimental mass, which had been dropped from the predetermined distance before making contact with the deceleration systems. The FEM simulation also indicated the mass overshooting zero velocity, implying that the retarded mass moved backwards after it came to rest. Without the visual playback mentioned previously (refer: Figure 56-Figure 59), the explanation would not easily have been understood. Viewing the playback it was possible to identify that the elasticity of the strip material caused some spring-back, which could be expected. The MATLAB program did not take this factor into account. Further comparison of the predicted performance was however, extremely favourable.

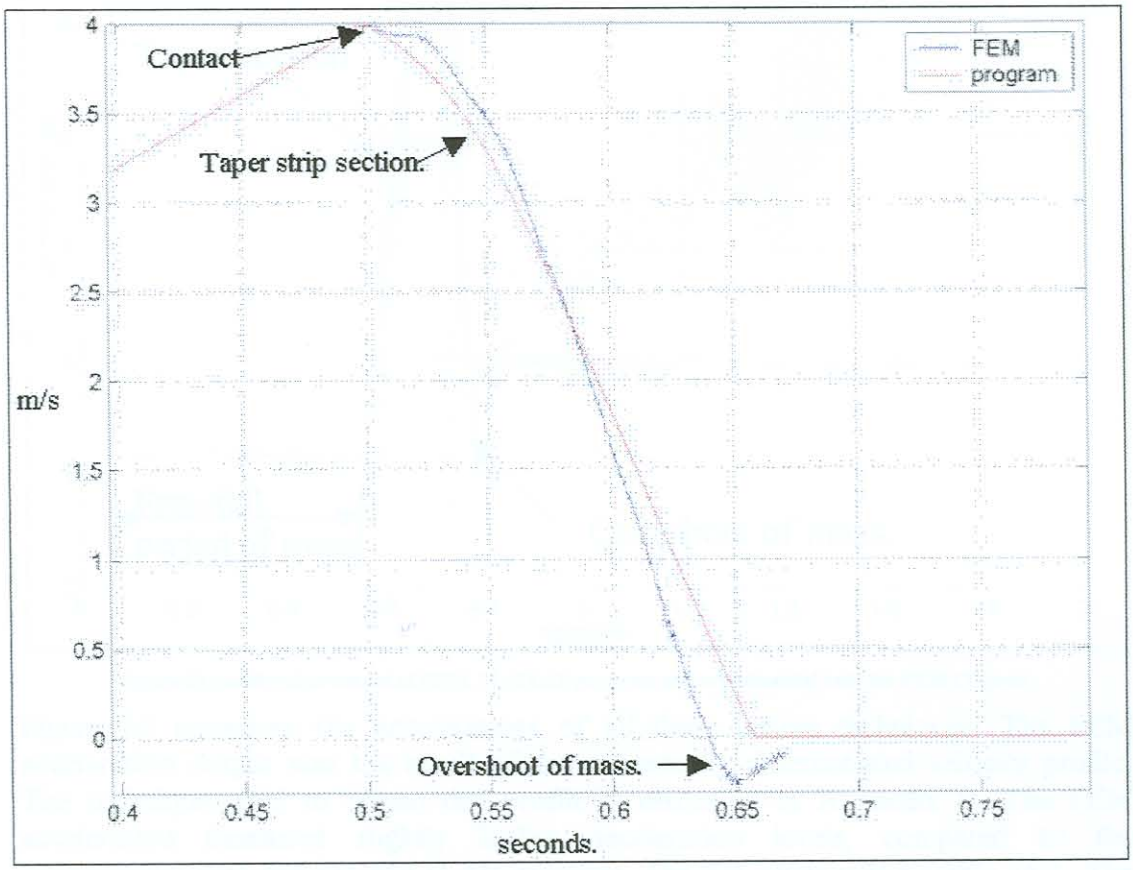

Figure 61 Velocity output of FEM and MATLAB program for FEMATaper3.

Once the velocity data of the FEM had been filtered and processed to yield an acceleration curve, it was compared to the data measured experimentally as well as the prediction from the MATLAB program (refer: Figure 62). The processing procedure performed on the data to obtain the acceleration plot is outlined in Appendix B.

Two or three test runs were performed per experiment for the sake of repeatability, which is the reason for more than one data plot in Figure 62. The initial negative 0.8Gs section in Figure 62 indicates free fall of the mass, bearing in mind that, for this experiment, the model cage dropped a certain distance before making contact with the deceleration systems installed in the shaft (refer: Figure 30, Figure 31). The MATLAB program takes this into account. In this section the effect of the friction in the rails of the conveyance can be seen. The conveyance only reached 0.8Gs when freefalling, indicating resistance. This was also accommodated for in the MATLAB program. The user describing the situation can make the choice of height above the arrestors.

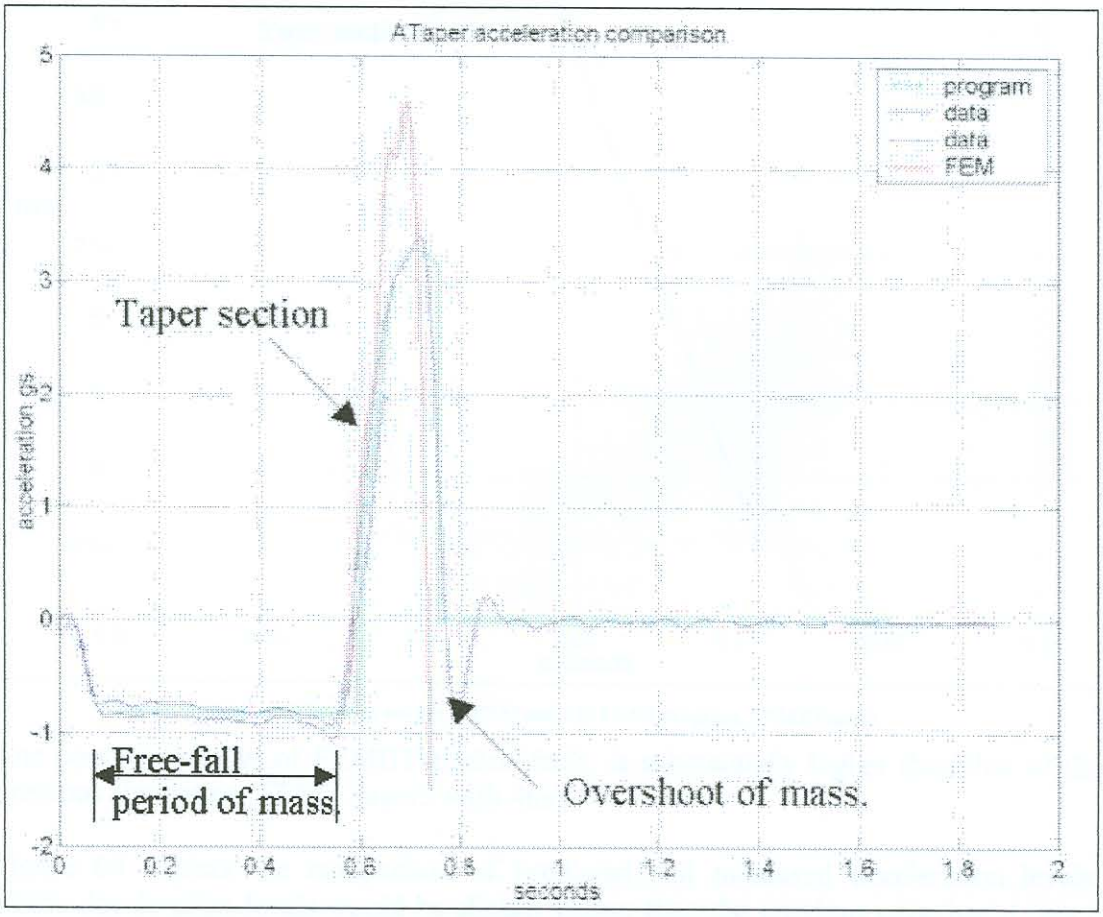

Figure 62 Acceleration output of FEM, MATLAB program and experimental data for FEMATaper3.

Figure 62 compares the accelerations of all three testing techniques. The FEM acceleration output was the result of the numerically differentiated velocity profile. The technique used to obtain this profile is discussed in Appendix B. The FEM acceleration measured slightly higher deceleration levels, compared to the experimental data and the MATLAB program. The difference was roughly 25%. The prediction of the MATLAB program, in this case was totally accurate, compared to the measured data.

The gradient of the initial deceleration showed the effect of the taper section of the strip gradually increasing the applied deceleration force (refer: Figure 62). The overshoot of the mass is clear from the experimental data recorded in Figure 62, as well as the FEM results. This similarity also confirmed the accuracy of the FEM simulation.

8.1.1.2 Second comparison set

The second comparison set, FEMBTaper3 also compared favourably, confirming the accuracy of the simulations already seen. The FEM simulation was interrupted at the final stages of the procedure thus not showing the mass coming to a halt, but the comparison proved to be of great accuracy (refer: Figure 63)

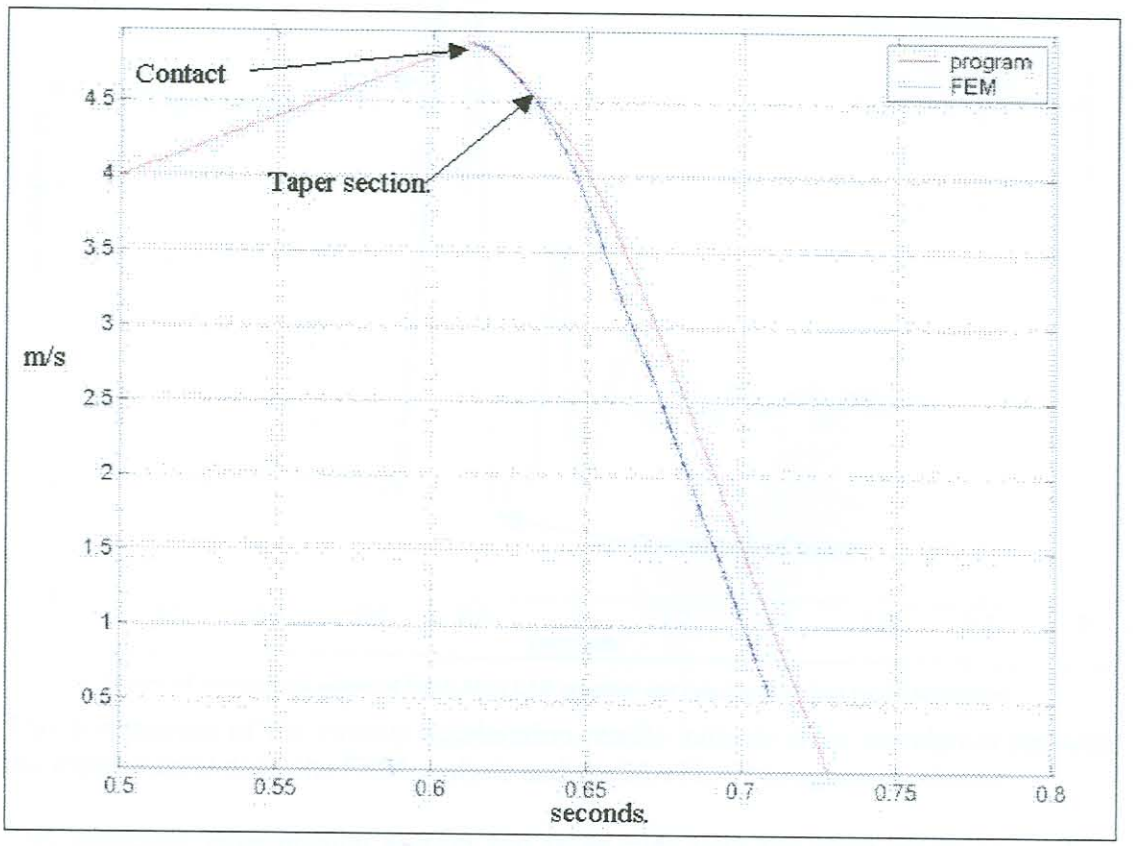

Figure 63 Velocity output of FEM and MATLAB program, FEMBTaper3.

The contact velocity of FEMBTaper3of 5m/s, is substantially higher than that of the previous simulation, FEMATaper3 with 4m/s.

Figure 64 depicts the comparison of predicted and measured deceleration levels. These deceleration levels would be slightly higher than the previous experiment, since with the scale experimental model at the University Pretoria, the space available to decelerate the mass at the bottom of the shaft was limited. Thus with the higher impact velocity required for the experiment, the deceleration rate of the mass had to be higher to allow for retardation within the distance available.

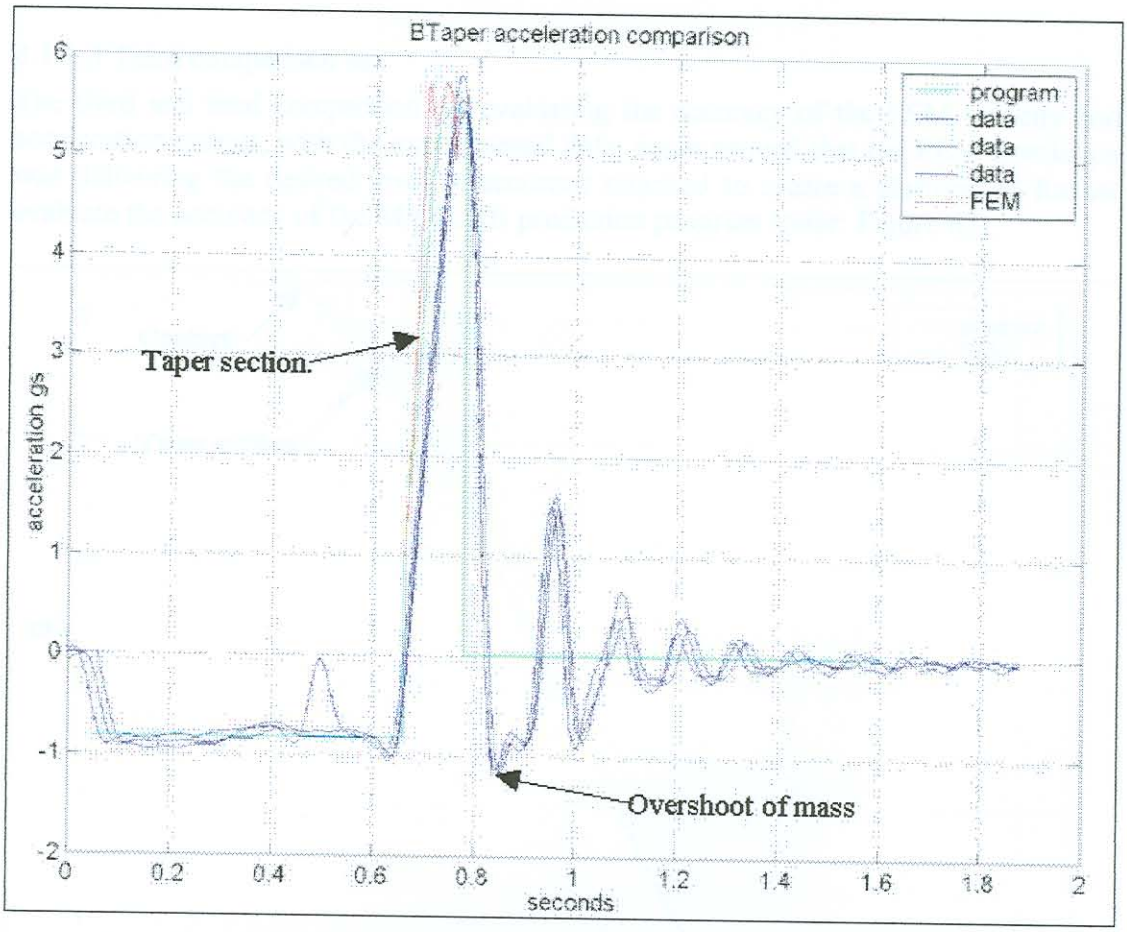

Figure 64 Acceleration output of FEM, MATLAB program and experimental data for FEMBTaper3.

This comparison of the various acceleration results indicate close correlation between the experimental data, the FEM analysis and the MATLAB program prediction.

This particular experimental section had three runs with the scale model to capture data. Figure 64 shows that the repeatability of the deceleration profile was close to perfect. The superimposed FEM acceleration profile corresponded closely to the data profile, including the maximum deceleration level expected, of approximately 5.8 Gs. Due to the interruption of the FEM calculation, the overshoot of the mass cannot be seen. The MATLAB program prediction again was extremely accurate, following the first two outputs of the experimental data and the FEM closely.

8.1.1.3 Third comparison set

The third and final comparison set evaluating the accuracy of the FEM velocity and acceleration output, with the experimental data, again proved that the FEM simulation was delivering the desired level of accuracy required to create a platform to further evaluate the accuracy of the MATLAB prediction program (refer: Figure 65).

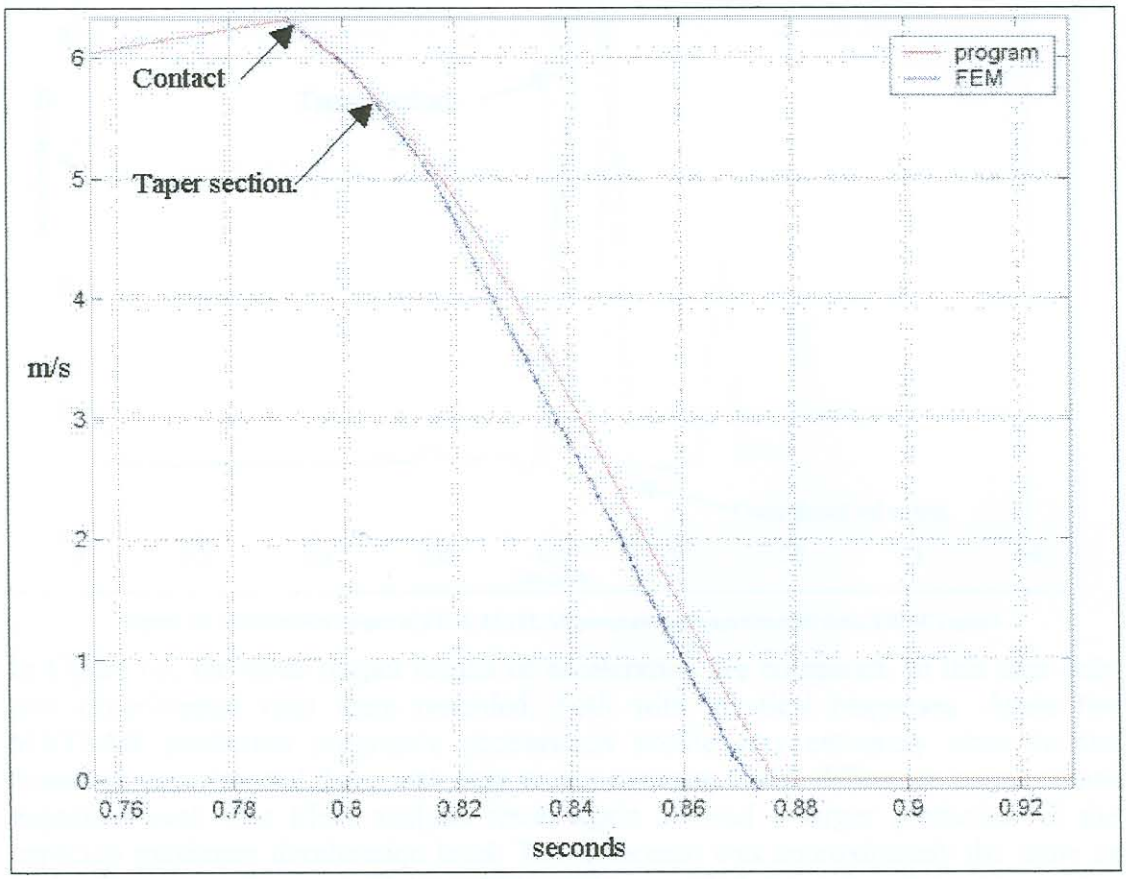

Figure 65 Velocity output of FEM and MATLAB program, FEMCTaper3.

The preliminary velocity plot shown in Figure 65 shows the close resemblance between the FEM velocity output and the MATLAB program velocity prediction.

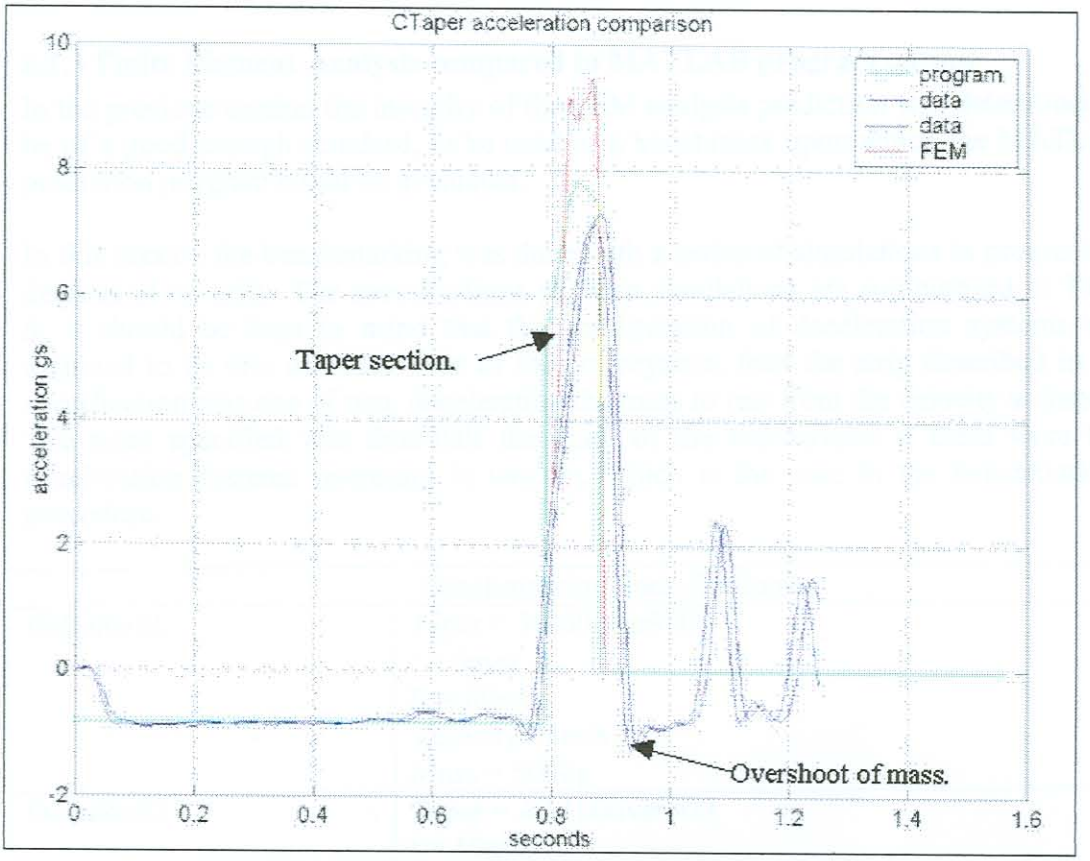

Figure 66 Acceleration output of FEM, MATLAB program and experimental data, FEMCTaper3

In Figure 66, the three output results of acceleration are compared. In this case only two experimental runs were recorded, both with identical responses. Again the MATLAB prediction program's acceleration profile was extremely close to the measured experimental data, with only an approximate 0.4Gs difference on maximum expected level. The FEM analysis result again showed a larger prediction of the expected maximum deceleration level. The difference was approximately the same as in the first comparison set of about 25% to the recorded data, as explained in section 8.1.1.1. The significance of this difference will be discussed at the end of this chapter (refer: section 8.1.2 and section 8.1.5).

8.1.2 Summary of Experimental Data and Finite Element Analysis Comparison

The objective of this section was to determine the quality of the FEM analysis prediction. The three phases of comparison clearly indicated that the proximity of the deceleration levels were adequate to accept that the prediction of the FEM analysis could be used as a benchmark to further evaluate the quality of the MATLAB program's output. In all three cases the MATLAB program was more accurate than the FEM, and delivered a conservative prediction of the expected deceleration levels. This tendency could be expected since the dynamic impact of the collision in the FEM attributes for higher decelerations encountered with the absence of cable damping as was the case in the experimental setup. The following section discusses the results of the FEM analysis for various simulated scenarios as compared to the MATLAB program outputs. By making use of the versatile FEA program and changing the density of the strip element material, the influence of inertial effects under braking conditions was also explored.

8.1.3 Finite Element Analysis compared to MATLAB program output

In the previous section the integrity of the FEM analysis prediction was determined to be of a good enough standard, to be used as a benchmark upon which the MATLAB prediction program could be evaluated.

In this section the benchmarking was done with a series of simulations in progressing degrees of severity. The specifications of these simulations are summarised in Table 5. It should be kept in mind that the configuration of deceleration systems was assumed to be one on either side of the conveyance, thus the strip described in the specification was one of two, decelerating the mass to rest from the velocity at impact. The mass specified was thus half the mass of the conveyance if there were two deceleration systems operating in tandem, which is the case in the benchmarking procedure.

Benchmarking Specifications.	
DeltaRoll1	Taper = 30-60over300 t = 6mm R = 80mm Velocity= 8m/s Mass = 500kg
DeltaRoll2	Taper = 40-100over500 t = 10mm R = 150mm Velocity= 12.5m/s Mass = 1000kg
DeltaRoll3	Taper = 100-250over1500 t = 20mm R = 300mm Velocity= 18m/s Mass = 5000kg

Table 5 Specifications of the MATLAB program Benchmarking.

The deceleration levels for the following scenarios were kept in the region of human tolerance, which is in the order of 2.5Gs (refer: section 2.1).

8.1.3.1 First Benchmark Scenario, DeltaRoll1

The first scenario was a simulation of a minor scale incident. The summary described in Table 5 gives all the specifications of the incident. Conceptually this scenario was equivalent to a 1000kg conveyance dropping four meters, at 0.8Gs or eight tenths of the gravitational acceleration. The reduced acceleration took into account the friction in the guide rails of the cage and this was measured experimentally on the scale model and was implemented into the MATLAB program's code (refer: Figure 62).

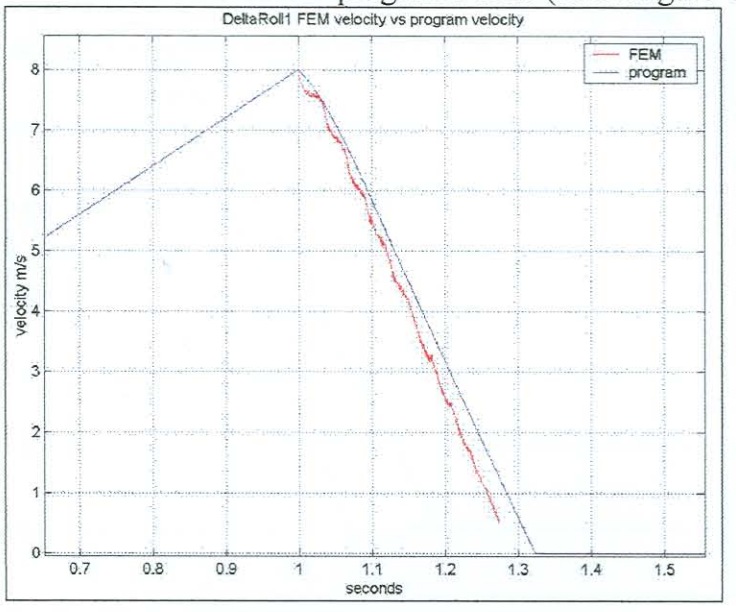

Figure 67 DeltaRoll1 velocity comparison.

In Figure 67 the velocity profiles of both predictions are compared. The velocity profile of the FEM analysis was then used to determine the acceleration performance by means of calculating the gradient of the curve. This procedure is further described in Appendix B.

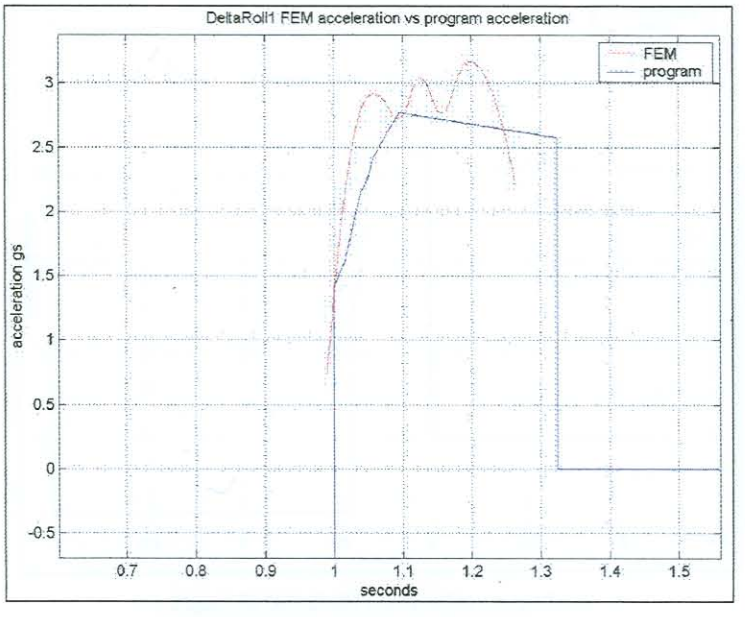

Figure 68 DeltaRoll1 acceleration comparison.

Figure 68 presents the result of the acceleration comparison. The predicted levels of deceleration were similar to the MATLAB program, once again delivering a conservative estimation as expected, based on previous performances observed.

8.1.3.2 Second Benchmark Scenario, DeltaRoll2

The conditions in the second benchmarking scenario were more severe than the first case. The equivalent situation could be described as a 2000kg conveyance, dropping ten meters at 0.8Gs or eight tenths of the gravitational acceleration, and being caught by two of the deceleration systems described in Table 5. The deceleration levels were again maintained in the region of the human tolerance limits as outlined in Table 2.

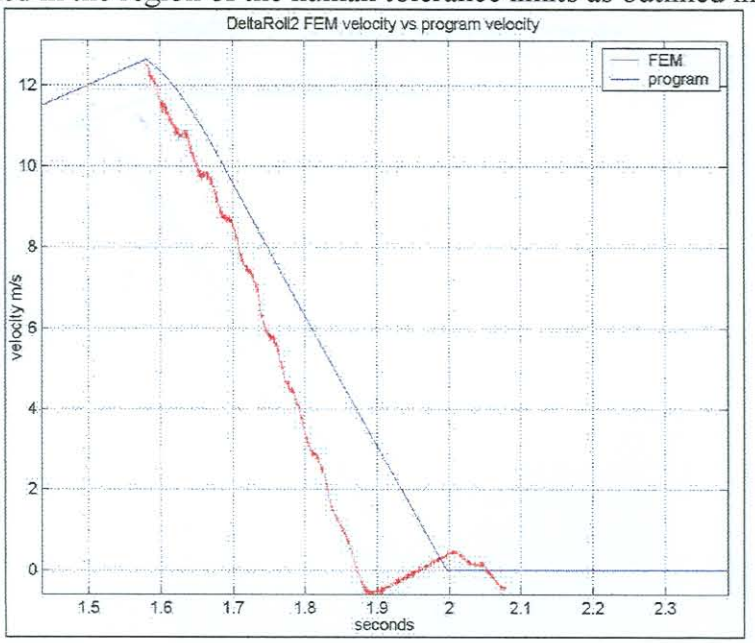

Figure 69 DeltaRoll2 velocity comparison.

The velocity comparison depicted in Figure 69 indicates a slightly sharper deceleration predicted by the FEM analysis, than the results of the MATLAB program.

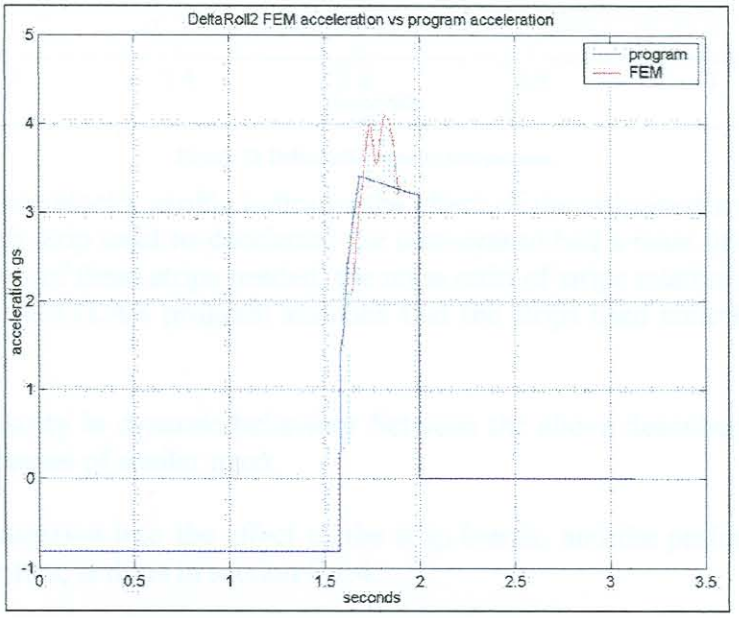

Figure 70 DeltaRoll2 acceleration comparison.

The deceleration levels shown in Figure 70, confirm the trend that the FEM analysis predicted a higher predicted level than the MATLAB program. The margin of error was in the order of 17%, which was consistent with the performance witnessed in the preceding section.

8.1.3.3 Third Benchmark Scenario, DeltaRoll3

In this scenario the situation was again more severe than previous. The equivalent description would be a 10000kg conveyance (10 Tonne), dropping twenty meters, before impacting two deceleration systems of the scale described in Table 5. This scenario is approaching the scale of real life application.

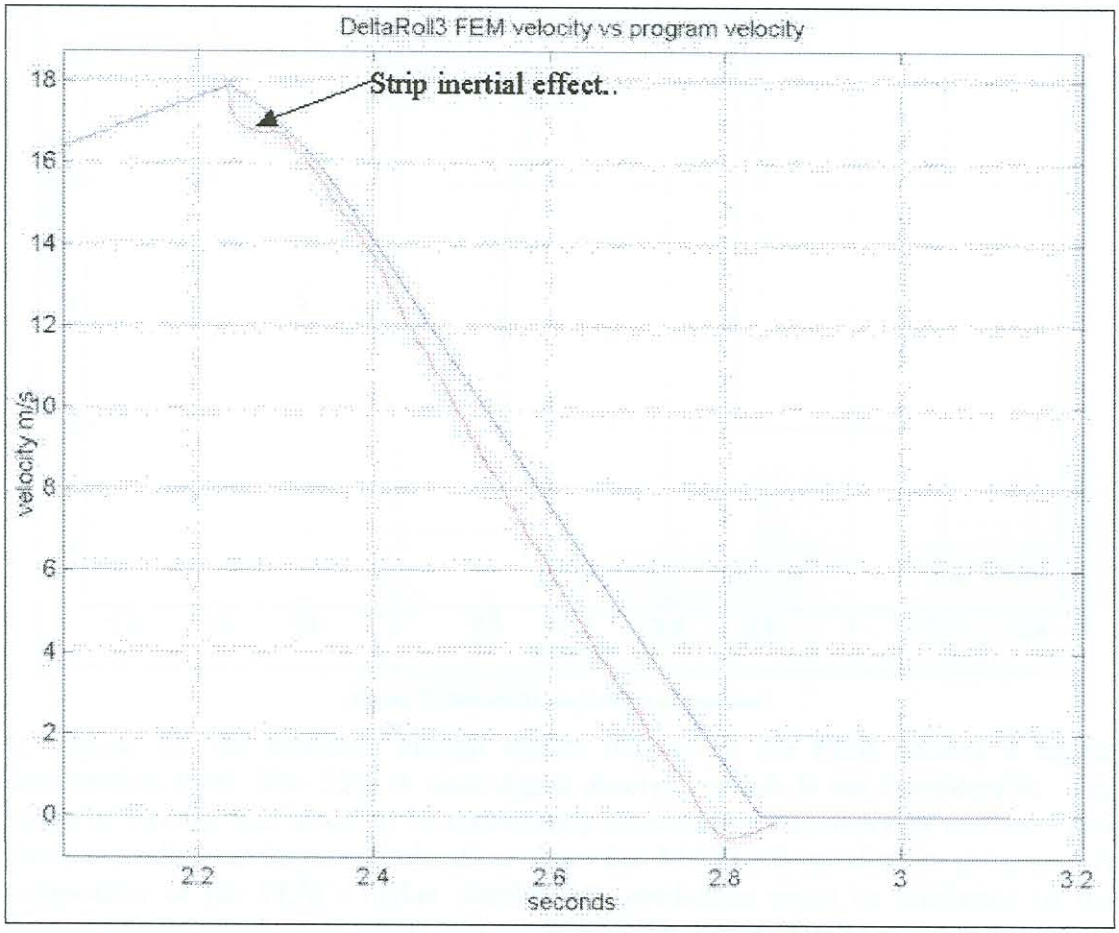

Figure 71 DeltaRoll3 velocity comparison.

In Figure 71, the velocity profile indicates the effect of the strip inertia on the system. In this case each strip used to decelerate the conveyance had a mass of approximately 273kg. With two of these strips needed, the mass ratio of strips relative to conveyance was 5.5%. The MATLAB program assumed that the strips used contributed no mass to the system.

There is a similarity in dynamic behaviour between the above described situation and two colliding masses of similar mass.

A further investigation into the effect of the strip inertia, and the performance impact made on the system, is done in section 8.1.4.

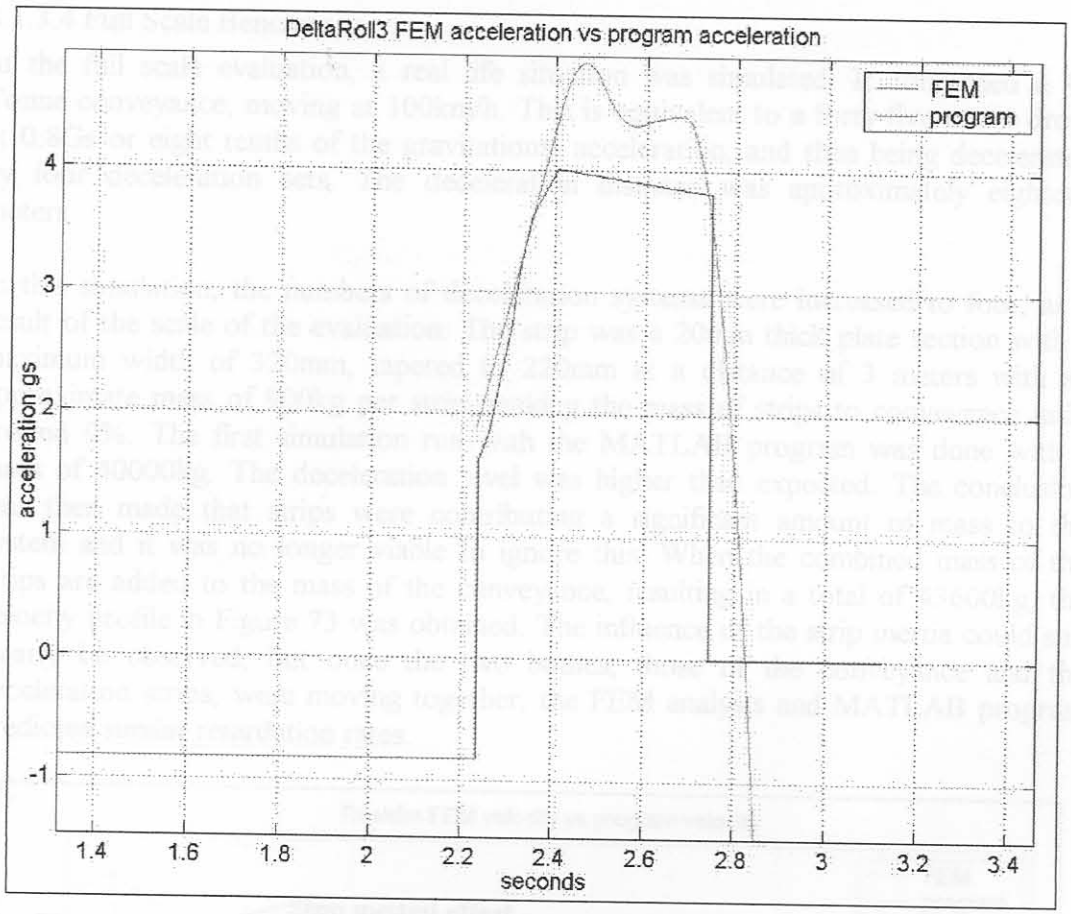

Figure 72 DeltaRoll3 acceleration comparison.

In Figure 72, the resulting inertial effects present in the FEM caused a higher deceleration level. The 25% is once again observed which is not considerable. The range of error is also noted to be consistently un-conservative, implying that the FEM always predicts a larger deceleration than the MATLAB prediction program. A component of the FEM's higher deceleration prediction could be attributed to the inertial effects which were taken into account in the model. The MATLAB prediction program ignored these effects.

A zero-density FEM was performed and compared to the MATLAB prediction program. The result of this comparison is discussed in section 8.1.4.

8.1.3.4 Full Scale Benchmark

In the full scale evaluation, a real life situation was simulated. It concerned a 40 Tonne conveyance, moving at 100km/h. This is equivalent to a forty-five meter drop, at 0.8Gs or eight tenths of the gravitational acceleration, and then being decelerated by four deceleration sets. The deceleration distance was approximately eighteen meters.

In this simulation, the numbers of deceleration systems were increased to four, as a result of the scale of the evaluation. The strip was a 20mm thick plate section with a maximum width of 320mm, tapered to 220mm at a distance of 3 meters with an approximate mass of 900kg per strip, making the mass of strips to conveyance ratio around 9%. The first simulation run with the MATLAB program was done with a mass of 40000kg. The deceleration level was higher than expected. The conclusion was then made that strips were contributing a significant amount of mass to the system and it was no longer viable to ignore this. When the combined mass of the strips are added to the mass of the conveyance, resulting in a total of 43600kg, the velocity profile in Figure 73 was obtained. The influence of the strip inertia could still clearly be observed, but once the two bodies, those of the conveyance and the deceleration strips, were moving together, the FEM analysis and MATLAB program predicted similar retardation rates.

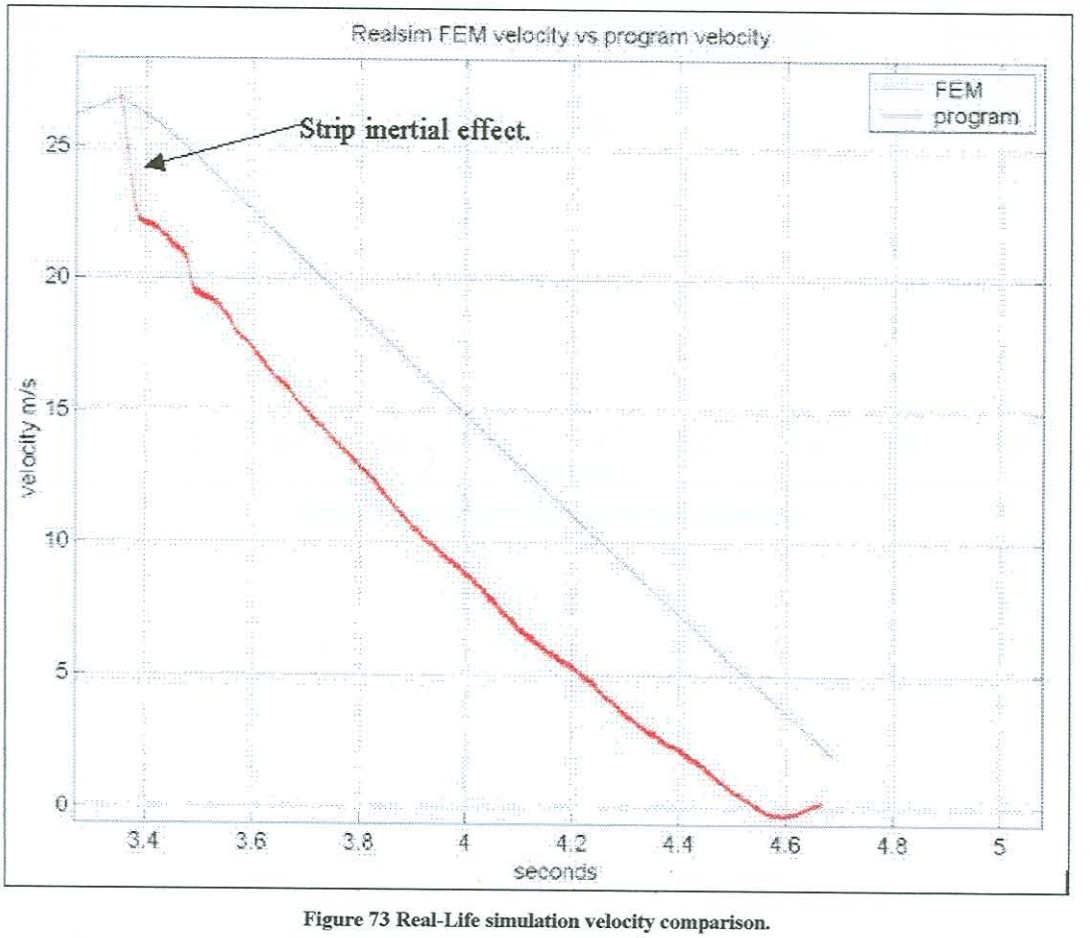

Figure 73 Real-Life simulation velocity comparison.

In section 8.1.4 a summary of the inertial effects of the strips is dealt with, and a combined graphical summary is presented to illustrate the contribution of these effects.

In Figure 74, the deceleration level predicted by the FEM analysis is in the order of 3.5Gs. This can be seen as an impulse with reference to the short length of time over which it occurs, which is approximately 0.2 seconds. With reference to section 2.1.2 dealing with the acceptable deceleration levels humans can endure, this deceleration situation would comfortably be survived by the average, fit person (refer: Table 1, Figure 8).

Apart from the initial discrepancy of the inertial effects caused by the mass inertia of the strips, the prediction of the MATLAB program was representative. Section 8.1.4 summarises the inertial effects of the strip inertia.

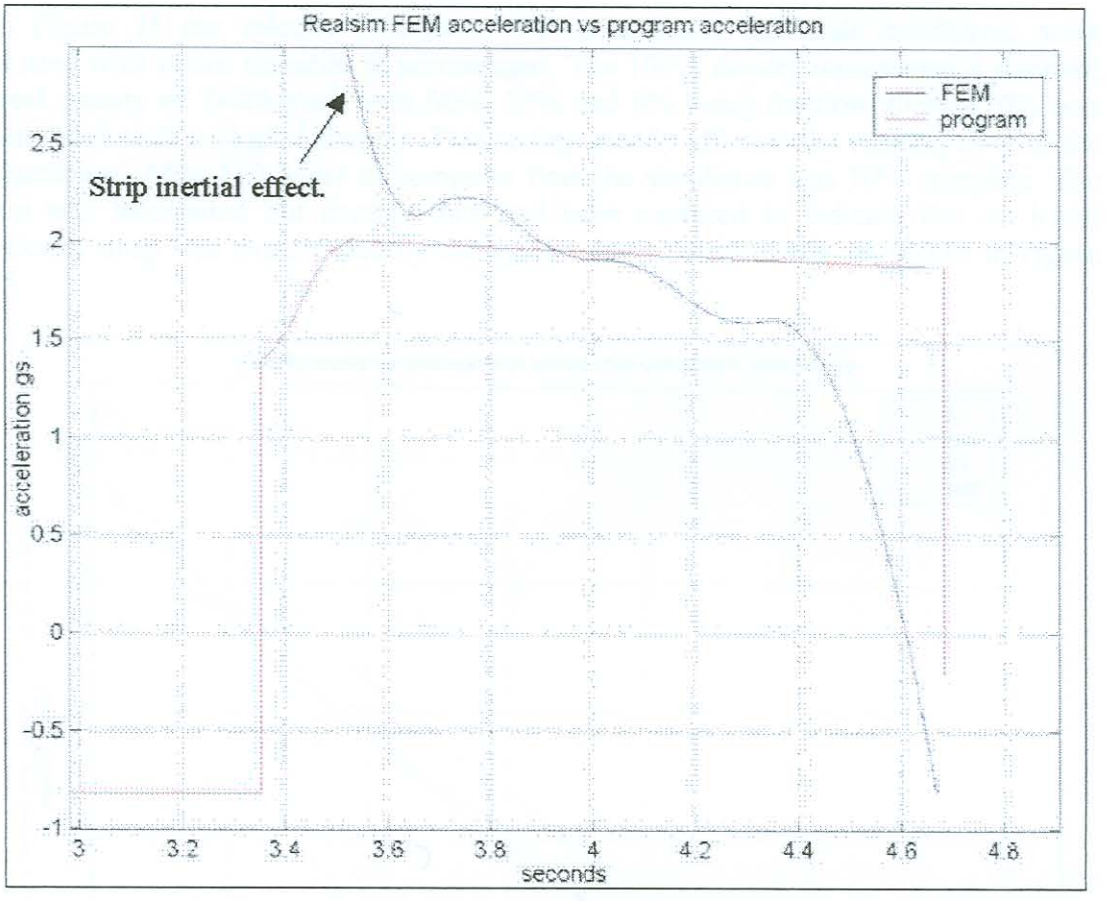

Figure 74 Real-Life simulation acceleration comparison.

8.1.4 Investigation of Strip Inertial Effect

An investigation was performed of the strip inertia effect on the performance of the cyclic bending deceleration systems. This was done by means of varying the density of the strips in the FEA package, MSC DYTRAN. The full scale scenario, as described in section 8.1.3.4, was re-simulated with the various modified strip densities and the resulting velocity and deceleration plots were compared. A comparison with the MATLAB prediction program was also drawn to clearly quantify the difference in performance of the systems relative to the strip density, which corresponded to the strip inertia.

In Figure 75 the velocity profiles of the re-simulated full scale conditions, were plotted with varied densities in percentages. The 100% density represented a standard steel density of 7800kg/m^3, with 60%, 25% and 0% being fractions thereof. 0% was simulated with a 1kg/m^3 density. This setting greatly affected the running time of the simulation. After 110 hours of computer time the simulation was 10% complete. The run was terminated but enough data had been captured to indicate that no initial velocity drop was experienced by the system due to strip inertia, as shown in Figure 75.

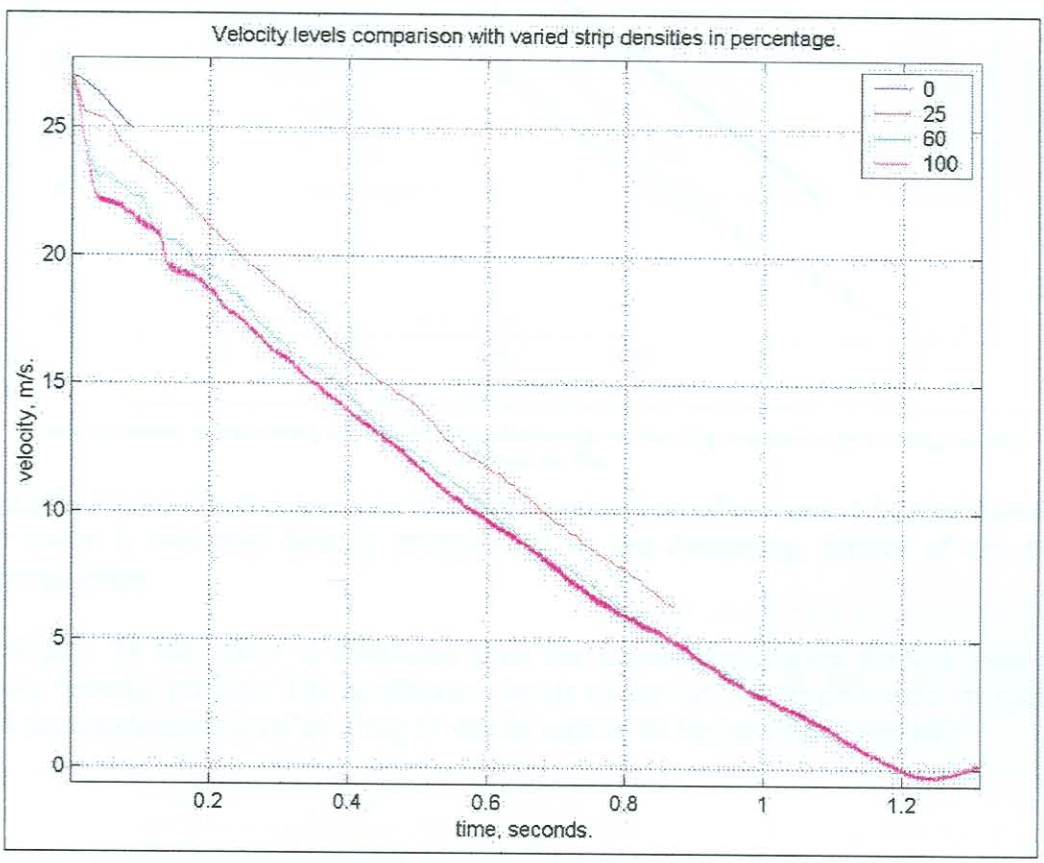

Figure 75 Velocity profiles of the full scale FEM simulation with varying strip densities. (In %)

The gradient of the velocity plots in Figure 75 are increasing (becoming steeper) as the strip density decreases. This effect can be attributed to the total mass of the system dropping, since the mass of the strips decreased. The deceleration capacity of the retardation system remained the same, and thus with less mass to accommodate, the deceleration logically became greater.

In Figure 76 the velocities were compared to the MATLAB prediction program output, with the mass of the strips included and excluded. 'Prog 0' neglected the strip mass and with the available braking force, the deceleration was greater than that experienced by the 'Prog 100' system, which included the mass of the strips. Referring to Figure 76, the gradients of 'Prog 0' and 'FEM 25' can be seen to be within the same order of magnitude, where 'Prog 100' and 'FEM 100' show their similarity in gradient.

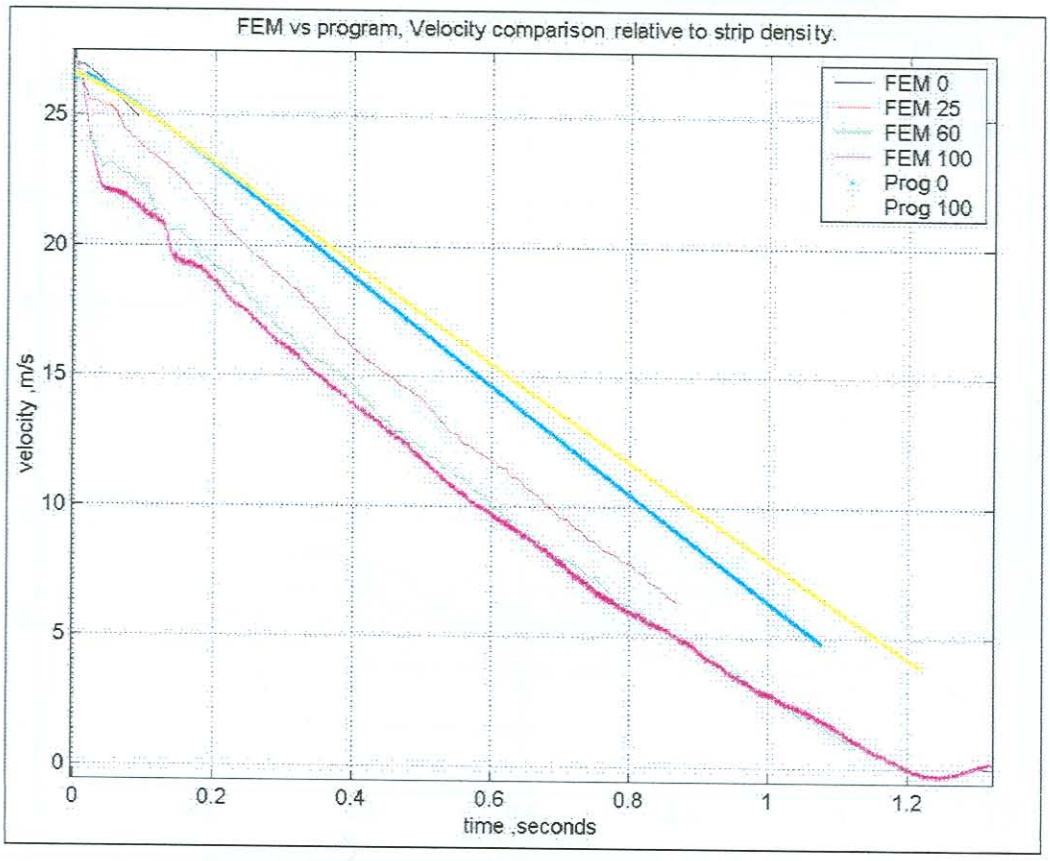

Figure 76 Velocity profiles of the full scale FEM simulation with varying strip densities vs. MATLAB prediction program. (In %)

Again in Figure 76, the decrease in initial deceleration effect caused by the inertia of the strips is evidently directly proportional to the decreasing density of the steel element strips.

In Figure 78 this effect is illustrated from the acceleration curves derived from the above velocity profiles. The acceleration levels of the various outputs were compared and the deceleration level of 'Prog 0' can be seen to be higher than 'Prog 100'.

Figure 77 is the result of differentiating the gradient of the previously plotted velocity profiles to obtain the deceleration experienced by the system. The only significant difference that can be noted in Figure 77 is the initial point of propagation. As the density of the strips decreased, so did the initial effect of the mass collision. This illustrated the crux of the investigation. 'FEM 0' shows no deceleration impulse since the mass struck a seemingly mass-less deceleration system.

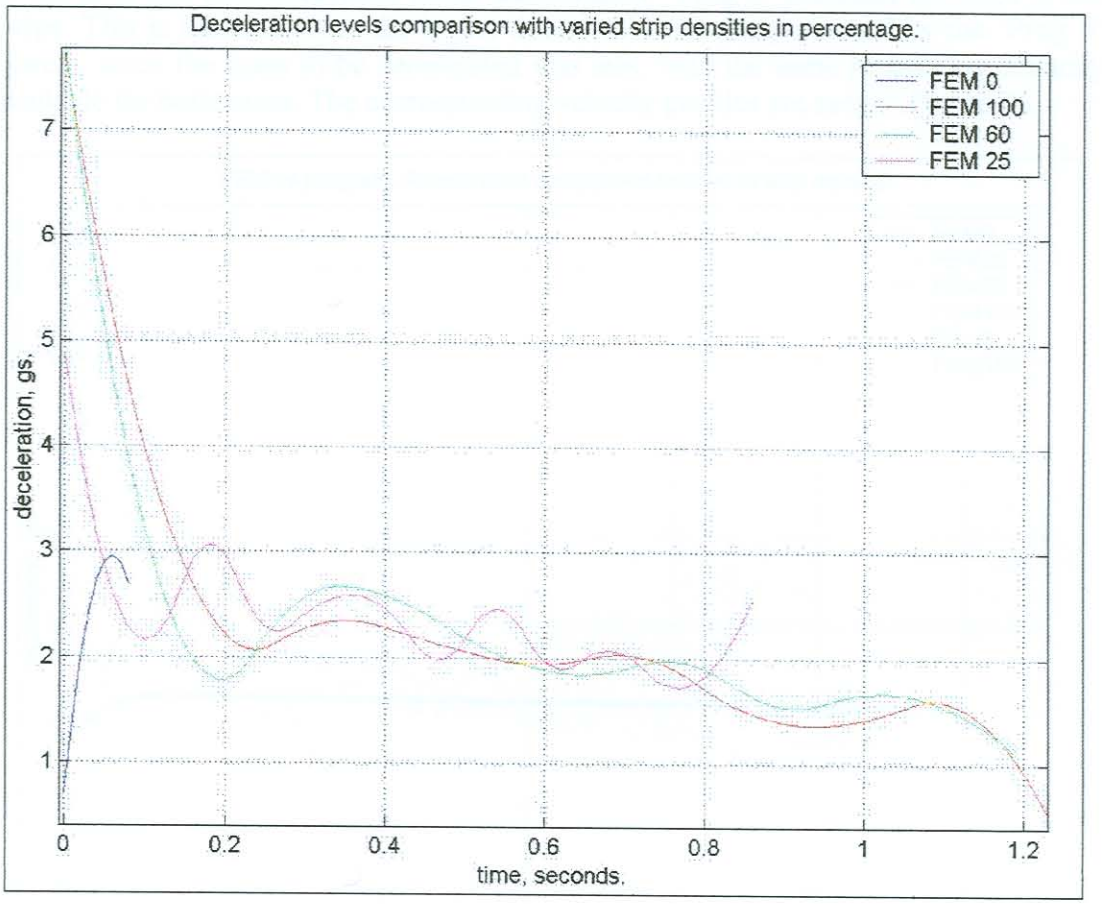

Figure 77 Acceleration profiles of the full scale FEM simulation with varying strip densities (as %).

In Figure 77 the retardation level of all the systems, once the deceleration strips had made contact with the mass, are the same.

If in the above hypothetical situation, a cage filled with occupants were subjected to these conditions of deceleration, the time interval they would have been subjected to the impact deceleration is very short. From Figure 77 the time interval for FEM 100 is estimated to be in the order of 0.15 seconds, with a peak deceleration level of 7.5Gs. In section 2.1.2 the human deceleration limits are quantified. With reference to those models and limits discussed, the occupants of the cage subjected to the full scale condition would probably have experienced deceleration levels which they could have survived while suffering only minor injuries.

In Figure 78 a further comparison was drawn between the FEM output and the MATLAB prediction program output. The initial impact of the MATLAB program output is not present in the graph, since the impact inertia of the strips was not included in the written prediction code.

The deceleration level of 'Prog 100' simulated the performance of the combined mass of the strip and the conveyance under deceleration. 'Prog 0' excluded the mass of the strips. This is the reason for the higher deceleration level experienced by the 'Prog 0' system, since the mass to be decelerated was less, with the same retardation capacity available for both cases. The corresponding velocity profiles are seen in Figure 76.

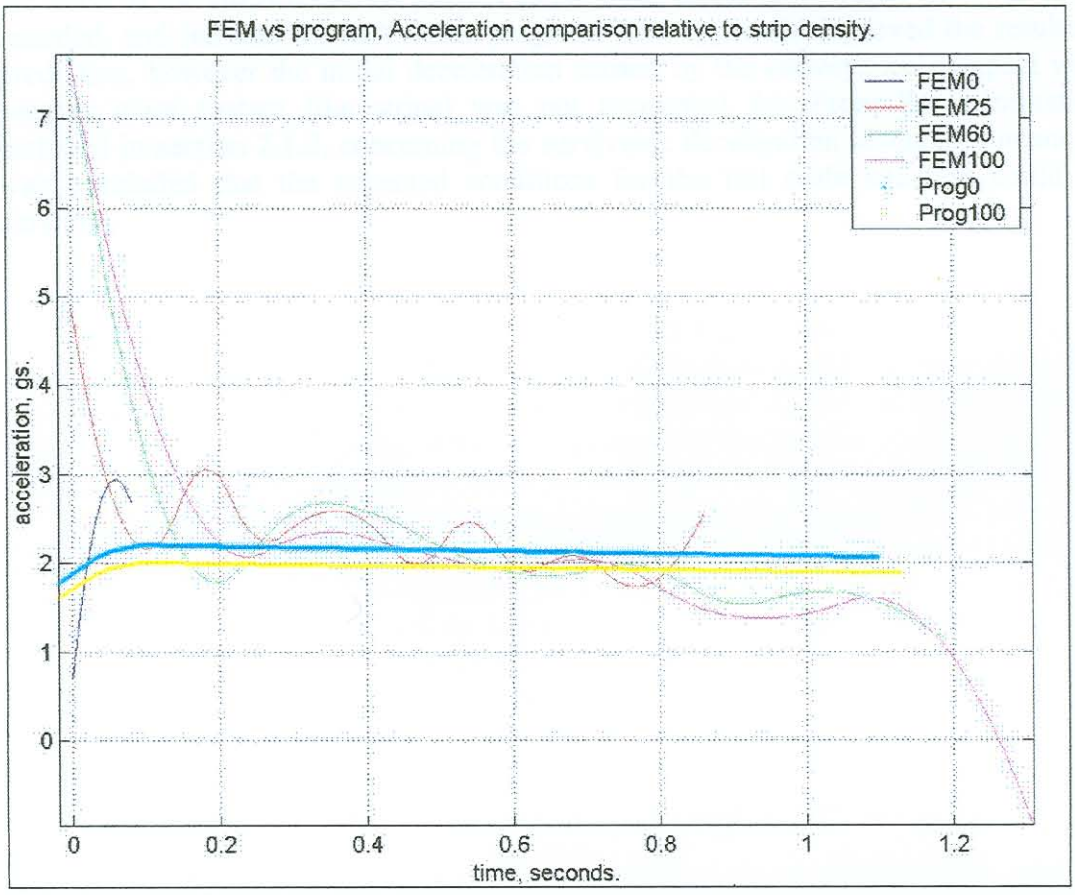

Figure 78 Acceleration profiles of the full scale FEM simulation with varying strip densities vs. MATLAB prediction program. (In %)

The constant region of deceleration, can be seen to be marginally affected by the inclusion or exclusion of the strip mass for the various simulations. The major effect of the strip mass is evident in the impact inertial effects which are directly proportional to the mass of the deceleration strips. The simulated results shown in Figure 78, bear testament to the decreasing initial impact levels for the corresponding lower strip densities.

8.2 Conclusion of Benchmarking Exercise

The comparison of outputs of the FEM analysis and the MATLAB prediction program, proved to be favourable and consistent in all cases. The prediction delivered by the MATLAB program was conservative in all cases of this investigation. The mass ratio between the combined mass of the strips and the conveyance plays a role in the accuracy of the prediction but was not crucial.

It was observed that the strip inertia contributed greatly to the high deceleration levels experienced during impact of the mass systems. When the mass ratio approached 5%, the mass of the strips could be totalled to the mass of the conveyance that was to be retarded, and fed into the MATLAB program. This approach improved the resulting prediction, however the initial deceleration caused by the conveyance's impact with another mass system (the strips) was not accounted for. From the information gathered in section 2.1.2, concerning the survivable deceleration levels of humans, it was concluded that the expected conditions for the full scale situation could be survived.

9. Conclusion and Recommendations

This investigation showed that the MATLAB prediction program promises to be a useful tool, which shows potential to be applied in various fields of industry and not only mining or conveyance applications. The MATLAB code was proved to be capable of accurately predicting the dynamic performance of the deceleration systems for a wide range of scenarios. The computational time for the MATLAB program to complete a prediction was substantially shorter than the FEM analysis. This is a great advantage. The processing time is in the order of 100 times faster and the degree of accuracy, based on the experiments conducted and the comparisons drawn, is of an acceptable standard.

As with all computer packages delivering prediction results, the user must be aware of the limitations of the program before it is applied to a problem situation.

The reason for FEM analysis consistently predicting a higher deceleration compared to the experimental data and the MATLAB program, can be a combination of the following factors:

1. The impact situation in the FEM analysis assumes that the rollers are frictionless. For this application it is a valid assumption since the contribution of friction in the rollers in the deceleration force is minimal. The MATLAB program also makes the same frictionless roller assumption.
2. Further, the FEM analysis assumed for a rigid connection between the strip and the mass. This assumption represents the worst case since the experimental set-up had a multi strand cable used for a connector (refer: Figure 4). In the FEM analysis, no energy was dissipated through the cable, where the cable did absorb impact energy in the experimental condition as well as the real-life application, and this helped alleviate some of the initial shock since the multi strand cables deliver a good amount of elasticity under load.

The finite element model and analysis was thus a more rigid system compared to the experiment set-up and would thus deliver a larger deceleration upon impact.

The MATLAB program also had no cable connection reference but it did not have an impact simulation included into the prediction. The execution of program code is such that the deceleration is applied once the mass passed the point of contact. At the point of contact the mass experienced no impact, which could influence the acceleration in terms of shock. For this reason the initial shock impulse is not seen in the graphs of the MATLAB program's predictions.

Much research would have to be done on the method and type of application of the cables proposed to be used as connectors between the deceleration systems, since their performance affects the overall effectiveness of the whole system. The ideal situation is for further work to be done on increasing the versatility of the MATLAB program code to accommodate both the inertial factors of the strips, as well as the elasticity of the cable connections.

Before this system is applied in industry, full scale tests need to be performed according to the predictions of the MATLAB program. The experimental data of these full-scale experiments then need to be closely analysed to determine the correlation between the prediction and the data captured.

The problem stated in section1.1, concerning the deceleration of a half full cage within the specified limits, can be solved practically by staggering the deceleration systems in banks of increasing deceleration capability. The idea is that when a half full cage under-winds, the first bank of deceleration systems decelerates the cage within the allowable levels of deceleration. If the conveyance is heavier or travelling faster than the deceleration capacity of the first bank of arrestors, a second bank, with larger decelerators is ready to apply a larger deceleration force. The second bank can then, for instance, be sized for a full cage under-wind, which would still be within limits of the specified human tolerance levels. A third bank could also be included with a much larger deceleration capacity, capable of accommodating a runaway cage, travelling faster than anticipated.

This third deceleration would probably be required to exceed the specified human tolerance levels, but could be used as a last line of defence, and under those conditions, injury would be better than death.

The details of such a system have to be tailor designed for each application depending on the amount of run through space at the bottom of the shaft, but the concept has potential to be investigated.

References.

1. Ottermann, R.W.
   von Wielligh, A.J
   Burger, N.D.L.
   de de de Wet, P.R.
   Blom, T.F.
   Visser-Uys, Dr. P.E.
   SIMRAC project GAP638c
   'The Identification, Investigation and Analysis of End-Of-Wind Protection Devices for Vertical and Incline Shafts.'
   December 2000

2. Jones, N.
   'Structural Impact'
   Cambridge University Press, 1989, pg. 422-428.

3. Rosslee, F.
   Coetzee, G.
   Pretorius, L.
   'Design and Analysis of an Energy Absorbing Mechanism for mine cages.'
   MIng. thesis, Rand Afrikaans University, Johannesburg 1996.

4. Johnson, W.,
   Mamalis, A.G.
   'Crash Worthiness of Vehicles,'
   Mechanical Engineering Publications,
   London, 1978, pg. 13-125

5. Seltrust Engineering
   'Strain Energy Linear Ductile Arrestor,'
   England. Bellamble Mining, ID9085806, 11 June 1999.

6. Willis, J.
   'Deep Drawing,'
   Butterworth Scientific Publications,
   London, 1954, pg. 10-39

7. Laubscher, R.F.
   van der Merwe, P.
   'Implementation of Strain Rate Sensitive Material Properties into Impact Related Problems,'
   Department of Mechanical Engineering, Rand Afrikaans University, Johannesburg, South Africa.

8. Cowper, G.R.
   Symonds, P.S
   'Strain Hardening and Strain-Rate Effects in the Impact Loading of Cantilever Beams,'
   Division of Applied Mathematics, Technical report 28.
   Brown University, Providence, USA. September 1957.

9. Hirsch, A.E.
   'The Tolerance of Man to Impact,'
   National Highway Safety Research Centre,
   US Dept. of Trans.Washington DC. 1968.

10. Harris, C.M
    Crede, C.E.
    'Shock and Vibration Handbook,'
    McGraw-Hill Book Company, 1976.

11. Eiband, A.M
    'Human Tolerance to Rapidly Applied Accelerations,'
    NASA Design memo, 5-19-59E, Washington DC 1959.

12. Stapp, J.P.
    'US Air Force technical report number 5915,'
    part. 1, 1949, part. 2, 1951

13. von Gierke — 'Symposium on Biodynamic Models and their Applications' 1970.

14. Specification code. — 'The Ministry of Mines for British Columbia,'

15. Dynamic Winder Testing Directive. — 'Department of Mineral and Energy Affairs,' Southern Africa. 10 February 1992.

16. Minerals Act South Africa. — 'Minerals Act and Regulations, Governing SA Mines,' 1998, Chapter 16, 'Winding'.

17. Macaulay, M.A. — 'Introduction to Impact Engineering,' Sectionman and Hall, London, 1987.

18. Harrigan, J.J. Reid, S.R. Peng, C — 'Inertial Effects in Impact on Energy Absorbing,' Material and Structures. Dept of Mech Eng UMIST. Manchester. 1999

19. Van Zelm, Jackson, M.A. — 'Patent on an Energy Absorbing Device,' Associated Inc. United States Patent No. 3/211/260 12 October 1965

20. Ezra, A.A. Fay, R.J. — 'An Assessment of Energy Absorbing Devices for Prospective use in Aircraft Impact Situations,' Dynamic Response of Structures, Pergamon Press, New York, 1972, pg225 – 246.

21. Lex Patria Publishers — 'Occupational Health and Safety Act and Regulations,' Act 85 of 1993. Driven Machinery Regulations. Sec 10.

22. De Vin, L.J. Streppel, A.H. Kals, H.J.J — 'The Influence of Material Behaviour of Air Bending,' The University of Ulster, Jordanstown, UK. 1996

23. Alexander, J.M — 'Metallic Energy Dissipating Systems,' Published by Johnson W. and Reid S.R Applied Mechanics Review vol. 31 No. 3 1978

24. Nine, H.D. — 'Drawbead Forces in Sheeet Metal Forming,' Mechanics of Sheet Metal Forming. General Motors Research Labs, Warren, Michigan. Plenum Press, New York, 1978

25. Thakur, A Nemat-Nasser, S. Vecchio, K.S. — 'Dynamic Baushinger Effect,' Dept. of Aplied Mechanics and Engineering Sciences University of California, 1995.

26. Dieter, G.E. — 'Mechanical Metallurgy,' McGraw-Hill Book Company, London, 1988.

27. Manjoine, M.J. 'Influence of Rate of Strain and Temperature on Yield Stresses of Mild Steel,' Journal of Applied Mechanics. Vol 11, 1944

28. Jones, N. 'Recent Studies on the Dynamic Plastic Behaviour of Structures,' Applied Mechanics Rev. Vol. 42 no 4 1989.

29. Perrone, N. 'On a Simplified Method for Solving Impulsively Loaded Structures of Rate Sensitive Materials,' Journal of Applied Mechanics, vol. 32, 1965.

30. Timoshenko, S.P. Gere, J.M. 'Mechanics of Materials Third Edition,' Chapman and Hall, London, UK, 1994.

Appendices.

Appendix A.

MATLAB prediction program code.

```
clear all

%=====================================================================
==================
%                Program to determine the effect of the
%                taper strip moving through a series of
%                rollers.


sigy = 280E6;                          %static yeild of material.
D = 40.4;                              %emp cnstant for mild steel.
p = 5;                                 %emp cnstant for mild steel.

v(1,1) = 0;                            %m/s
M = input(What it is the mass of the conveyance? kg - );  %kg
n = input(How many roller sets are needed? - );
N = input(Number of rollers in the set?  -  );          %#
t = input(What is the thickness of the sheet used? m  );
dia = input(What is the diameter of the rollers? - );    %m

s = pi*dia/4;                          %qrtr dstnce of roller.
R = dia/2;

tme(1,1) = 0;
delta_t = 0.0003125;

start_w = input(The thinnest width of the taper? m  - );
stop_w = input(The thickest width of the taper? m  -  );
overdst = input(Over what distance does the taper occur? m  -  );
itter = 15000;                         %must be more than 2000
xdrop = input(How high above the arrestors is the mass? - );

x(1,1) = 0;
x(1,N) = (2*N - 3)*s;

strp_taper_in = x(1,N);
strp_taper_end = x(1,N) + overdst;     %the taper geometry

for p = 2:(N-1)                        %Initial locations of the strp
   x(1,p) = (2*p-2)*s;                 %position on the rollers.
end                                    %Before any motion

r = 1;
x(r,:) = x(r,:) - xdrop;               %The initial position of
                                       %the mass
```

```
%-----------------------------------------------------------------------
            %Main program for the forces with fixed delta time.


     while x(r,:) <= strp_taper_in
         tme(1,(r+1)) = tme(1,r) + delta_t;
         accel(1,r) = -8;                              %The rated G with
         v(1,(r+1)) = v(1,r) - accel(1,r)*delta_t); %friction factor
         delta_x(1,r) = 0.5*(v(1,r)+v(1,(r+1)))*delta_t;
         x((r+1),:) = x(r,:) + delta_x(1,r);
         r = r+1;
     end


for z = r:itter;                          %For  itter time increments.
      for y = 1:N;
         if x(z,y) <= strp_taper_in
         w(z,y) = start_w;
         elseif x(z,y) <= strp_taper_end
         w(z,y) = ((stop_w - start_w)/(strp_taper_end -
strp_taper_in))*x(z,y) + (start_w - ((stop_w -
start_w)/(strp_taper_end - strp_taper_in))*strp_taper_in);
         else
         w(z,y) = stop_w;
         end


         if v(1,z) <= 0;
            v(1,z) = 0;
         end

   strnrate(1,z) = v(1,z)/(12*R + 6*t);%strain rate.
                                       %Same for each roller.
   sigyd(1,z) = (1 + (strnrate(1,z)/D)^1/p)*sigy;  %Dynamc yield,
                                                   also the same.
                                                   %for each
                                                   %roller
F(z,y) = (4*sigyd(1,z)*w(z,y)/sqrt(3))*(t - 2*R*sqrt(1 + t/R) + 2*R);

     end

%for
%------------------------ End of the independant roller calcs-----

 Fset = sum(F,2);                  %sums all the rollers in the set.

   Ftot = n*Fset;                  %Combined force of n brakes


   accel(1,z) = Ftot(z,1)/M;       %combined decceleration that the
                                   %strip applies
   if v(1,z) <= 0;
      accel(1,z) = 0;
   end
```

```
----------                          %The motion part.

tme(1,(z+1)) = tme(1,z) + delta_t;              %next time step
v(1,(z+1)) = v(1,z) - (accel(1,z)*delta_t);%velocity change with
                                                %accel

delta_x(1,z) = 0.5*(v(1,z)+v(1,(z+1)))*delta_t; %movement in
                                                %time increments
x(z+1,:) = x(z,:) + delta_x(1,z);       %adds displacement increment
                                        %to the individual roller pos.
end

sig_strp = max(Fset)/(start_w*t);
Safety_Factor = sigy/sig_strp

                                %MAIN END!!!!!!

secs = linspace(1,(itter/3200),(length(tme)-1));%3200 is the sampling
                                                %frq in experiment.
figure(1)
plot(secs,Ftot,.)
hold
grid
plot(secs,F)
title(Independant forces (one roller) and then the combined effect
(both))
xlabel(seconds)
ylabel(Newtons)

gs = accel/9.8;

figure(2)
plot(secs,gs,r)
grid
title(The decceleration experienced by the mass in Gs)
xlabel(seconds)

figure(3)
plot(tme,v)
hold
plot(tme(1,r),strp_taper_in,r.)
plot(tme(1,r),strp_taper_in,r+)
plot(tme(1,r),strp_taper_in,ro)
grid
title(The velocity profile of the skip/mass)
ylabel(m/s)
xlabel(seconds)

figure(4)
plot(tme,x(:,3))
hold
grid
plot(tme(1,r),strp_taper_in,r.)
plot(tme(1,r),strp_taper_in,r+)
plot(tme(1,r),strp_taper_in,ro)
title(Displacement of the mass/skip, from fall to stop. Mark is
contact with brakes.)
ylabel(meters)
xlabel(seconds)
```

Appendix B.

Technique for converting velocity profile to acceleration.

The technique used to determine the gradient of the velocity profile was as follows:

1. The data files of the time series and velocity series were loaded.
2. A number of points between which to sample in the data string were chosen.
3. The values of the positions were determined.
4. A spline was fitted through the positions.
5. The gradient of the spline was derived.
6. The derivation was plotted as an acceleration curve.

```
clear all
clear session
close all

eval(load vel)        %loading FEM velocity data
eval(load tt)         %loading FEM time data

vel_orig = vel;
time_orig = tt;

no_int = 8;              %the number of sampling points through which
                         %to fit the spline

temp = length(vel_orig);

interval = linspace(1,temp,no_int);

for j=1:length(interval)
    interval(j) = round(interval(j));
end

for j=1:length(interval)
    t_samp(j) = time_orig(interval(j)); %sampling values determined
    v_samp(j) = vel_orig(interval(j));
end

t_fit = time_orig;
v_fit = interp1(t_samp,v_samp,t_fit,spline); %spline fit

figure(1)                      %plot of sample positions vs spline fit
plot(t_samp,v_samp,o,t_fit,v_fit)

for j=1:(length(t_fit)-1)              %determining of gradient
    del_y = v_fit(j+1) - v_fit(j);
    del_x = t_fit(j+1) - t_fit(j);
    a_fit(j) = del_y/del_x;
end

figure(2)                              %plot of derived acceleration
t_acc = t_fit(1:(temp-1));
plot(t_acc,a_fit)
```

Appendix C.

Parallel profile strip results.

The experimental procedure regarding this section was done with two inline dampers (refer: Figure 79). The damper system consisted of a steel tube with a coil spring inside. The spring absorbed the initial impact and then activated the decelerating strip systems. The problem with this application was the spring back and the mass ratio of the tubes with the springs compared to the conveyance/mass itself. The masses of the tubes were 15kg each and the conveyance was 130kg. In section 8.1.3.4 a conclusion of mass ratio not exceeding 10% was reached. In this case the ratio was over 20%. The arrangement is shown in the following figures.

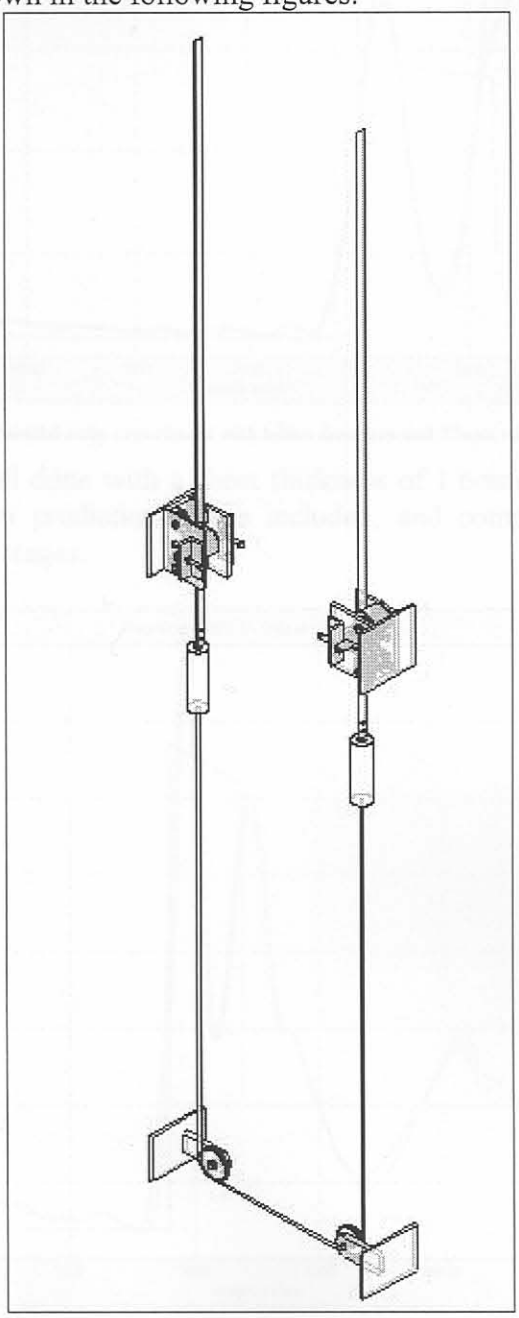

Figure 79 Schematic representation with inline damping systems included.

The double acceleration peak was generated by the spring back of the coil spring. The dynamic performance was similar to a two-mass-spring-damper-system, under an impulse excitation, with the double stage action. For this reason the arrangement was changed to the tapered strip set-up, where the mass of the tube could be eliminated.

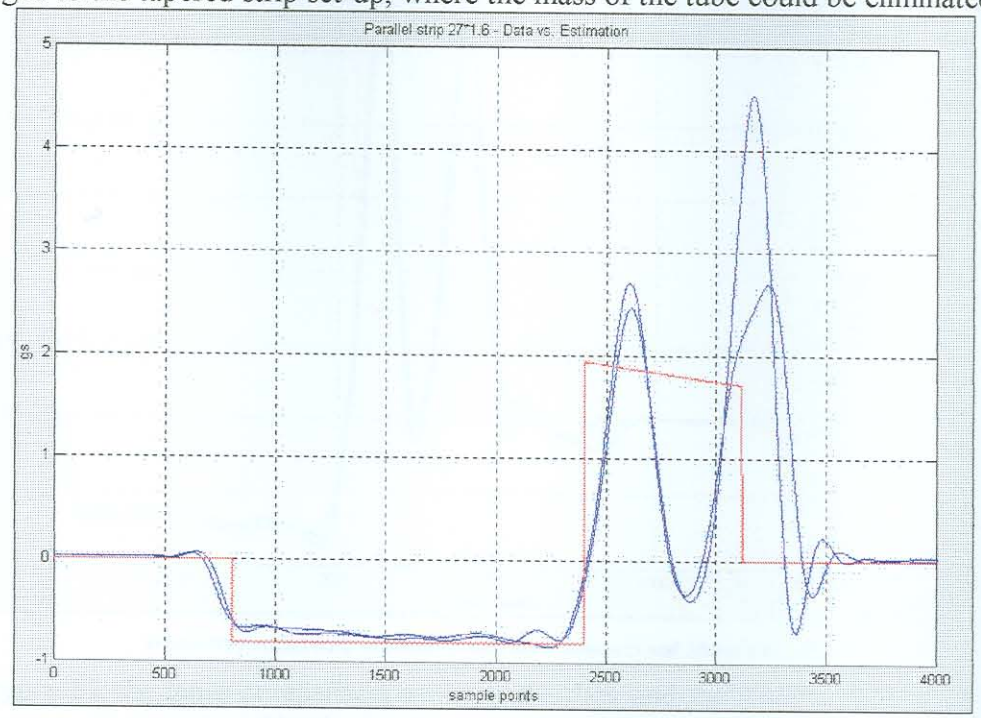

Figure 80 Parallel strip experiment with inline dampers and 27mm wide strip.

The experiments were all done with a sheet thickness of 1.6mm and parallel sections. The MATLAB program predictions were included, and compared reasonably well during the development stages.

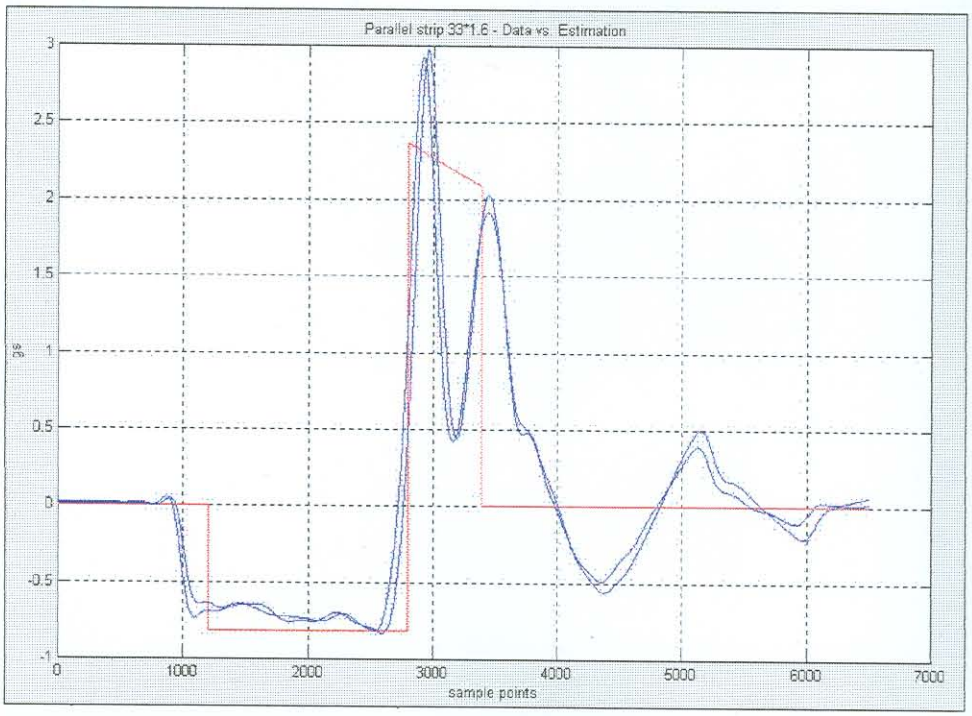

Figure 81 Parallel strip experiment with inline dampers and 33mm wide strip.

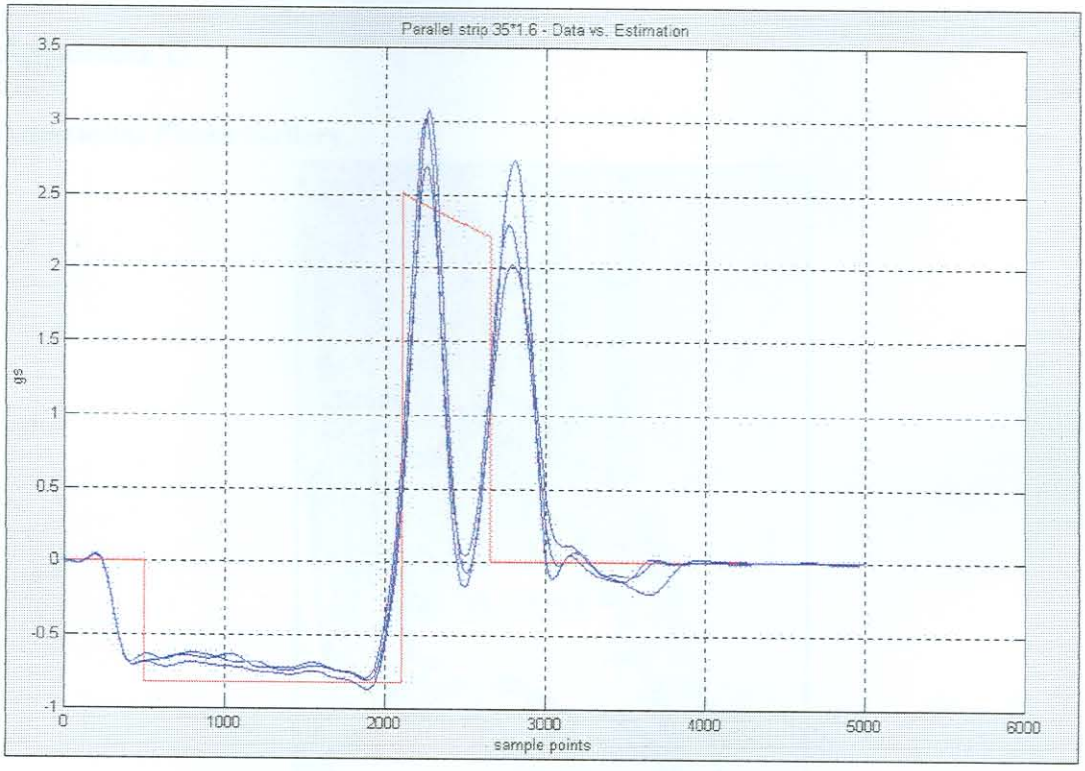

Figure 82 Parallel strip experiment with inline dampers and 35mm wide strip.

In Figure 82 the close comparison between the data and the prediction is evident. In this series of tests the objective was to decelerate the conveyance at no more than 2.5Gs and it can be seen from the resulting acceleration plot that this was achieved. The sizing of the strips was done by means of using the MATLAB prediction program.

Even though the technique was altered it served as a valuable development stage.

Appendix D.

Additional Photo Gallery.

Figure 83 Pulley system at the bottom of the model shaft.

Figure 84 View through the mouth of the shaft.

In Figure 84 the strips can be seen threaded between the rollers. Here the strips had been drawn through the rollers, and the model cage retracted from it's rest position at the bottom of the shaft.

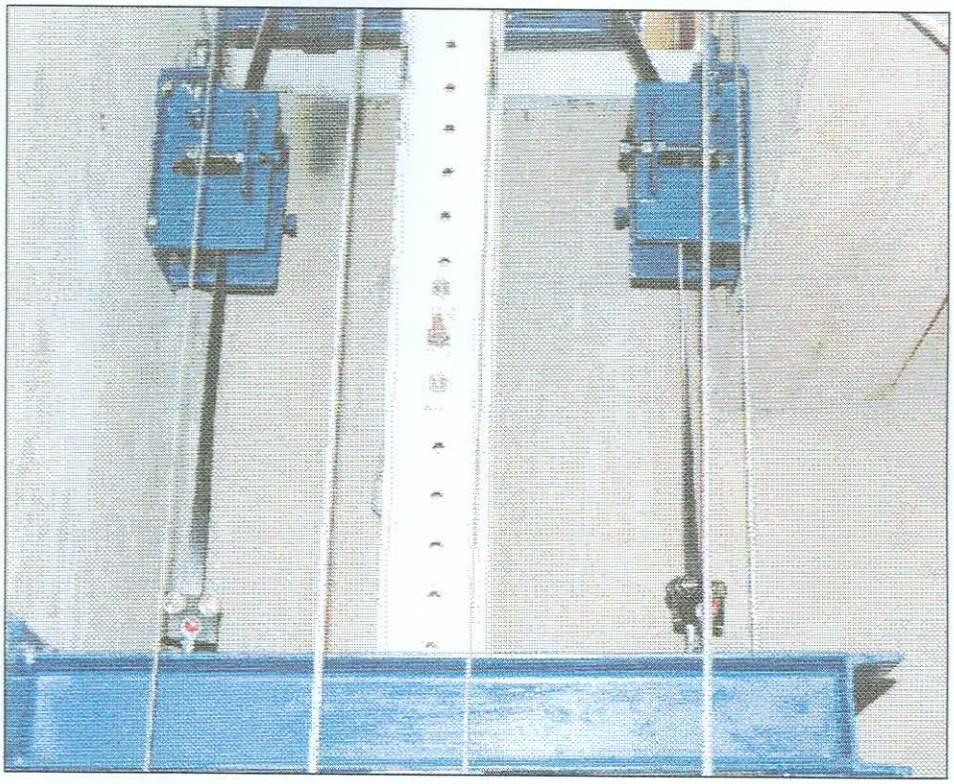

Figure 85 View of strips drawn through the rollers.

Figure 86 View of all the taper strips of which data was recorded.